Tracing biogeochemical processes using sulfur stable isotopes: two novel applications

by

Mélanie Lyne Cousineau

A thesis submitted
to the Faculty of Graduate and Postdoctoral Studies
in partial fulfilment of the requirements for the degree of
Ph.D. in Earth Sciences,
Specialisation in Chemical and Environmental Toxicology

University of Ottawa
Ottawa, Ontario

We have not succeeded in answering all our problems. The answers we have found only serve to raise a whole set of new questions. In some ways, we feel we are as confused as ever, but we believe we are confused on a higher level, and about more important things.

Attributed to Earl C. Kelly, 1951.

uOttawa

Abstract

Dissimilatory microbial sulfate reduction (MSR)

The specific objectives of the study were to provide the first measurements of sulfur isotope fractionation associated with acidophilic sulfate reducing-microorganisms, and to examine whether pH influences sulfur fractionation during MSR. The fractionation associated with the strains investigated was comparable to that of neutrophilic strains with similar metabolisms (4-12‰), but varied with pH. Two fractionation regimes were identified: one regime is consistent with fractionation during exponential growth, while the other – not identified previously - is not linked to active sulfate reduction and may result from internal sulfate accumulation. This would represent the first measurement of sulfur fractionation during sulfate uptake, the first step of MSR.

Geological processes at the Cretaceous-Paleogene (KPg) boundary

The KPg boundary is associated with one of the largest biological extinctions in the history of our planet. Two major geologic events - the Chicxulub bolide impact with evaporite terrane and the eruption of the Deccan continental flood basalts - coincide with the KPg boundary and have been identified as possible triggers for the extinctions, but their relative timing remains unresolved. The objectives of this study were to identify the contribution of these processes to the sulfur burden in the sedimentary environment of two freshwater KPg sections, and to determine their relative timing. The results demonstrate that the peak of Deccan volcanism post-dates the Chicxulub impact and the associated abrupt KPg mass extinction, thus precluding a direct volcanic causal mechanism, but shedding light on the underlying causes for the delayed recovery of ecosystems in the early Paleogene.

Résumé

Réduction microbienne non-assimilatoire des sulfates (RMS)

Les objectifs spécifiques de cette étude étaient d'effectuer les premières mesures du fractionnement isotopique du soufre associé à la réduction des sulfates par des micro-organismes acidophiles et d'examiner le rôle du pH dans le fractionnement durant la RMS. Le fractionnement associé aux souches étudiées est comparable à celui de souches neutrophiles à métabolisme semblable (4-12‰), mais varie en fonction du pH. Deux régimes de fractionnement ont été identifiés: l'un est en accord avec le fractionnement durant la phase exponentielle de croissance, alors que l'autre - qui n'avait pas été identifié précédemment - n'est pas associé à la réduction active de sulfates et pourrait résulter de leur accumulation à l'intérieur de la cellule, dans quel cas il correspondrait au fractionnement durant la première phase de la RMS, l'entrée des sulfates dans la cellule.

Processus géologiques à la frontière du Crétacé-Paléogène (KPg)

La frontière du KPg est associée à l'une des plus grandes extinctions massives dans l'histoire de notre planète. Deux événements géologiques majeurs - la collision d'un météorite avec un terrane composé d'évaporites, et l'inondation basaltique continentale des trappes du Deccan - coïncident dans le temps avec la frontière KPg et ont été identifiés comme déclencheurs possibles des extinctions, mais leur répartition relative dans le temps n'a pas encore été résolue. Les objectifs de cette étude étaient de mesurer la contribution relative en soufre de chacun de ces processus géologique à l'environnement sédimentaire en eau douce de deux sections de la frontière, ainsi que de déterminer leur répartition relative dans le temps. Les résultats indiquent que l'apogée des éruptions volcaniques est survenue après l'impact météoritique et l'extinction massive abrupte. Ceci écarte donc la possibilité que le volcanisme ait joué un rôle direct dans l'extinction massive, mais jette de la lumière sur les causes sous-jacentes du rétablissement retardé des écosystèmes au début du Paléogène.

Table of Contents

List of Figures

List of Tables

Acknowledgements

I extend my sincere thanks to Danielle Fortin, my supervisor, for her positive attitude and continuous support, and for giving me the opportunity to work under her tutelage. A special thank you as well to Boswell Wing, my co-supervisor, without whom this degree would have been considerably different and definitely not as fascinating. The chance to work with him and members of his lab has opened my eyes to a whole new - ancient - world. His advice, support, and deep knowledge of the intricacies of stable isotope systematics and mathematics have been instrumental in making my four years always challenging, but certainly motivating.

Throughout my time as a PhD candidate, many fellow graduate students have generously shared their knowledge and expertise with me. I am indebted to the members of the Fortin and Wing labs for their generous assistance, and to the many undergraduate students who donated their precious time to help with my complex and often failing experiments. A special thanks to Marc-André Cyr and Kizil Reder.

To the many people with whom I shared an office, thank you for your friendship and for the many fascinating conversations. Tea Laurila, Lilian Navarro, Matt Herod, Fritz Griffith and Nathan Steeves: I hope to continue to be the bringer of good coffee!

To Hélène DeGouffe: thank you for always knowing exactly how to answer my sometimes-complicated administrative questions.

A special thanks to the staff at the University of Ottawa Science Store, who are most likely often forgotten, but who have been instrumental in the success of my laboratory experiments. Pierre, Dan, Claude, and others: you were always friendly, helpful, and ready to help - sometimes with quirky requests, at the last minute, or from across the world.

I am grateful to Teruyuki Maruoka for offering me the opportunity to experience research in a Japanese laboratory and for helping me integrate in Tsukuba upon my arrival there: my summer in Japan is an experience I will always remember fondly. I am also indebted to François Therrien for willingly sharing his precious samples, time and expertise on the KPg project. It was a pleasure working with him, and I hope our paths will cross again (perhaps for a second visit in the fascinating storage rooms of the Royal Tyrell Museum!),

To my husband, Greg Brown, I extend my infinite gratitude for his friendship, love, and understanding. His encouragement and support are what kept me going.

I would like to dedicate this work to the memory of Moire Wadleigh, who was my MSc supervisor at Memorial University. She passed away much too early, but her encouragement and support were significant in my decision to pursue doctoral studies. She will be remembered fondly.

Finally, I would like to acknowledge the financial support of the Natural Sciences and Engineering Research Council, the Fonds de recherche du Québec - Nature et Technologies, the Japan Society for the Promotion of Science, the Mineralogical Association of Canada, and the University of Ottawa.

General Introduction

Because different environmental conditions (temperature, pH, etc.) and reaction pathways (biological, chemical, physical) can lead to distinct fractionation patterns of stable isotopes, the isotopic composition of a given material can provide valuable information on the environmental conditions prevailing during its formation. Thus the study of sulfur isotope fractionation finds applications in countless fields in the geo- and biosciences.

This thesis focuses on two applications of sulfur stable isotopes as novel tracers of biogeochemical processes. The first application concerns the fractionation of sulfur stable isotopes during the microbial reduction of sulfate. This has implications for undertanding the origin of biogenic sulfides, and the conditions prevailing during their formation. An extensive field of research making use of these principles and focussed on understanding the history of oxygenation of the Earth and oceans has developped in recent decades. This is discussed further in this introductory chapter and is the focus of the paper presented in Chapter 3.

A second application of sulfur stable isotopes is the investigation of global geological processes at the time of the Cretaceous-Tertiary (KPg) mass extinction, ≈65.5 million years ago. Although the scientific community appears to lean heavily on a bolide impact with evaporite terrane as the trigger for the extinctions, the contribution of the Deccan continental flood basalts has long been in question. Chapter 2 features an introduction to this key event in Earth history, and is completed by Chapter 4, which presents the results of an investigation of the contribution of these two geological processes to the sulfur record of two well-preserved terrestrial KPg sections. Appendices include recipes for chemically-defined media used in the culturing of the sulfate-reducting micro-organisms used in the experiments described in Chapter 3, as well as a detailed description of the sulfur extraction line constructed by the candidate in the course of her doctoral studies at the University of Ottawa.

Chapter 1: Microbial and atmospheric sulfur cycling

The focus of this first introductory chapter is on two components of the global sulfur cycle: microbial and atmospheric cycling. Fundamental principles and how they apply to the study of the reactions that characterize the cycling of sulfur by micro-organisms and the atmosphere are explored. Basic principles and the notation used in the study of sulfur stable isotopes are also included.

1.1 Stable sulfur isotopes and notation

Sulfur is the fourteenth element in abundance in the Earth's crust, occurring to the extent of 0.047% (Grinenko and Ivanov, 1983). With an atomic mass of 32.06 amu, it has four stable isotopes ^{32}S, ^{33}S, ^{34}S, and ^{36}S, occurring in proportions of 95.04%, 0.75%, 4.20% and 0.014%, respectively (Ding et al., 2001). Sulfur exists in nature in five valence states (-2, 0, +2, +4 and +6) and is essential to living systems. The biogeochemical sulfur cycle has changed considerably through the planet's history, mainly due to the appearance of new metabolic pathways and changes in their importance (Schlesinger, 1991), but its present state reflects extreme human-induced perturbations.

The sulfur isotopic composition of a given material is given relative to a reference material and expressed in units of per mil (‰). The historical reference material for relative isotope ratio measurements of sulfur was an iron sulfide (FeS) mineral (troilite) from the Cañon Diablo iron meteorite, and was believed to represent the primordial solar system ratio of ^{34}S to ^{32}S. However, because of large variability in its composition (up to 0.4‰; Beaudoin et al., 1994), its use has been discontinued. The reference materials now used in the study of sulfur stable isotopes are based on the Vienna-CDT (V-CDT, Vienna Cañon Diablo troilite) scale, on which the $\delta^{34}S$ value of the international reference Ag_2S material IAEA-S-1 is defined as -0.3‰. The isotopic

composition of a sample is related to that of a reference material according to the following equation:

$$\delta^{A}S\ (‰) = [(^{A}S/^{32}S_{sample})/\ (^{A}S/^{32}S_{reference})] - 1$$

where $^{A}S=^{33}S$, ^{34}S or ^{36}S. A positive $\delta^{A}S$ value indicates enrichment (depletion) in the heavier (lighter) isotope relative to the reference, whereas a negative value denotes enrichment (depletion) in the lighter (heavier) isotope. In part because it was expected that fractionation of sulfur isotopes would take place strictly according to mass differences between the various isotopes (mass-dependent fractionation) and in part because of the technical difficulty in analyzing the less-abundant isotopes ^{33}S and ^{36}S, until fairly recently the study of sulfur isotope fractionation had been mostly limited to the most abundant isotopes of sulfur, ^{32}S and ^{34}S. However, analytical improvements and the discovery of unexpected isotope effects (mass-independent fractionation, see Section 1.1.2) in the geological record has led to expansion of research in the study of the minor isotopes of sulfur.

Separation of the various isotopes between the product and reactant of a reaction is referred to as “fractionation” and results from isotope effects, physical phenomena that cause the separation of isotopes between the product and reactant. Two general types of isotope effects can be identified: equilibrium isotope effects and kinetic isotopes effects. Equilibrium effects cause certain isotopes to accumulate in a particular component of a system in equilibrium, and follow the general rule that heavy isotopes preferentially accumulate in the chemical compound in which they will be bound more strongly (Bigeleisen, 1965; Thode, 1991). For example, equilibrium fractionation between aqueous sulfide and sulfate in a high-temperature and -pressure hydrothermal systems leads to the preferential accumulation of ^{34}S in the sulfate fraction (Sakai and Dickson, 1978). Kinetic isotope effects occur when the rate of a chemical reaction is sensitive to the atomic mass of one of the reacting species. In most cases, kinetic

isotope effects cause the lighter species to react faster because of greater translational and vibrational velocities associated with lighter isotopes. At thermodynamic equilibrium, the distribution of sulfur isotopes in a given system is predictably controlled by mass differences between the isotopes: this is referred to as “mass-dependent fractionation”.

Fractionation can be described in terms of the fractionation factor α, defined as:

$$\alpha=({}^{A}S/{}^{32}S_{\text{after fractionation}})/({}^{A}S/{}^{32}S_{\text{before fractionation}})$$

or quantified in terms of the enrichment factor ε, which, when expressed in parts per thousand (per mil), is related to α by the following (Clark and Fritz, 1997):

$$\varepsilon=1000\bullet\ln\alpha$$

Because α is very close to 1,this equation can be simplified to:

$$\varepsilon=(\alpha-1)\bullet1000$$

The use of this simplified equation yields a relative error of less than 2‰ for enrichment factors below 40‰ (Bolliger et al., 2001).

1.1.1 Mass-dependent fractionation of sulfur

Mass-dependent isotope fractionations are those that result from atomic mass differences between the different isotopes involved in a reaction. In the case of sulfur, the fractionation between ^{34}S and ^{32}S, as well as ^{36}S and ^{34}S, occurs primarily because of the ≈2 unit difference in atomic mass between the two isotopes, while in the case of ^{33}S and ^{32}S, it occurs primarily because of a difference of ≈1 in atomic mass (Hulston and Thode, 1965; Miller, 2002). Thus with processes that lead to mass-dependent fractionation of sulfur isotopes, which include all those at thermodynamic equilibrium as well as many non-equilibrium processes, expected variations between sulfur isotopes can

be described by $\delta^{33}S \approx 1/2 \cdot \delta^{34}S$ and $\delta^{36}S \approx 2 \cdot \delta^{34}S$ (Hulston and Thode, 1965). In the geological record, mass-dependent fractionations of sulfur isotopes can be predictably described by the fractionation array given by $\delta^{33}S \approx 0.515 \cdot \delta^{34}S$ (and $\delta^{36}S \approx 1.90 \cdot \delta^{34}S$): the "terrestrial mass fractionation array", which represents an average of mass-dependent fractionations found to occur on Earth. Because of the dependence of isotopic fractionations between two species of sulfur, i and j (e.g., sulfate, sulfide), on the natural logarithm of the fractionation factor α, mass-dependent fractionations between ^{33}S and ^{34}S isotopes can be expressed as (IAEA, 2000):

$$\theta_{ij} = \ln(^{33}\alpha_{ij}) / \ln(^{34}\alpha_{ij})$$

Equilibrium mass-dependent fractionations produce θ values in the range of 0.514 to 0.516 for $^{33}S/^{32}S$ and $^{34}S/^{32}S$ (Farquhar et al., 2003), while fractionations arising from unidirectional or physical processes produce values of θ that are more variable, falling between 0.500 and 0.516 (Craig, 1968; IAEA, 2000; Young et al., 2002).

Mass-dependent sulfur fractionations can also be described by λ, defined by the relationship between the natural logarithm of sulfur isotope compositions for two reservoirs of sulfur. For the product and reactant of sulfate reduction, this yields:

$$^{33\text{-}34}\lambda_{H2S\text{-}SO4} = (\delta^{33}S'_{H2S} - \delta^{34}S'_{SO4}) / (\delta^{33}S'_{H2S} - \delta^{34}S'_{SO4})$$

where $\delta^{3X}S' = 1000 \ln (1 + \delta^{34}S/1000)$ [Hulston and Thode, 1965].

In most cases, λ and θ are equal (e.g., Angert et al., 2003), with values between 0.5146 and 0.5150 for sulfur isotope exchange betweeen H_2S and SO_4^{2-} in the 0-100°C temperature range (Farquhar et al., 2003).

1.1.2 Mass-independent fractionation of sulfur isotopes

Processes that deviate from the expected mass-dependent variations are said to

lead to “mass-independent fractionation” (MIF) and are characterized by $\Delta^{33}S$ and $\Delta^{36}S$ values that deviate from zero within a few percent (±0.2‰ for $\Delta^{33}S$ and ±0.4‰ for $\Delta^{36}S$), where $\Delta^{33}S=\delta^{33}S-1000((1+ \delta^{34}S/1000)^{0.515}-1)$ and $\Delta^{36}S=\delta^{36}S-1000((1+ \delta^{34}S/1000)^{1.9}-1)$.

Our understanding of mass-independent fractionation of sulfur isotopes is incomplete at best, but known causes include photochemical reactions (photolysis of sulfur gases; e.g., Farquhar et al., 2001), photopolymerization of dimethyl sulfide (Colman et al., 1996; Zmolek et al., 1999) and hyperfine interactions in solid and liquid phases (Thiemens, 1999).

1.1.3 Fractionation in a closed system

An implicit condition of fractionation is that a reaction that occurs quantitatively will not lead to observable fractionation. An isotopic separation measurable at some intermediate point in the reaction will not be measurable once the reaction is complete, as all of the reactant will have been transformed into the product, with an isotopic composition identical to that at the start of the reaction. Thus fractionations arising from kinetic effects can be preserved only if a system is open, or if the reactions do not proceed to completion.

If the reservoir of a reactant is finite and the fractionation between the reactant and product is large, significant isotopic variation can arise from progressive fractionation processes. In such conditions, many of the equilibrium and kinetic fractionation processes can be described as Rayleigh distillation processes:

$$R=R_0 f^{(\alpha-1)}$$

where R_0 is the initial isotopic ratio when a fraction f of the initial amount of reactant available remains, and α is the fractionation factor (IAEA, 2000). In the delta notation

for sulfur isotopes, this yields:

$$\delta^{34}S = (\delta^{34}S_0+1000)f^{(\alpha-1)} - 1000$$

The Rayleigh distillation model is applicable to processes such as the precipitation of minerals from solution, precipitation of rain or snow, and the bacterial reduction of sulfate to sulfide (Seal, 2006).

The isotope effect of a given reaction or set of reactions in a closed system can be derived by comparing the initial isotopic composition of the reactant (δ_{ro}) to that of the remaining reactant (δ_{rf}) using the approximation discussed above ($\varepsilon=[\alpha-1]\bullet1000$):

$$\varepsilon=(\delta_{rf}-\delta_{ro})/\ln(1-f)$$

With this approximation (Mariotti et al., 1981), when the isotopic composition of the remaining reactant is plotted as a function of the logarithm of the remaining fraction (ln[1-f]), the value of ε, the enrichment factor, is given by the slope of the straight line. If fractionation is not constant for the duration of the reaction, a straight line will not be obtained.

1.2 The global sulfur cycle

Three major global reservoirs of sulfur can be identified in the modern sulfur cycle, these are: the reduced sulfide of sediments (mainly shales), the oxidized sulfate of evaporites and other sediments, and seawater sulfate (Holser et al., 1989; Schlesinger, 1991). The sulfur cycle is driven by transformations between the different valence states, which are accomplished in part through inorganic processes and in part through microbial activity. Microbial processes, including microbial sulfate reduction (Section 1.2.1.2), ensure that the cycle is completed by enabling the transformation of the oxidized sulfur back to its reduced forms.

The three global reservoirs and the interactions between them are illustrated in Figure 1.1. Weathering on the continents mobilizes the sulfur bound in pyrite minerals and evaporites, while river flow carries this sulfur to the oceans. During this process, reduced sulfur becomes oxidized to sulfate, the thermodynamically-stable form of sulfur in our oxidizing atmosphere. The fate of marine sulfate is then either to be precipitated as sulfate minerals in evaporite deposits (mainly anhydrite, $CaSO_4$, and gypsum, $CaSO_4 \cdot 2H_2O$), or reduced by biological processes and subsequently deposited as pyrite in marine sediments (Holser et al., 1989). Recrystallization of sulfate can result in a small fractionation of ≈1.3‰, which can usually be ignored, as the $\delta^{34}S$ values of marine evaporite rocks have been found to approximate that of the seawater brine from which they crystallized because seawater brine in marine evaporite basins is dominated by inflowing marine sulfate (Holser et al., 1989; Claypool et al., 1980).

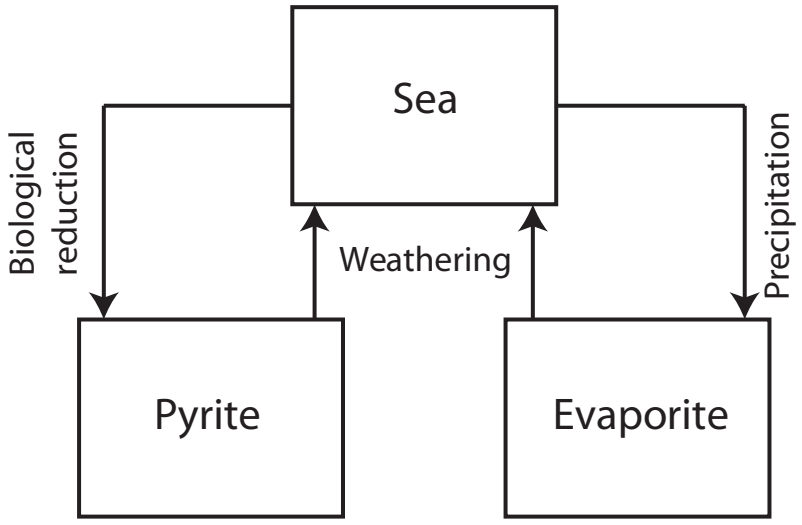

Figure 1.1: Simplified box model of the sulfur cycle. After Holser et al. (1989).

The concentration of sulfate in the oceans is currently in the order of 28 mM (2712 mg/kg; Holland, 1978), making it the third ion in importance in ocean water after sodium and chloride. Marine sulfate and sulfur mobilized and oxidized during weathering can also be recycled directly to the atmosphere in the form of sulfate aerosols, “sea spray” (Brimblecombe et al., 1989). Ocean-to-atmosphere transfer mechanisms also include

the production of biogenic gases, volcanic eruptions and the release of S compounds at hydrothermal vents. Without the current anthropogenic input to the sulfur cycle, with anthropogenic S emissions at present accounting for approximately 55% of the total sulfur input to the continental atmosphere (Brimblecombe et al., 1989), net transport of sulfur would occur from sea to land (Brimblecombe et al., 1989; Schlesinger, 1991). Two major aspects of the global sulfur cycle will be considered here in greater detail: these are microbial cycling (Section 1.2.1) and atmospheric cycling (Section 1.2.2).

1.2.1 Microbial cycling of sulfur

Sulfur is required by living systems and can be found in a wide variety of compounds, only few of which are considered to be necessary for normal cell function. Some examples are the amino acids cysteine and methionine, glutathione, thiamine, vitamin B, biotin, ferrodoxin, lipoic acid, and coenzyme A (Krouse et al., 1991). Sulfur constitutes on average ≈1% of the dry mass of living organisms and is mainly found in its reduced state (-2), while accessible sulfur in the planet's oxidizing environment is found mostly in its oxidized form (+6). This entails that organisms must first reduce sulfur before it can be incorporated into cellular organic compounds. This is accomplished via assimilatory sulfate reduction, a metabolic pathway that represents an overall loss of energy, in contrast to dissimilatory sulfate reduction, which is an energy-yielding process.

The biological dissimilatory sulfate reduction of sulfate to sulfur, a key step in the global sulfur cycle, is carried out by anaerobic sulfate-reducing bacteria (Roy and Trudinger, 1970) and one group of archaea (Shen and Buick, 2004). The overall reaction for microbial sulfate reduction (MSR) can be expressed as:

$$SO_4^{2-} + CH_2O \rightarrow S^{2-} + CO_2 + 2H_2O$$

where CH_2O represents any degradable organic carbon and S^{2-} represents any completely reduced sulfide (Holser et al., 1989). This process can be thought of in terms of

a process similar to denitrification, with the SO_4^{2-} acting as an alternative electron acceptor during the oxidation of organic matter. The term “dissimilatory” implies that the sulfate is not used as a nutrient by the microbes carrying out the reaction, but rather as a means of obtaining the necessary energy for metabolic functions. From this point on, the expression “sulfate reduction” will be used solely to refer to the metabolism dissimilatory sulfate reduction.

In coastal marine sediments, the importance of bacterial sulfate reduction is such that it is estimated to account for more than 50% of the total carbon mineralization on the ocean floor (Jørgensen, 1982; Canfield, 1993). MSR has an influence on the pyrite content of sedimentary rocks and the fate of organic matter in sedimentary basins, and thus ultimately on the redox conditions of the atmosphere, hydrosphere and lithosphere. Without MSR, some types of mineral deposits would not form and the mineral assemblage landscape would be dramatically different.

1.2.1.1 Antiquity of microbial sulfate reduction

Sulfate reducers are widely distributed in anaerobic terrestrial and oceanic environments and, as a group, can withstand a wide range of ecological conditions, from very cold (e.g., Isaksen and Jørgensen, 1996) to very hot (e.g., Jørgensen et al., 1992). Sulfate reducers are also phylogenetically diverse, with some groups branching very early in the Tree of Life (e.g., Stackebrandt et al., 1995) and perhaps representing some of the very earliest life forms to have appeared on Earth, as the early Archaean oceans would have been dominated by anaerobic microbes (Knauth, 2005). Thus, understanding how the sulfate reduction metabolism evolved, and how it functions, can help us understand the conditions prevailing on early Earth.

Evidence of early sulfate reduction is found mostly in the form of characteristic sulfur stable isotope signatures in rocks and sediments, as molecular markers of sulfate

reduction do not survive geological conditions in any recognizable form, and fossils of early sulfate-reducers would not be morphologically-distinct enough to tell apart from those of other microorganisms (Shen and Buick, 2004). During MSR, the reactant sulfate is depleted in the lighter isotope of sulfur ^{32}S (and enriched in the heavier isotope ^{34}S), while the product sulfide is enriched in ^{32}S (and depleted in ^{34}S). Similar levels of fractionation as those resulting from MSR can be accomplished through the abiological reduction of sulfates, termed "thermochemical sulfate reduction", but this process is understood to take place only at high temperatures (80-100°C < T < 150-200°C), beyond those in which sulfate reducers are able to metabolize (Machel et al., 1995). As a result, significant depletions of sedimentary sulfides in ^{34}S relative to coeval sulfate from low-temperature deposits are a powerful proxy for the involvement of microbial sulfate reduction in sulfur cycling.

Currently, MSR is known to be accomplished by five phylogenitically-distinct groups of microbes: archaea of the genus *Archaeoglobus* (hyperthermophilic: >70°C), the hyperthermophilic genus of bacteria *Thermodesulfobacterium*, the genus *Thermodesulfovibrio* of the Nitrospirae phylum (thermophilic: 40-70°C), the genera *Desulfotomaculum* and *Desulfosporosinus* of the Firmicutes, and several genera of Proteobacteria, including the thermophilic genus *Thermodesulforhabdus* and several mesophilic (15-45°C) genera, including the common genus *Desulfovibrio* (Shen and Buick, 2004).

Leaving aside some of the complicating effects of mass-independent fractionation (Farquhar et al., 2008), some of the oldest terrestrial S-isotopic records suggestive of MSR have been found in the banded iron formations of the Isua supracrustal rocks of West Greenland (>3.7 Ga; Monster et al., 1979) and show the narrow range of $\delta^{34}S$ values characteristic of rocks of Archaean age (e.g., Anbar and Knoll, 2002). In sedimentary sulfides younger than 2.8 Ga, however, for example in those of the Michipicoten and Woman River Iron formations of Canada (Goodwin et al., 1976), sulfide

$\delta^{34}S$ values are distinctly shifted towards negative values, with fractionation relative to coeval sulfates in the order of the tens of per mil (e.g., Kakegawa et al., 1999; Grassineau et al., 2000). This has been interpreted as strong evidence that MSR had evolved by 2.7 Ga. Large fractionations (40-45‰), which are typical of MSR in non-limiting sulfate conditions, (Shen and Buick, 2004) are found in the rock record from 2.3 Ga and could indicate an increase in oceanic sulfate concentrations resulting from increased atmospheric oxygen content (Cameron, 1982). This record of large fractionations extends continuously from 1.0 Ga, suggesting that today's complex modern sulfur cycle was fully established by this time (Canfield and Teske, 1996) [Figure 2].

The low S fractionations recorded in ancient Archaean rocks have been attributed to either MSR in limiting sulfate conditions, implying that the oceans had not yet fully oxygenated, or to sulfides of abiological origin, implying that MSR had not yet evolved (Cameron, 1982; Walker and Brimblecombe, 1985; Habicht et al., 2002; Canfield et al., 2000). Before the establishment of the oxygenic weathering cycle (≈2 Ga), sulfate could be provided in small amounts by volcanic activity, through the oxidation of volcanic and volcanogenic sulfur gases (Perry et al., 1971; Walker and Brimblecombe, 1985). An alternate hypothesis has been put forth and maintains that atmospheric oxygen reached present-day levels by 3.8 Ga, its presence persisting until now (Ohmoto et al., 1993; Ohmoto, 1997), but our current understanding of isotopic fractionation during MSR does not appear to support this view (e.g., Shen and Buick, 2004). If the modern ocean is rich in sulfates, sulfate concentrations in the Archaean oceans were probably very low, increasing with the rise of oxygenic photosynthesis, but likely remaining below 1 mM levels until ≈2.3 Ga (Canfield and Raiswell, 1999). Some Archaean environments may have been sulfate-rich, as indicated by the precipitation of evaporitic sulfate minerals (e.g., Buick and Dunlop, 1990). These sulfates may have originated from the anoxygenic phototrophic oxidation of mantle-derived sulfide (Canfield and Raiswell, 1999) or the hydrolysis of volcanogenic SO_2 from relatively

oxidized magmas (Hattori and Cameron, 1986).

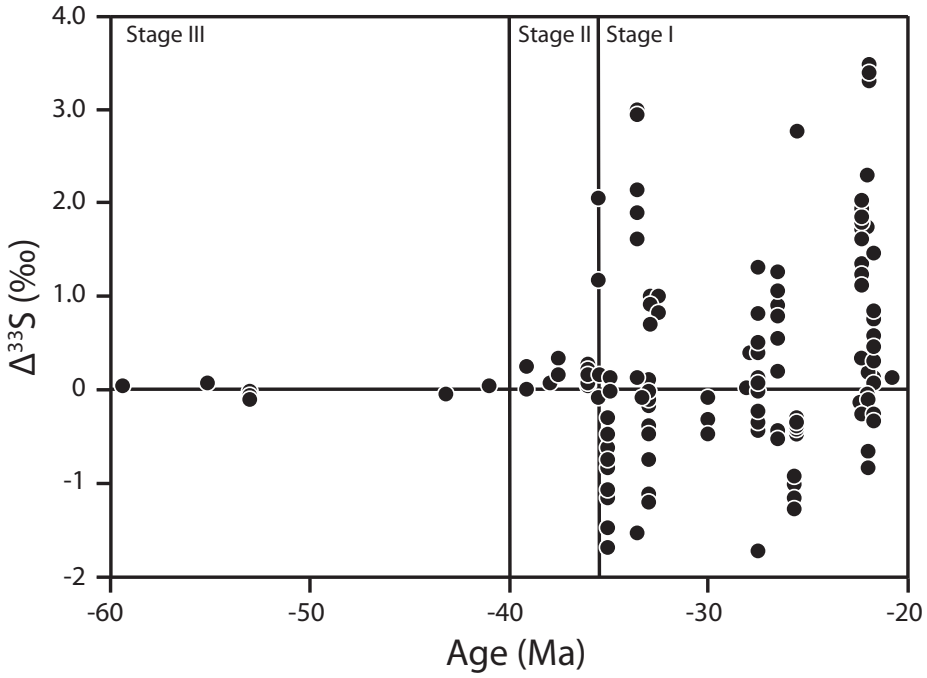

Figure 1.2: Plot of $\Delta^{33}S$ versus age (Ma), showing variability the Earth's sulfur stable isotopic composition record: Stage I is characterized by variable $\Delta^{33}S$ and interpreted to represent a period of Earth history with low atmospheric oxygen concentration. Stage II is thought to represent a transition stage, with more subdued $\Delta^{33}S$ values arising from the onset of oxidative weathering. Stage III has been interpreted to indicate the absence of photolysis reactions involving sulfur oxide gases due to high atmospheric oxygen concentrations. After Farquhar and Wing (2003).

Sulfur-based metabolism, sulfate reduction included, may be the earliest metabolism used by archaea, which would imply that archaea must have preceded eubacteria in the phylogenic evolutionary tree (Achenbach-Richter et al., 1987; Woese, 1987). In modern times, hypothermophilic sulfate-reducing bacteria can be isolated from hot springs containing reduced sulfur in significant amounts (Zeikus et al., 1983). This suggests that conditions prevailing on Earth when the sulfate-reduction metabolism appeared were similar to those observed in these environments. Futhermore, the fact that the deepest-branching sulfate-reducers (of the genus *Thermodesulfobacterium*) are hypothermophilic, with a temperature maximum of 85°C, may be indicative of higher ocean temperatures during the Archaean, when the earliest biogenic sulfide

deposits could have formed (Stackebrandt et al., 1995). Recent sulfur isotopic data from barite deposits in North Pole, Australia, indeed suggest that sulfate-reducers can be traced back to ≈3.5 Ga (Shen et al., 2001), but whether the small fractionations observed in these early Archaean deposits are indeed indication of biological implication remains controversial.

1.2.1.2 Microbial sulfate reduction metabolism

The metabolism of microbial sulfate reduction has been extensively studied over the last several decades, with fractionation experiments conducted as early as in the 1950s (e.g., Thode et al., 1951; Harrison and Thode, 1958). Early models of the MSR metabolism assumed that the reactions involved in the reduction of sulfate to sulfide were first-order with respect to the concentration of sulfur species (e.g., Harrison and Thode, 1958). The later Rees model (Rees, 1973), however, used zero-order kinetics to explain the isotopic fractionation of sulfur stable isotopes during sulfate reduction by *Desulfovibrio desulfuricans*. More recent studies have expanded on this model and revised the expected sulfur fractionation thresholds associated to MSR (Brunner and Bernasconi, 2005; Brunner et al., 2005). These are discussed below.

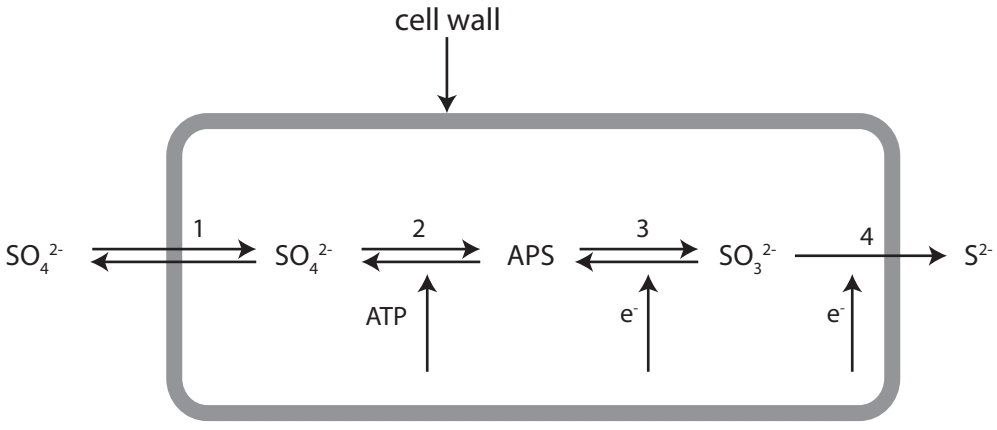

Figure 1.3: Model for microbial sulfate reduction (Rees, 1973). Modified from Shen and Buick (2004).

In the Rees (1973) model, the first step (step 1, Figure 1.3) of the obligately anaerobic sulfate reduction metabolism is the active uptake of the sulfate ion across the cell wall. This fully reversible step (Cypionka, 1989; Warthmann and Cypionka, 1990; Kreke and Cypionka, 1995) occurs via an electroneutral proton-anion symport driven by the pH gradient across the membrane (Cypionka, 1987). It has been shown that in the absence of a natural proton gradient, the entry of sulfate into the cell is severely limited, but some strains are apparently able to self-generate such a gradient by pumping protons across the cytoplasmic membrane (Fitz and Cypionka, 1989). The strain *Desulfovibrio vulgaris*, for example, has been shown to generate a proton gradient by vectorial proton translocation across the cytoplasmic membrane and by extracellular proton release, this via a periplasmic hydrogenase enzyme (Fitz and Cypionka, 1991).

For most freshwater species, sulfate is taken up in the form of undissociated sulfuric acid, while for marine species, protons are replaced by sodium ions to balance the negative charge of sulfate (Cypionka, 1987; 1989; Warthmann and Cypionka, 1990; Stahlmann et al., 1991). Once the sulfate ion has entered the cell, it reacts with adenosine triphosphate (ATP) to form adenosine-5'-phosphosulfate (APS) - the enzyme ATP sulfurylase is involved in this activation step (step 2). The reduction of APS to sulfite (step 3) is then catalyzed by the enzyme APS reductase. The final reduction of sulfite to sulfide is mediated by the enzyme sulfite reductase (step 4). It is yet unclear whether this last step involves a single, direct, 6-electron reduction mechanism, or whether sulpihte is reduced via intermediate (thiosulfate and trithionate) compounds (Kobayashi et al., 1974; Chambers and Trudinger 1975; Fitz and Cypionka, 1989; 1990; Brunner and Bernasconi, 2005). The reduced sulfide sulfur exits the cell through passive diffusion in the form of hydrogen sulfide (step 4). At least in the case of the $2H^+/SO_4^{2-}$ symport found in freshwater species, this results in an overall electroneutral cellular uptake mechanism, with two protons entering the cell during the uptake step and two protons exiting the cell with the reduced sulfur (Cypionka, 1987).

The ability of sulfate-reducing microorganisms to accumulate internal sulfate to concentrations far exceeding those in the outside environment has been clearly demonstrated. This process results in alkalinization of the growth medium without sulfide production, and can lead to up to several thousand-fold sulfate accumulations (e.g., Cypionka, 1987; 1989). Experiments suggest that sulfate accumulation is greatest after growth in sulfate-limiting conditions (Warthmann and Cypionka, 1990) and that it is a function of the transmembrane proton gradient, thus becoming severely inhibited at high pH, perhaps as a result of the disappearance of a natural proton gradient between the environment and the cytoplasm (Cypionka, 1989). There is evidence that at least some strains of sulfate-reducing microbes possess two distinct sulfate accumulation mechanisms, each with different energy requirements (Cypionka, 1989; Warthmann and Cypionka, 1990): a low-accumulation system with $3H^+$ taken for every sulfate anion would be used at high sulfate concentrations, regulated to avoid unnecessary energy-spoiling accumulation, while a high-affinity accumulation system with $2H^+$ per sulfate anion would be favoured in sulfate-limiting conditions. The latter may represent a survival mechanism developed in response to prolonged exposure to low sulfate concentrations (Warthmann and Cypionka, 1990; Kreke and Cypionka, 1992).

Isotopes effects during the microbial reduction of sulfate to sulfide arise from the reactions that involve the breaking of S-O bonds, thus from steps 3 (the conversion of APS to sulfite), and 4 (the reduction of sulfite to sulfide) in the Rees model (Figure 1.3). An approximate value of a 25‰ depletion in ^{34}S relative to the source of sulfate was originally assigned to each of these steps, while sulfate uptake was associated to a reverse effect, with enrichment in ^{34}S by 3‰ (Rees, 1973). This assumption was based on the hypothesis that the isotope effects associated with the backward reaction of steps 3 and 4 are close to zero because they involve the oxidation of sulfur or reactions where the oxidation state of sulfur is not changed. The inverse isotope effect for the uptake of the sulfate ion into the cell was explained by the favouring of

the sulfate ion with ^{34}S compared to ^{32}S. Restrictions to the validity of the Rees model included the following: 1) the uptake of sulfate is independent of sulfate concentration at high sulfate concentrations, 2) the flow between the external sulfate and the internal sulfite is reversible, 3) measurements of isotope effects are made when the bacterium is operating in the steady-state regime to allow sulfate concentrations to reach limiting conditions, and 4) the hydrogen sulfide product is sampled when the system has reached steady-state. The results of the studies presented in Chapter 3 suggest that the uptake of sulfur inside the cell is indeed associated to low fractionation, but that its direction is the same as that of subsequent metabolic steps (preferential uptake of light sulfur).

A perceived short-coming of the Rees model has been that the maximum level of fractionation it allows (≈46‰) fails to explain the discrepancy with modern microbial sulfide deposits (70‰). A later model (Brunner and Bernasconi, 2005) suggested that these larger fractionations could indicate the alternate pathway proposed by Rees (1973) in the sulfate reduction metabolism, one that would see the sulfite-to-sulfide reduction taking place in multiple steps instead of a single 6-electron step. Studies conducted using ^{35}S-labelling support the single-step theory (Chambers and Trudinger, 1975), but others show that intermediates such as thiosulfate and trithionate can be produced (e.g., Kobayashi et al., 1974; Fitz and Cypionka, 1990). A revised version of the Rees model (Brunner and Bernasconi, 2005) holds that intermediates are indeed formed during the reduction of sulfite to sulfide (step 3). The proposed trithionate pathway involves three reactions: 1) the formation of trithionate from three sulfite molecules, a step mediated by the enzyme sulfate reductase, 2) the formation of thiosulfate and sulfite by the enzyme trithionate reductase, and 3) the formation of sulfide and sulfite by thiosulfate reductase (Cypionka, 1995). This revised model suggests that the maximum isotopic fractionation associated to steps 3 and 4 as defined by Rees (1973) [Figure 1.3] represents the minimum fractionation possible rather than

the maximum. Thus, the theoretical maximum for sulfur isotopic fractionation during microbial sulfate reduction should be revised to approximately 70‰, in accordance with the maximum observed in modern sulfide deposits (Brunner and Bernasconi, 2005), instead of the upper limit of 46‰ proposed by Rees (1973) and reproduced in laboratory experiments. Before the publication of the results of a recent study that demonstrated the possibility of >46‰ fractionations in laboratory conditions (Sim et al., 2011), it had been hypothesized that the full range of isotopic fractionation required combined hypersulfidic and substrate-limiting conditions at a non-limiting supply of sulfate (Wortmann et al., 2001; Brunner and Bernasconi, 2005), or additional fractionation during the extracellular oxidative sulfur cycle (Canfield and Thamdrup, 1994). A possible alternate explanation for the previous absence of high fractionations in laboratory experiments is that the sulfate reduction pathway must be operating in a highly reversible manner in order for the full isotope effects to be expressed, a condition that approaches equilibrium conditions between sulfate and sulfide and is thus difficult to attain (Sim et al., 2011; Brunner and Bernasconi, 2005).

1.2.1.3 Sources of sulfur fractionation during microbial sulfate reduction

A number of biological, chemical and physical variables have been found to influence the extent of kinetic fractionation processes taking place during MSR and in the past few decades, an impressive body of research has been dedicated to studying, either in natural settings or in laboratory conditions, the effect of these environmental factors on S isotope fractionation. These variations as a function of environmental conditions arise from biological, chemical, and physical factors, and are discussed below.

1.2.1.3.1 Biological factors

Biological factors known to affect sulfur fractionation during MSR include phylogeny (genetic differences between species), enzymatic differences, and carbon oxidation

pathway. Phylogeny may play a role in the fractionation of S-isotopes during bacterial sulfate reduction insofar as it reflects different metabolic characteristics (Brüchert et al., 2001) and thus physiological differences (Widdel and Hansen, 1992). These may include differences in cell membrane composition, structural differences between APS and dissimilatory sulfite reductase enzymes, the use of different enzymes in the electron transport chain, and varying capacity in terms of substrate use (Hansen, 1994). Genetic evidence for the existence of different APS reductases and dissimilatory sulfite reductases in sulfate-reducing bacteria has been uncovered (Minz et al., 1999; Wagner et al., 1998) and different strains of sulfate-reducing bacteria may possess different cytochromes for the regulation of the electron flow from the organic substrate (Hansen, 1994). Enzymes with different structures would be expected to possess different activation energies, which may in turn influence the isotopic fractionation associated to each step in the sulfate-reduction metabolism (Brüchert et al., 2001). Additionally, the carbon oxidation pathway used for the oxidation of organic substrate during bacterial sulfate reduction may play a role in the fractionation of S isotopes, with its influence potentially related to the energy yield associated to the organic substrate used (see Section 1.2.1.3.2).

The microbial metabolism of a given substrate can involve complete or incomplete oxidation. Acetate is a common product of the incomplete oxidation of some fatty acids whereas complete oxidation yields CO_2 as a product (Hansen, 1994). The term “complete oxidizer” is generally used to refer to sulfate reducers that are able to oxidize the C_2-unit of acetyl-CoA to CO_2, but acetate can nevertheless be excreted in considerable amounts during growth (Hansen, 1994). Differences in fractionation between pathways can be rationalised in terms of the energy conserved during the oxidation of the organic substrate: more energy is conserved per mole of sulfate for incomplete oxidation compared to complete oxidation (Detmers et al., 2001). For example, complete oxidation of acetate to CO_2 yields three times less energy than the incomplete

oxidation of lactate to acetate (Detmers et al., 2001). An extensive study of 32 strains of sulfate-reducing microbes showed that while all strains discriminated against ^{34}S, the largest fractionations were observed with complete oxidizers, which fractionated between 15.0‰ and 42.0‰, while for the acetate-excreting incomplete oxidizers fractionations were between 2.0‰ and 18.7‰ (Detmers et al., 2001). In a similar study, it was found that complete oxidizing strains fractionated sulfur to a greater extent (13-22‰) than incomplete oxidizing strains (4.6-10‰) [Brüchert et al., 2001].

The nature of the substrate used for MSR also appears to have an effect on the extent of fractionation with, for example, MSR using lactate rather than acetate leading to smaller fractionations (Brüchert et al., 2001).

Very few studies have investigated the role played by enzymes involved in the sulfate reduction metabolism and its subsequent influence on the extent of fractionation. However, the role of the enzyme dissimilatory sulfite reductase, which mediates the last reduction step of APS to sulfite, has been investigated in experiments where nitrite – an inhibitor of this enzyme – was added. The results indicate that sulfate reduction is in part regulated by kinetic conversions during the metabolism: without nitrite to inhibit the enzyme's activity, fractionation is low, indicating fast sulfite-to-sulfide reduction, but with nitrite, the reaction rate associated to the enzyme becomes the rate-limiting step (Mangalo et al., 2008; Brunner and Bernasconi, 2005).

1.2.1.3.2 Chemical factors

Type of electron donor - substrate type

As a group, sulfate-reducers are very versatile in the variety of electron donors they can couple to the reduction of sulfate. At least 125 compounds have been identified as usable electron donors in studies using pure cultures of sulfate reducers (Hansen, 1993), most of which are typical fermentation products and intermediate metabolic

compounds, such as amino acids, fatty acids, and glycerol. This versatility likely stems from the necessity, in natural environments, to adapt to varying conditions in substrate composition and availability. Although acetate and lactate are most frequently used for bacterial growth in microcosm experiments, a variety of other fatty acids can serve as electron donors. For example, low molecular weight fatty acids appear to be the preferred substrate in saline sediments (acetate, butyrate and propionate, together with hydrogen; Sørensen et al., 1981), perhaps because they are natural products of the anaerobic fermentation of organic matter in natural environments (Trudinger, 1992). Ethanol and a number of petroleum hydrocarbons have also been used successfully as a source of carbon in laboratory experiments. Growth using organic matter as the electron donor is heterotrophic, but some sulfate reducers can grow autotrophically using H_2.

An effect of carbon substrate type on sulfur stable isotope fractionation would be expected from its relationship with sulfate reduction rates (Kaplan and Rittenberg, 1964; Kemp and Thode, 1968), as these may depend on the quantity and quality of the organic matter available for oxidation (Westrich and Berner, 1984). The oxidation pathway - complete or incomplete - and the free energy change associated with the oxidation of electron donors are also likely key factors in determining sulfate reduction rates, and by extension the extent of fractionation (Hansen, 1994; Widdel and Hansen, 1992): more negative free energy changes tend to be associated to lower fractionations (e.g., lower fractionations with lactate compared to acetate; Kaplan and Rittenberg, 1964; Brüchert et al., 2001; Detmers et al., 2001) [Table 1]. Furthermore, acetate, which is likely a key substrate in natural settings, has received relatively little attention (Canfield, 2001). The underlying causes for the link between free energy change and isotope fractionation remains unclear (Detmers et al., 2001), but there is evidence that any electron donor effect on fractionation may not be due solely to ensuing changes in sulfate reduction rates. The mechanism of sulfur isotope fraction-

ation remains unclear, and the relationship between substrate type and the extent of fractionation is complex. Investigations at the enzymatic level may be necessary to fully understand the mechanism of S isotope fractionation during bacterial sulfate reduction.

Table 1.1: Free energy changes at standard state ($\Delta G^{0'}$) and corresponding range of isotope fractionations (ε) during dissimilatory sulfate reduction with various electron donors for complete and incomplete oxidation (from Detmers et al., 2001).

Electron donor (type of oxidation)	**Stoichiometry**	**$\Delta G^{0'}$ (kJ mol^{-1} SO_4^{2-})**	**ε (‰)**
Pyruvate (incomplete)	$4CH_3COCOO^- + 4H_2O + SO_4^{2-} \rightarrow 4CH_3COO^- + 4HCO_3^- + HS^- + 3H^+$	-340.9	8.1
Lactate (incomplete)	$2CH_3CHOHCOO^- + SO_4^{2-} \rightarrow 2CH_3COO^- + 2HCO_3^- + HS^- + H^+$	-160.1	2.0-17.0
Hydrogen	$4H_2 + SO_4^{2-} + H^- \rightarrow 4H_2O + HS^-$	-152.2	14.0
Formate	$4HCOO^- + SO_4^{2-} + H^+ \rightarrow 4HCO_3^- + HS^-$	-146.9	5.5
Ethanol (incomplete)	$2CH_3CH_2OH + SO_4^{2-} \rightarrow 2CH_3COO^- + HS^- + 2H_2O + H^+$	-146.6	18.7
Pyruvate (complete)	$4CH_3COCOO^- + 4H_2O + 5SO_4^{2-} \rightarrow 12HCO_3^- + 5\,HS^- + 3H^+$	-106.3	16.1; 25.7
Proprionate (imcomplete)	$4CH_3CH_3COO^- + 3SO_4^{2-} \rightarrow 4CH_3COO^- + 4HCO_3^- + 3HS^- + H^+$	-50.2	5.5; 6.8
Benzoate (complete)	$C_7H_5O_2^- + 3.75SO_4^{2-} + 4H_2O \rightarrow 7HCO_3^- + 3.75HS^- + 2.25H^+$	-49.7	15.0-42.0
Butyrate (complete)	$CH_3CH_2CH_2COO^- + 2.5SO_4^{2-} \rightarrow 4HCO_3^- + 2.5HS^- + 0.5H^+$	-49.2	23.1-32.7
Acetate (complete)	$CH_3COO^- + SO_4^{2-} \rightarrow 2HCO_3^- + HS^-$	-47.6	18.0-22.0

A limited number of organic substrates have been investigated in both pure and enrichment cultures of sulfate-reducing bacteria in comparison to the variability occurring in natural environments and very few studies have investigated the effect of organic substrate concentration on S isotope fractionation. In most studies investigating S-isotope fractionation during bacterial sulfate reduction, organic substrate is provided in excess. In natural environments, however, sulfate-reducers may experience organic substrate limitation (Isaksen et al., 1994; Sagemann et al., 1998). Experimental evidence suggests that when an organic substrate becomes limiting, sulfur is increasingly found in intermediate species (Cypionka, 1995), increasing the likelihood of back

reactions from intermediates to sulfite occurring, and effecting a change in isotope fractionation (Chambers et al., 1975; Fitz and Cypionka, 1990). Substrate limitation, combined with excess sulfate and hypersulfidic conditions, may explain some of the fractionations in nature greater than the 46‰ value reported in most experiments with pure cultures (Brunner and Bernasconi, 2005), although a recent study has shown that these conditions are not necessary to generate larger fractionations (Sim et al., 2011).

Sulfate availability

An obvious prerequisite of MSR is presence of sulfate in sufficient quantity, but sulfate reduction has been demonstrated to take place at even minute concentrations of sulfate (<50 μM; e.g., Habicht et al., 2002). A consistent relationship has been found between level of fractionation and sulfate concentration, this both in pure and enrichment cultures. At low (limiting) sulfate concentrations, fractionations are generally small (<10‰; Habicht et al., 2002), while high fractionations (up to 50‰; Harrison and Thode, 1958; Habicht & Canfield, 1996; Canfield et al., 2000; Canfield, 2001) are reported at non-limiting concentrations. As a general rule, fractionation increases with increasing sulfate concentration in sulfate-limiting conditions, but appears to be uncorrelated to sulfate concentration in non-limiting conditions (e.g., Harrison and Thode, 1957; Chambers et al., 1975; Kaplan and Rittenberg, 1964; Kemp and Thode, 1968; Habicht and Canfield, 1997; Canfield, 2001). A possible explanation for this apparent first-order dependence of S-isotope fractionation on sulfate concentration is that when sulfate becomes limiting, sulfate-reducers must actively pump sulfate into the cell, which reduces the free exchange of sulfate in and out of the cell. The energy increase associated to active uptake leads to a reduction in growth yield; to maintain energy for growth, specific sulfate reduction rates are increased, which in turn leads to lower fractionations (Habicht et al., 2005) as sulfate is processed rapidly within the

cell. There may also be a link with the high-accumulation mechanism of sulfate uptake described in some strains of sulfate reducing bacteria (Kreke and Cypionka, 1992).

Environmental pH

Until recently, the vast majority of isolated strains of sulfate reducing bacteria were neutrophilic (preferring pH 6-9) and it was thought that communities of sulfate-reducers in acidic environments (e.g., acid mine drainage environments) were not genetically diverse (Kolmert and Johnson, 2001). It is now recognized that the biodiversity of these environments may be considerable (Johnson, 2000). If many bacteria species in these environments are neutrophilic but acid-tolerant and thus able to survive and metabolise at low pH, truly acidophilic strains would be expected to be present as well. Recently, such bacteria have been isolated from acid mine drainage-impacted sites and geothermal environments: grown in laboratory media, these were shown to conduct sulfate reduction at pH values as low as 3 (Sen and Johnson, 1999; Senko et al., 2009). Acidic waters often contain excess sulfate and dissolved metals. Additionally, they are often-carbon limited (Koschorreck, 2008). As sulfate reduction is a proton-consuming reaction, the potential free energy associated to the reaction increases with lower pH, creating an energetic advantage to sulfate reduction at low pH (Koschorreck, 2008). Very few studies, if any, have investigated the effect of pH on isotope fractionation during microbial sulfate reduction. In fact, most sulfate reduction studies have investigated neutrophilic strains of sulfate-reducers at either near-neutral or optimum pH values, and those that have attempted to investigate sulfate reduction at low pH have not considered isotopic fractionation. Thus at the present time, information on the effect of pH on the fractionation of sulfur stable isotopes during bacterial sulfate reduction is inadequate. Considering the acidic and reducing conditions that are thought to have prevailed during the Archaean, investigating sulfur fractionation by acidophilic or acidotolerant strains of sulfate-reducers at low pH may help understand

the large range of sulfur fractionation observed in biogenic sulfide deposits. There is evidence that cells can accumulate sulfate internally in concentrations significantly higher than those present in the environment and that at least some sulfate reducers possess two distinct accumulation systems (e.g., Warthmann and Cypionka, 1990; Kreke and Cypionka, 1992), which could play a role in determining the overall fractionation of sulfur between the sulfate and sulfide fractions. Chapter 3 presents the results of a series of experiments designed to investigate the fractionation of sulfur isotopes during MSR by two strains of acid-tolerant sulfate reducers. One goal of the study was to determine whether pH exerts an an effect on the level of fractionation taking place during MSR. Additional objectives were to determine the level of fractionation associated to MSR by acid-tolerant sulfate-reducing bacteria.

1.2.1.3.3 Physical factors

Sulfate reduction rate

There is evidence suggesting that a link between sulfate reduction rates and sulfur isotope fractionation exists. This inverse relationship of fractionation increasing as sulfate reduction rates decrease - and vice versa - has been reported in a number of earlier studies (Harrison and Thode, 1958; Kaplan and Rittenberg, 1964; Chambers et al., 1975) as well as in recent publications (Habicht and Canfield, 1997; Canfield, 2001; Brüchert et al., 2001). However, detailed studies of S-isotope fractionation over a wide range of sulfate reduction rates found no correlation between fractionation and reduction rate (Canfield and Teske, 1996; Rudnicki et al., 2001; Farquhar et al., 2008). It has been suggested that when sulfate reducers are grown in optimal conditions, isotope fractionation is independent of sulfate reduction rates (Bolliger et al., 2001; Detmers et al., 2001). Phylogenetic differences may play a more important role than sulfate reduction rate in determining the level of sulfur fractionation (Brüchert et al., 2001).

Sulfate reduction rates may also depend on the concentration of dissolved sulfate, but experiments suggest that the rate of sulfate reduction is independent of the concentration of dissolved sulfate until low concentrations (< 3 mM) are reached (Boudreau and Westrich, 1984; Ingvorsen et al., 1984; Ingvorsen and Jørgensen, 1984; Habicht et al., 2002). A link between sulfate reduction rate and temperature has also been suggested, although sulfate reduction signatures appear to deviate from equilibrium considerations, suggesting that they are independent of temperature (Johnston et al., 2007) within an organism's tolerance range. The apparent inverse relationship between isotope fractionation and sulfate reduction observed may arise from the influence of the specific sulfate-reduction rate on the exchange of sulfate across the cell membrane, and on the reversibility of each step in the metabolism of sulfate reduction (Canfield, 2001). As such, the extent of isotope fractionation rate may be correlated with the specific rate of sulfate reduction, but not the absolute rate, which may serve to explain discrepancies in reported results. Cell-specific rates of sulfate reduction (csSRR) are calculated as a function of cell density, and are represented by dividing the sulfate reduction rate by the cell density in the culture. Specific rates of sulfate reduction are more easily obtained in controlled growth media.

Temperature

Temperature has the potential to influence S-isotope fractionation through its effect on membrane fluidity and its impact on the uptake of sulfate into the cell. At low temperatures, cell membrane fluidity may be reduced (Scherer and Neuhaus, 2002), leading to small fractionations (e.g., Kaplan and Rittenberg, 1964; Rees, 1973) resulting from reduced sulfate transport across the membrane. Higher temperatures within the organism's tolerance limit would likely facilitate sulfate transport by increasing membrane fluidity, and if sulfate concentrations are low, then sulfate transport across the membrane could become rate-limiting. Because only little fractionation is associ-

ated with this step (Rees, 1973; Chapter 3), the full extent of fractionation for subsequent steps in MSR would not be expressed and small overall fractionation would be expected. Temperatures exceeding optimal growth conditions may lead to reduced sulfate reduction rates due to damage to cell membranes and/or enzymes (Brüchert et al., 2001). These mechanisms would predict low fractionation at low and high temperatures, and high fractionation in the intermediate temperature range (Kaplan and Rittenberg, 1964). An influence of temperature on the extent of fractionation not necessarily following this model has been uncovered in a number of studies for some strains and some substrates (Habicht and Canfield, 1997; Brüchert et al., 2001; Canfield, 2001). However, other studies have found no consistent link between temperature and fractionation (Brüchert et al., 2001; Canfield, 2001; Rudnicki et al., 2001), suggesting that in natural populations at least, varying fractionation levels within a given microbial community may result more from differences between strains and optimal temperatures for MSR rather than a temperature effect. In pure cultures, the influence of temperature on fractionation may be dependent upon the exchange path for the reduction of sulfate to sulfide, more specifically: 1) the rate of sulfate transport in and out of the cell, and 2) the exchange of sulfur between sulfur pools internal to the organism, with different sulfate reducing populations balancing the importance of these two paths differently (Canfield et al., 2006). Possible confounding effects - both biological and chemical - may be at play.

1.2.1.4 Distinguishing between sulfur isotope signatures from multiple microbial metabolisms

By its significant (>50%) contribution to sedimentary organic matter respiration (Jørgensen, 1982), the microbial sulfate reduction metabolism was likely the major influence on the sulfur isotopic composition of biogenic sulfides throughout the planet's history. However, the microbial cycling of sulfur is accomplished via a variety of meta-

bolisms, yielding the potential for confounding sulfur isotopic signatures observed in sedimentary sulfides. Among these metabolisms is sulfur dispropornation, which uses a variety of intermediates (elemental sulfur, sulfite, and thiosulfate) and produces both oxidized (sulfate) and reduced sulfur species (hydrogen sulfide) [e.g., Bak and Pfennig, 1987; Canfield and Thamdrup, 1994; Habicht et al., 1998].

The different steps involved in each of these metabolic processes can impart differences in multiple isotope signatures (e.g., between ^{33}S and ^{34}S), which in turn allow their recognition. For example, with the disproportionation of elemental sulfur and thiosulfate, $^{33\text{-}34}\lambda_{H2S\text{-}SO4}$ values (see Section 1.2.1.4) generally lie above the equilibium fractionation line for H_2S and SO_4 (from 0.5145 to values greater than 0.5187), while for sulfate reduction values are found below this line (between 0.5103 and 0.5125; Figure 1.4; Johnston et al., 2005).

These measurable differences in the isotope signatures of sulfur metabolic pathways and their deviation from the equilibrium isotope exchange values for H_2S and SO_4 indicate that microbial sulfur metabolic processes cannot be approximated by equilibrium isotope exchange. This signifies that their implication in the formation of biogenic sulfides can often be evaluated through a close look at multiple sulfur isotope signatures (Johnston et al., 2005).

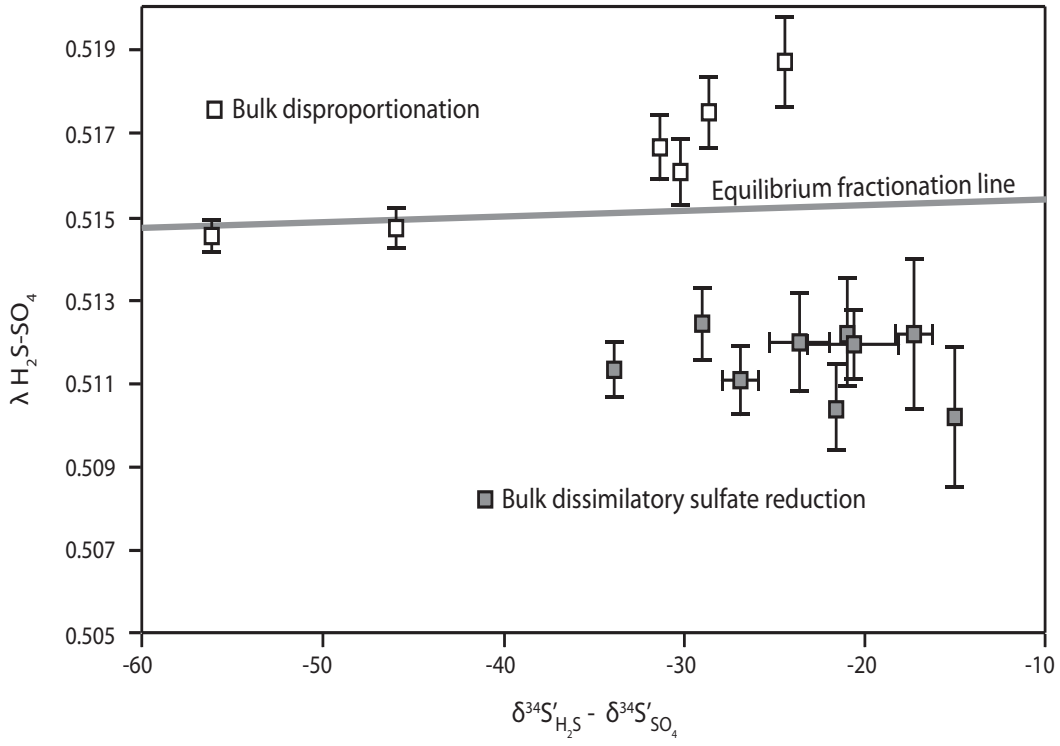

Figure 1.4: Plot of $\lambda_{H2S\text{-}SO4}$ versus $\delta^{34}S'_{H2S}$-$\delta^{34}S'_{SO4}$ from experiments with sulfate reducing microbes. The gray line represents equilibrium exchange between H_2S and SO_4 (from Johnston et al., 2005).

1.2.2 Atmospheric sulfur cycling

The atmosphere is a very mobile system in which most processes take place in no more than a few days. Sulfur enters the atmosphere in gaseous or particulate form from a variety of sources. The major natural fluxes influencing the global atmospheric sulfur budget are: i) biogenic emissions from coastal regions, the open ocean and land, ii) aeolian weathering of sulfates, iii) sea spray sulfate from the ocean, and iv) volcanic exhalations. Sulfur compounds in the atmosphere can occur in the gaseous, liquid, and solid phases. Reduced species released into the planet's oxidizing atmosphere are initially oxidized to sulfur dioxide (SO_2) and methane sulfonic acid (CH_3SO_3H or "MSA") [oxidation state +4], and ultimately to sulfuric acid (H_2SO_4, +6), the thermodynamically stable form of sulfur in the presence of oxygen.

1.2.2.1 Input of sulfur compounds from the atmosphere

Biogenic sources of sulfur are estimated to constitute as much as 50% of the total atmospheric sulfur burden (Kellogg et al., 1972; Ryaboshapko, 1983). Biogenic emissions - largely produced by vegetation and anaerobic respiration processes in anoxic environments - occur predominantly in the form of reduced sulfur. Plants can emit sulfur in the form of hydrogen sulfide (H_2S), dimethylsulfide (CH_3SCH_3, "DMS"), carbonyl sulfide (COS) and carbon disulfide (CS_2) (Aneja and Cooper, 1989). Biologically-active areas, for example sea marshes and the tidal flats of marine environments, serve both as sources and sinks for a number of sulfur compounds, and so sulfur plays an important role in biological processes in these environments, notably via oceanic sulfate, the major electron acceptor for respiration in anoxic sediments (Ingvorsen and Jørgensen, 1982). In the oceans, DMS is produced by benthic and mostly planktonic marine algae (Andreae and Barnard, 1984) and represents 50% of all biogenic gases emitted to the atmosphere (Ferek et al., 1986). In the atmosphere, DMS forms sulfate aerosols, which in turn serve as a source of cloud-condensation nuclei over the oceans, playing an important role in the regulation of the Earth's climate (Charlson et al., 1987; Cropp et al., 2005).

The second most important flux in the atmospheric component of the sulfur cycle is the aeolian weathering of sulfates from the continental surface. This flux is difficult to quantify and may vary greatly in time and space. Arid regions and areas where dust storms are frequent may contribute the largest portion of aeolian sulfur material to the atmosphere (Grinenko and Ivanov, 1983). At present, the contribution of this source to the atmospheric sulfur budget is estimated at less than 6% of total S emissions (Brimblecombe et al., 1989), but is thought to have increased significantly as a result of human activities that increase erosion (Brimblecombe et al., 1989).

The contribution of sea spray sulfates (or sea salt sulfates) to the global sulfur budget

has been estimated to be in the order of 144 Tg (S), representing approximately 42% of the total sulfur input to the atmosphere (Brimblecombe et al., 1989). Sulfate aerosols enter the atmosphere in the form of tiny droplets that have become airborne as a result of the bursting of bubbles at the water surface (MacIntyre, 1974; Wu, 1981). The salt left behind when the water evaporates from the bubbles crystallizes and forms the seasalt aerosols, which crudely approximate the composition of seawater (Glass and Matteson, 1973). Seaspray sulfates are found everywhere in the oceanic atmosphere and along the coasts, but only a small proportion of the seawater sulfate passes over land (≈10%), and only in coastal locations (Moss, 1978; Whelpdale, 1992). Modern oceans are rich in sulfates (28 mM), with sulfate currently one of the most abundant ions in seawater, and a major component of the alkalinity budget (Morel and Hering, 1993). Ancient oceans, however, including the Archaean ocean, were probably sulfate-poor, with concentrations increasing with the development of oxygenic photosynthesis (Canfield and Raiswell, 1999). The oceanic sulfate concentration has varied significantly over time, with concentrations stabilizing at current levels ≈50 million years ago (Paytan et al., 1998).

Volcanic activity releases a number of compounds into the atmosphere (water vapour, carbon dioxide, sulfur dioxide, hydrogen sulfide, hydrogen chloride, various sulfates, some sulfur trioxide), as well as solid matter (ash, lava) [Kellogg et al., 1972; Robock and Oppenheimer, 2003]. Reduced sulfur gases in the lower troposphere are typically rained out or rapidly oxidized to sulfate to form sulfate (sulfuric acid) aerosols, which affect the Earth's radiative balance directly by scattering solar radiation and indirectly by serving as cloud condensation nucleii, increasing cloud cover and albedo (Textor et al., 2003). Volcanic ash, when exposed to water, can also mobilize a range of sulfate and halide compounds (Witham et al., 2005). Although most of the sulfur on the Earth's surface apparently originated from outgassing of deep crustal and mantle regions, the contribution of volcanoes to the present sulfur budget is quite small, with

estimates as low as 2% (Nielsen, 1974). H_2S is also emitted in significant amounts by hydrothermal vents in the oceans (Brimblecombe et al., 1989).

1.2.2.2 Removal of sulfur compounds from the atmosphere

Sulfur compounds in the atmosphere can be brought back to the surface through various mechanisms, including wet deposition (precipitation) and dry deposition (processes that do not involve precipitation). In wet deposition processes, sulfur gases are removed during uptake into raindrops within clouds (in-cloud scavenging), uptake into raindrops as they are falling to the ground beneath the clouds (sub-cloud scavenging) [Ryaboshapko, 1983], or through their adsorbtion onto frozen precipitation elements (Whelpdale, 1992). Sulfate particles are efficient cloud condensation nuclei (CCN) and can thus be incorporated into precipitation or scavenged by cloud droplets and falling drops (Whelpdale, 1992). The efficiency of sulfur removal by wet deposition processes depends on their form and on characteristics of precipitation (type, intensity, duration, frequency). For aerosol particles with diameters between 0.1 and 1 μm, the primary removal mechanism is thought to be precipitation scavenging (Brasseur et al., 1999). Particles with diameters of 10 μm or more may be removed by gravitational sedimentation. Smaller particles and gases are more efficiently brought back to the surface by turbulent atmospheric motions. The actual uptake of these smaller particles may be accomplished by chemical reaction, dissolution, adsorption and other mechanisms (Whelpdale, 1992).

The sulfur dioxide entering the atmosphere is mostly deposited locally via precipitation and dryfall, with the remainder undergoing long range transport (Schlesinger, 1991). Sulfur dioxide in the atmosphere can be oxidized in the gas phase, on the surface of soil particles, and in the liquid phase of droplets in clouds and fog (Ryaboshapko, 1983). The dominant process is by far oxidation in the gas phase and is attributable primarily to reaction with the OH radical to form sulfate (Cox and Sheppard, 1980).

The rate of SO_2 oxidation through this process is highly variable due to OH concentrations in the atmosphere varying with cloudiness, time of day, season and latitude (solar radiation intensity). For example, in cold and dark conditions, SO_2 is not efficiently oxidized (Hobbs et al., 1991). The half-life of sulfur dioxide and sulfate in the lower atmosphere is estimated at approximately 10 hours and 48 hours, respectively, with a half-life for transformation of sulfur dioxide to sulfate of 60 hours (Prahm et al., 1975). Removal of sulfate aerosols from the atmosphere occurs primarily via wet deposition within a few days, but their stratospheric lifetime can range from months to years.

1.2.2.3 Sulfur isotope fractionation in the atmosphere

From modern studies, a broad distinction can be made between sulfur that has and has not participated in the sedimentary cycle, with the latter showing a much wider range of isotope values. Volcanic gases and rocks tend to have a relatively narrow range of $\delta^{34}S$ values, centred around 0‰ (e.g., Grinenko and Thode, 1970; Hoefs, 1997), but with a wider spread than those associated with sulfur of meteoritic or magmatic (basaltic) origin (e.g., Grinenko et al., 1970). However, as some volcanoes can act as pumps for a variety of sources of sulfur compounds, the isotopic composition of volcanic gases depends on the nature of the source material. The isotopic composition of magma-derived sulfides can range to 4-5‰ of the mantle value (Schneider, 1970). Sulfur compounds of biological origin display a large range of isotopic compositions, hence igneous rocks with isotopic compositions departing significantly from 0‰ can be said with some certainty to contain some component of sedimentary sulfur.

There appears to be minimal enrichment in ^{34}S (1.5-2.6‰) between sulfate and its source SO_2 when the sulfate is formed in the combustion process or at high temperatures (Forrest et al., 1973; Nriagu and Coker, 1978), but marine sulfate aerosols tend to have $\delta^{34}S$ compositions that are somewhat lower than that of the source sulfate, potentially due to the contribution from the oxidation of biogenic sulfides (Van

Everdingen et al., 1982; 1985). For reduced volcanic species such as H_2S, some fractionation is predicted as a result of the oxidation process, but this fractionation is smaller than predicted by equilibrium exchange between sulfur species: $\delta^{34}S$ values for H_2SO_4 fallout are similar to the precursor H_2S, but ambient SO_2 is ≈5‰ depleted in ^{34}S (Newman et al., 1991). Sulfate aerosols collected at basaltic vents are enriched in ^{34}S, with $\delta^{34}S$ values ≈8‰ (Mather et al., 2006).

Chapter 2: The Cretaceous-Paleogene extinction event

The Cretaceous-Paleogene boundary (KPg) boundary[1] marks a significant biological turnover in our planet's history ≈65.5 million years ago (Gradstein et al., 2004). Along with the Permian-Triassic, Triassic-Jurassic, Late Devonian, and Ordovician-Silurian extinction events, it is known as one of the "big five": extinction events in the Phanerozoic that stand out against a background of continuous extinctions in our planet's history through their role in the disappearance of >50% of well-preserved genera and perhaps more than 70% of their species (Sepkoski, 1996). Although the KPg event is perhaps best known for having led to the extinction of all non-avian dinosaurs, it is also associated with the disappearance of many other groups of species, including ammonites (Kennedy, 1989; Marshall, 1995), belemnites (Iba et al., 2011), heterohelicid planktic foraminifera (Keller, 1989; Molina et al., 1998), mosasaurs and sauropterygians (marine reptiles; Russell, 1967; Motani, 2009; Polcyn and Bell, 2005), plants (e.g., Tschudy and Tschudy, 1986; Nichols and Johnson, 2008), and insects (Labandeira et al., 2002). The KPg boundary is marked by a continuous bedding plane that is apparently partly consists in debris and dust from a bolide collision with evaporitic and carbonate rocks (Schulte et al., 2010). This bedding plane is referred to as the "KPg boundary" or "boundary claystone" and can be found at sites worldwide.

Many causes to the extinctions have been proposed, including the explosion of a supernova (Russell and Tucker, 1971), a comet shower (Carlisle, 1995), flood basalt eruptions (e.g., Officer & Drake, 1985), an asteroid or large comet impact (Alvarez et al., 1980; Smit and Hertogen, 1980; Prinn and Fegley, 1987), changes in oceanographic or climatic conditions (e.g., Tappan 1968; McLean, 1978; O'Keefe and Ahrens,

1. The KPg boundary was formerly known as the K/T or K-T (Cretaceous-Tertiary) boundary". This usage has been abandonned since the Tertiary is no longer recognized as a valid chronostratigraphic descriptor by the International Commission on Stratigraphy.

1989), a magnetic reversal (Simpson, 1966), and an arctic lake flooding the ocean surface with freshwater (Gartner and Keany, 1978). With the finding of an iridium enrichment in the boundary layer (Alvarez et al., 1980) and the subsequent discovery of the Chicxulub structure (Hildebrand et al., 1991), followed by decades of extensive research, the impact model has garnered significant support from the scientific community (e.g., Schulte et al., 2010). This stems from overwhelming evidence for an impact event at the end of the Cretaceous and its stratigraphic coincidence with the abrupt disappearance from the fossil record of entire groups of species. KPg boundary sites around the world feature direct evidence of an impact coeval with the emplacement of the boundary claystone (tektites, shocked quartz) and indirect evidence that can easily be reconciled with a rapid and catastrophic process with global consequences (Section 2.3).

In their seminal paper, Alvarez et al. (1980) hypothesized that the mechanism of extinction at the boundary was the blocking of sunlight at the Earth's surface by dust and debris from a bolide impact, leading to the collapse of the food chain. The specific mechanisms responsible for the biotic turnover, however, are still cause for debate and have been thought to include other factors, including greenhouse-induced warming (O'Keefe and Ahrens, 1989), wildfires (Wolbach et al., 1985), intense surface heat and radiation (Melosh et al., 1990; Robertson et al., 2004), and ocean anoxia (Kajiwara and Kaiho, 1992).

This chapter completes the information presented in Chapter 4. It includes a detailed review of the nature of the boundary layer, an overview of the biotic impacts of the KPg catastrophe, and some background information on the Deccan continental flood basalts.

2.1 The Deccan continental flood basalts

The “Deccan Traps” are continental flood basalts that cover ≈500 000 km^2 today, but that may have originally covered up to one million square kilometers (Krishnan, 1960). The current thickness of the lava flows ranges from 2000 m in western India to 100-200 m in central India (Bose, 1972). Continental flood basalts are a type of large igneous province that erupt mostly subaerially, with the unique feature of being characterized by the repeated eruption of large amounts of lava over short periods of geologic time (Rampino and Stothers, 1988). Deccan volcanism is thought to have originated from the passing of the Indian lithosphere over the deep mantle plume of the Réunion hotspot, after the Indian plate became detached from Gondwanaland (Morgan, 1972; Gupta and Gaur, 1984; Ganerød et al., 2011). Hot spot activity would have bored through the lithosphere and extruded great volumes of tholeiitic basalts, generating the structures know today as the Deccan traps.

The observation of modern eruptions associated with basaltic fissures (e.g., Laki volcano, 1783 A.D.) hints at the formation of violent “fire fountains” during prolonged flood basalt eruptions, reaching heights of up to 1.5 km (Thordarson and Self, 1998) and perhaps 13 km at times in the case of convective plumes (Self et al., 2005). Estimates of sulfur release by ancient flood basalt eruptions are complicated by weathering and element mobilization by groundwater, but recent studies suggest that ≈75% of volatile sulfur species in the rising melt are released at vents as SO_2 and lofted in the atmosphere at heights >10 km, with the remainder of gas release occurring above the surface of lava flows, in the lower troposphere (Self et al., 2005; 2006). Continental flood basalt eruptions maintained over long periods of time thus have the potential for the release of massive amounts of sulfur, leading to rapid depletion of stratospheric ozone and hydroxyl radicals (OH^-) - key agents in the removal of sulfur from the atmosphere (Bekki, 1995).

The environmental impact of volcanic eruptions is a function of various factors, including the nature of the eruptions (aerial or subaerial), the latitude at which they occur, the amount of sulfur and carbon dioxide they release, their ability to inject gases into the stratosphere, and cumulative effects from prolonged eruptions (Kaminski et al., 2011). In the case of large-scale volcanic eruptions such as the Deccan continental flood basalts, the potential for injection into the stratosphere would have been facilitated by penetrative convection phenomena above large lava flows from the heating of the atmospheric boundary layer, providing additional buoyancy (Kaminski et al., 2011) and would have contributed to the rapid spreading of volcanic gases, dust, and aerosols around the planet.

Estimates of sulfur release from individual short-lived (tens of years) Deccan eruptions are in the order of 10 000 Tg sulfur (Self et al., 2006). The amount of sulfur degassed from Deccan lava fields and source vents has been estimated at ≈1200 ± 100 ppm sulfur, yielding 6.5 Tg SO_2 per cubic kilometer of lava: an estimated range would be between 6500 - 65,000 Tg SO_2 per eruption for the Deccan Basalt Group as a whole (Wai sub-group; Self et al., 2006). If a total lava volume of $1X10^6$ km^3 for the Deccan continental flood basalts is assumed, the eruptions may have had the potential to release up to $6.5X10^6$ Tg SO_2 (Self et al., 2006).

2.1.1 Deccan timing and duration

Estimates of the duration of Deccan volcanism are varied and range from close to 1 My (McLean, 1985; Courtillot et al., 1986; Duncan and Pyle, 1988; Hofmann et al., 2000; Self et al., 2006), to at least 8 My (Sheth et al., 2001), to less than 30 My (Alexander, 1976) and over 85 My (Kaneoka, 1980). More recent studies, however, suggest that the total Deccan continental flood basalt eruptions were of short duration, lasting only a few hundred thousand years (Sen et al., 2006; Chenet et al., 2007; 2008).

Absolute age dating of lava flows points to the emplacement of the Deccan traps in three major phases: an initial phase ≈68-67 Ma, a main eruptive phase at or near the KPg boundary (≈66 Ma) and a shorter, less intense phase after the emplacement of the KPg boundary claystone layer (Courtillot et al., 2000; Chenet et al., 2007; 2009). Courtillot et al. (2000) proposed that Deccan volcanism would have started within uppermost Maastrichtian normal chron C30n (66.5-67 Ma). After a ≈1-2 My period of quiescence, it would have resumed near the KPg boundary (65 Ma, main phase), within reversed chron C29r. The occurrence of an earlier phase of volcanism, some 2 My before the boundary, appears to be well supported, as is the eruption of a smaller sequence after the emplacement of the boundary layer, beginning in chron C29r and ending in C29n (Chenet et al., 2007). The uncertainty lies in the timing of the eruption of the main Deccan phase relative to the KPg boundary, the bulk of which may have erupted within reversed chron C29r (e.g., Courtillot et al., 1986; Duncan and Pyle, 1988; Courtillot et al., 2000; Chenet et al., 2007; 2008). The establishment of the relative timing of the two events is beyond the resolving power of any absolute dating technique available today.

2.1.2 Deccan eruptions and the KPg extinctions

The terminal Cretaceous extinctions have been attributed to Deccan volcanism, and there is indeed evidence that the timing of at least the main Deccan phase took place close in time to the formation of the KPg boundary. Additionally, some of the geochemical and paleontological signals observed near the KPg boundary are consistent with at least some of the expected effects of prolonged large-scale volcanism. For example, volcanic exhalations from the Deccan traps would have released massive amounts of CO_2 into the atmosphere, with the potential of severely disrupting the global carbon cycle by lowering the pH of the surface and deep ocean and impacting carbonate stability (McLean, 1985). The release of isotopically light CO_2 from volca-

nic exhalations could perhaps account for at least part of the negative excursion in $\delta^{13}C$ values at the boundary (Section 2.3.5). One of the key extinction scenarios put forward by proponents of the volcanism extinction mechanism have suggested that massive volcanic eruptions at KPg boundary time obscured the skies with dust - a mechanism akin to that proposed by Alvarez et al. (1980), spewed toxic gases in the atmosphere and caused a drop in temperature, resulting in global climate change (Officer and Page, 1996). However, the difficulty in reconciling the sudden character of the KPg extinctions with prolonged volcanic eruptions, as well as the discreditation of the climate cooling hypothesis following the eruptions (Huber et al., 1995; Wilf et al., 2003) make the establishment of a causal link between the eruptions and the extinctions difficult. The sudden nature of the extinctions at the KPg event - although still under debate (e.g., Keller et al., 1995) - is incompatible with gradual environmental changes resulting from the long-term eruption of Deccan continental flood basalts. The establishment of a direct link between Deccan volcanism and the end-Cretaceous mass extinctions is further complicated by the rarity of age diagnostic fossils in intertrappean sediments of the Deccan continental flood basalts (Keller et al., 2008).

In Chapter 4 we present evidence that the initiation of the main Deccan phase, the largest of the Deccan eruption events, is coeval with the boundary itself, and therefore could not have contributed to the sudden biological extinctions observed in the fossil record (see Chapter 4). If such results preclude a direct causal link between the KPg extinctions and Deccan volcanism, they do, however, point to a link between volcanism and the recovery time of both the terrestrial and oceanic ecosystems post-impact.

2.1.3 Deccan volcanism at the KPg boundary triggered by a bolide impact?

There is abundant evidence to suggest that the main Deccan eruptive phase and the impact were roughly contemporaneous. It is therefore not surprising that a direct

causal link between a bolide impact and the initiation of Deccan volcanism has been proposed (Alt et al., 1988; Negi et al., 1993; Carlisle, 1995). Before the discovery of the Chicxulub structure (Hildebrand et al., 1991), it was even suggested that the KPg impact site was located beneath the Deccan traps themselves (e.g., Alvarez et al., 1982; Courtillot et al., 1986; Clube and Napier, 1990). A recent study of the geophysical consequences of large meteorite impacts suggest that the energy released by an impact of Chicxulub magnitude could trigger seismicity, volcanism, fracturing of rock, melting and tsunamis and that the seismic waves would reach the antipode of the impact site (Meschede et al., 2011). Paleotectonic reconstruction of continents at KPg boundary time suggests that the Deccan Plateau was in the vicinity of the antipode of the Chicxulub impact site, a coincidence that is certainly intriguing, especially in light of the timing of events proposed in Chapter 4, with the initiation of the Main Deccan phase of eruption coeval in time with the bolide impact.

2.2 Selectivity of species survival and recovery of ecosystems

The study of paleontological evidence to understand extinction patterns is fraught with difficulties: some taxa within a taxonomic group may be more abundant or less common, or even rare, and disappearances in the stratigraphic range of some taxa may appear to be gradual, even though their disappearance was abrupt and catastrophic (Signor-Lipps effect; Signor and Lipps, 1982; Meldahl, 1990). A thorough look at the stratigraphic record and the comparison of several coeval sections may be necessary to ensure an accurate understanding of taxonomic changes across geological time, but at the KPg boundary, the paleontological evidence appears to point to a sudden change in the composition of ecosystems worldwide, both marine and terrestrial (e.g., Fastovsky and Sheehan, 2005).

Walter Alvarez and colleagues (Alvarez et al., 1980) were among the first to propose a clear extinction mechanism linked to the terminal Cretaceous bolide impact. They

postulated that the impact was followed by shock waves and extensive wildlfires that raised an enormous cloud of dust that spread rapidly around the Earth: the dust obstructed solar radiation for a few years, suppressing photosynthesis and primary production, the effects of which rapidly trickled up the food chain, creating an ecological catastrophe resulting in major extinctions. This proposed mechanism appears to be in general agreement with the patterns of extinctions observed in the paleontological record. For example, in the botanical world, the large-scale impact would likely have resulted in the destruction of surface vegetation, inhibiting the subsequent growth of plant taxa unable to regenerate from seeds or rootstocks. This is consistent with the observation, in KPg terrestrial sections, of a “fern-spore spike” (Section 2.3.4), which points to a drastic change in floral assemblages, from a diversified assemblage dominated by the flowering gymnosperms to one dominated by pioneer-species, grown from spores or rhizomes. In the case of animals, the survival of taxa of smaller size characterized by the use of burrows and scavenger feeding behavior also suggests rapid changes in ecosystem functions following the impact that would have resulted in the preferential survival of these taxa over those that relied directly on plant matter for their nutrition, or those that were unable to find shelter. Survivors include numerous mammalian taxa, many of which are the taxonomic ancestors of species currently found on the planet (Archibald, 2011).

The long-lasting effects of the KPg catastrophe can be observed in the fossil record at the KPg boundary through a sudden drop in the diversity of taxa, significantly different assemblages of both mega- and micro-fossil floras on either side of the boundary, the unusual abundance of pioneer fern taxa in the fossil record above the level of pollen extinctions, and the persistence in the fossil record of these new less-diversified floral assemblages (Nichols and Johnson, 2008). The fossil record also suggests that the extinctions in plant taxa were less severe outside of North America, further away from the impact site, and that some taxa were able to re-colonize devastated areas

because of the presence of plant refugia (Nichols and Johnson, 2008). There is some indication that survival was better among mire plants than dry-land plants, and that topography (e.g., proximity to a mountain range) played a role in determining which taxa survived the impact (Nichols and Johnson, 2008).

In the marine realm, it is apparent that benthic species and non-calcareous marine phytoplankton (dinoflagellates, diatoms) were little affected by the catastrophe, but that calcareous microplankton (e.g., foraminifera and coccolithophorids) and invertebrate species that reside in the mixed layer of the ocean at some point in their lifetime experienced catastrophic drops in their numbers and species diversity, perhaps due to significant pH changes in the first layers of the ocean (McLean, 1985) following the catastrophe. Such a change in chemical conditions of the ocean would help explain the extinction of other taxa linked to the mixed layer, including brachiopods, ammonoids, and belomnoids. The disappearance of primary producers may have also played a major role in the extinction of these organisms, which relied on photosynthetic organisms for food (McLean, 1985). McLean (1985) attributes changes in pH in the mixed layer to mantle degassing from the eruption of the Deccan traps, but an impact with sulfate-containing rocks, such as those of the Chicxulub structure, would have led to a significant input of sulfuric acid to the ocean, an extinction mechanism that is favored by some (Sigurdsson et al., 1992; Maruoka et al., 2002). Microfossil groups that survived the KPg event have some characteristics in common, which include the ability to form cysts rather than rely on sexual reproduction, and detritus-feeding behavior rather than a dependence on primary production (Sheehan and Hansen, 1986).

Numerous lines of evidence support the assumption of a delayed recovery of marine ecosystems compared to terrestrial ones, but carbon stable isotopes are one of the main geochemical markers used to constrain ecosystem recovery times after the terminal-Cretaceous extinction event (Section 2.3.5). In the terrestrial realm, the isotope

signature of atmospheric CO_2 is recorded in facies, hence the recovery of the carbon isotope signature to pre-boundary values is interpreted to indicate a complete recovery of the terrestrial carbon cycle and terrestrial ecosystems. In marine systems, the signal for recovery is the restoration to pre-boundary values of the surface-to-deep gradient of carbon isotope values.

There is general consensus that following the KPg catastrophe, the recovery of terrestrial ecosystems occurred much more rapidly than that of marine ecosystems. Terrestrial systems appear to have recovered in a period of a little over one hundred thousand years post-impact (Beerling et al., 2001; Therrien et al., 2007), while the initial recovery of the surface-to-deep water carbon isotope gradient occurred in the first 500 ky (Keller and Lindinger, 1989; Robin et al., 1991; D'Hondt et al., 1998; Arens and Jahren, 2000). The complete reestablishment of the marine carbon cycle, however, may have taken place only much later (over several million years; e.g., D'Hondt et al., 1998; Keller and Lindinger, 1989; Beerling et al., 2001). This discrepancy in ecosystem recovery times has been attributed to lower extinction rates among land plants compared to marine producers (e.g., Arens and Jahrens, 2000) and the development of ocean anoxia.

2.3 The KPg boundary claystone layer

The KPg boundary is a unique marker of geological time in that it represents an event of extremely short duration (decades at most) that is nevertheless visible in the geological record. The boundary, especially in marine rocks, features a claystone layer generally 1-2 cm-thick thought to be the product of diagenetic alteration of the debris from a meteorite impact (Hildebrand and Boynton, 1988; Smit, 1999). It is represented by the Global Stratotype Section and Point established by the International Commission on Stratigraphy in marine rocks at El Kef, Tunisia, and marks the transition from the Cretaceous (Maastrichtian stage) to the Paleogene (Danian stage). Both

stages are defined by their content in marine fossils, making the direct comparison with equivalent terrestrial rocks difficult. The use of complementary information, such as magnetostratigraphy, and pollen and geochemical (e.g., stable isotope) analysis, can help improve time resolution and facilitate the comparison between marine and terrestrial sections of the KPg boundary.

The KPg boundary occurs within subchron C29r, which lasted between 570 and 833 thousand years (e.g., Cande and Kent, 1995). Well-preserved sections feature a clear paleontological extinction horizon and elevated iridium concentrations, as well as spherules, shock-metamorphosed mineral grains, and a characteristic increase in the relative abundance of fern spores immediately above the level of extinction of Cretaceous pollen in terrestrial sections (Orth et al., 1981; Tschudy, 1984). Other characteristic features of KPg boundary sections may include an abrupt negative shift in $\delta^{13}C$ values (e.g., Schimmelmann and DeNiro, 1984; Arens and Jahren, 2000; Therrien et al., 2007), a positive shift in $\delta^{34}S$ values (Holmes and Bohor, 1994; Maruoka et al., 2002; Chapter 4), and the presence of microscopic diamonds (e.g., Carlisle and Braman, 1991; Hough et al., 1995). A more in-depth look at each of these markers of the KPg boundary is featured in the next few paragraphs.

2.3.1 The iridium “anomaly”

Platinum-group elements are much more abundant in chondritic meteorites than in the Earth’s upper crust and mantle, likely owing to the concentration of these elements in the Earth’s core. In 1980, Alvarez et al. published a seminal paper describing the finding of an abnormally-elevated iridium content in the sedimentary rocks of two KPg sections in the Italian Umbrian Appenine mountains, the Bottacione and Contessa sections (“Gubbio”, in the Scaglia rossa formation, a continuous pelagic limestone sequence), and the Danish Stevs Klint section.

The “iridium anomaly” as measured by Alvarez et al. (1980) represents an increase in iridium abundance relative to background values of up to 160 times, and is most often found in association with a unique claystone layer of kaolinitic and smectitic composition. Similar peaks in iridium abundance have been detected in numerous KPg sections, both marine and terrestrial. In North America, the iridium enrichment from background values is generally in the order of a few tenths of a ppb to ≈70 ppb (Nichols and Johnson, 2008). Alvarez et al. (1980) determined the concentration in the boundary clay and adjacent Cretaceous and Paleogene sediments of 28 elements that would be expected to be enriched similarly were the iridium enrichment in the boundary layer the result of concentration from a crustal source or iridium-enriched localized sources (e.g., nickel sulfide and chromite ores). They also considered whether the iridium could have been concentrated by marine chemical processes, which would have disposed of the other elements in a different fashion, but reasoned that the probability of this same process occurring elsewhere was rather low. Subsequent investigations of terrestrial sections, where the iridium anomaly can also be found, more or less resolved this issue: if an identifiable mechanism had been responsible for the concentration of iridium in marine KPg sections from an intrinsic source, then the absence of this mechanism in terrestrial environments would result in the absence of a coeval iridium enrichment in these sections.

An iridium-enriched layer has been found in intertrappean sediments in some regions of the Deccan volcanic province and associated with the KPg boundary impact (Bhandari et al., 1995). However, the absence of extraterrestrial diagnostic material in many of these sections has also prompted some researchers to speculate that the enrichment in Pt-group elements is plume-related (Bajpai and Prasad, 2000). It has been proposed that the emplacement of the Ir “anomaly” was gradual rather than sudden, leading to the suggestion that its source is not linked to a bolide impact. McLean (1985), for example, calculated that the duration of the marine KPg boundary Ir en-

richment was 10^5 years and attributed the source of the Ir to the release of IrF_6 gas from the mantle.

2.3.2 The Chicxulub structure and ejecta material

At the time of publication of the 1980 Alvarez et al. paper, only three craters of diameter 100 km or greater - the minimum size calculated to be necessary for the impacting bolide to provide the influx of iridium leading to the measured enrichment - were known, but these were either too young or too old to correspond in age to the timing of the Cretaceous-Paleogene extinctions. Alvarez et al. (1980) postulated that there was a 66% chance that the bolide responsible for the extinctions had fallen into the ocean, rendering its eventual discovery challenging at best.

The Chicxulub impact structure was “re-discovered” in 1991 (Penfield and Camargo, 1981; Hildebrand et al., 1991) and is believed to have been generated by the bolide impact linked to the end-Cretaceous extinctions. Despite some apparently contradictory evidence of its too-old age (Keller et al., 2003), it has now been confirmed to be coeval with the KPg boundary (Swisher et al., 1992). Other structures were however postulated to be possible KPg impact sites, including the Manson crater in Iowa, U.S.A. (French, 1984; Kunk et al., 1989; Hartung et al., 1990; Anderson and Hartung, 1992), and the Popigai structure in Northern Siberia (Deino et al., 1991). The Manson structure was ruled out because of its small size (Izett et al., 1993), while the Popigai structure was confirmed to be of Late Eocene age (Bottomley and York, 1989; Bottomley et al., 1993; 1997).

The Chicxulub crater is a 180-km-diameter structure located on the Yucatán peninsula of Mexico. It consists in a thick (up to 3500 m) sequence of Lower Cretaceous to Quaternary carbonate and evaporitic rocks lying atop basement crystalline rocks of Paleozoic age (Hildebrand et al., 1991). The shocked material contained in brec-

cia within the crater and rim is consistent with ejecta material (shocked quartz and alkali-feldspar grains, high-Ca tektites) found in the KPg boundary layer in proximal Carribean KPg sites. The carbonate and evaporite nature of the impacted rocks is also consistent with the large-scale climatic impacts proposed in many of the extinction scenarios for the biotic turnover (e.g., release of dust and aerosols, generation of sulfuric acid).

Tektites, glass-melt droplets formed by instantaneous fusion of terrestrial rocks during impact events, have been found at various KPg sites and present features consistent with the Chicxulub structure as a source material. The Beloc, Haiti, tektites occur in conjunction with an Ir anomaly and shock-metamorphosed quartz grain at the paleontological KPg boundary and are enclosed in iron-rich smectitic material (Izett et al., 1991) that is interpreted to result from the alteration of the Chicxulub source material (Swisher et al., 1992). The tektites are broadly similar to other tektites found at impact sites elsewhere, but some show unusually high Ca and S contents (Izett et al., 1991; Dalrymple et al., 1993), pointing to a source material of continental terrane rocks rich in carbonate and sulfate minerals (Sigurdsson et al., 1991a; 1991b). Oxygen isotope analyses are consistent with high-Ca sedimentary rocks as the source material for the tektites (Blum and Chamberlain, 1992) and the tektites are devoid of the features characteristically found in volcanic glass (Blum and Chamberlain, 1992; Dalrymple et al., 1993), precluding a volcanic source. The Beloc and other tektites have been dated using $^{40}Ar/^{39}Ar$ and found to be indistinguishable in age from the KPg boundary (Izett et al., 1991) and glassy melt rocks from the Chicxulub structure (Swisher et al., 1992).

2.3.3 Microstratigraphy of the KPg boundary claystone

In marine sections, the KPg boundary layer generally presents itself as a single mm-thick layer of kaolinitic clay containing anomalous iridium concentrations and altered impact spherules (e.g., Alvarez et al., 1980).The iridium is found in the finest material

at the top of the marine KPg beds. In terrestrial sections, however, especially those found in North America, two, and sometimes three, distinct layers can often be identified. The three layers are interpreted to represent (Alvarez et al., 1995): 1) “hot fireball”: vaporized material from the bolide and the target carbonate and sulfate rocks, 2) melt-ejecta: ejecta material containing shocked rock fragments from the impact, including kaolinitic clay originating from the alteration of glassy spherules, and 3) “warm fireball”: shocked mineral grains, including shocked quartz. The iridium generally found in the top-most layer of the boundary claystone, in association with the “warm fireball” layer, would have been launched first, but deposited later because of its occurrence as finer-sized particles. This late deposition of the iridium is consistent with the finding of the iridium anomaly in association with the top of the boundary layer at marine locations.

2.3.4 The “fern-spore spike”

The “fern-spore spike” found at many terrestrial KPg sections is defined by an assemblage of 70-100% fern spores of a single species occurring 0-15 cm above the KPg boundary (Fleming and Nichols, 1990). It is thought to represent a significant shift in floral composition after the impact, from a diversified assemblage of gymnosperm and angiosperm (flowering plants) taxa to a dominance of so-called “disaster species”; species able to resurface quickly after the devastation due to their ability to grow quickly from spores and buried rhizomes (Nichols and Johnson, 2008). In these sections, the ratio of angiosperm pollen to fern spores drops abruptly just above the paleontological extinction level, reestablishing itself a few centimeters above (e.g., Orth et al., 1981; Lerbekmo et al., 1987).

Terrestrial KPg sites where palynological investigations have been applied consistently show major changes in floral assemblages across the KPg boundary, with a drastic reduction in species richness and the sudden dominance of pioneer species (Nichols

and Johnson, 2008). The abruptness of this shift - which is believed by some to have occurred in as little time as one season of growth - is indicative of sudden ecological disruption (Sweet et al., 1999; Therrien et al., 2007; Nichols and Johnson, 2008), a scenario that is apparently largely incompatible with the environmental consequences of a long-term gradual process such as the emplacement of the Deccan continental flood basalts.

2.3.5 Carbon stable isotopes

Significant shifts in bulk and organic carbon stable isotope compositions have been measured at KPg boundary sites worldwide, both in marine and terrestrial sections. In terrestrial sections, the shift presents itself in a sudden ≈2‰ decrease (≈1.5‰ to 2.8‰), followed by a slow recovery to pre-boundary values and ecosystem conditions continuing into the Paleogene (Arens and Jahren, 2000; Beerling et al., 2001; Therrien et al., 2007). As the $\delta^{13}C$ signature in terrestrial facies records the isotope signature of atmospheric CO_2, this sudden decrease is thought to have resulted from an increased supply of ^{12}C to the atmosphere, with some potential sources of this light carbon including biomass burning resulting from the impact (Ivany and Salawitch, 1993; Beerling et al., 2001), or perhaps volcanic exhalations from the Deccan continental flood basalts (McLean, 1985). As the floral assemblage gradually recovered after the KPg catastrophe, low-biomass pioneer species were replaced by higher-biomass woody angiosperm taxa, progressively sequestering an increasing amount of light carbon, resulting in a progressive increase in the $\delta^{13}C$ composition towards pre-boundary values.

A shift in $\delta^{13}C$ values of dissolved inorganic carbon of a similar magnitude (1.5‰ to 2.0‰) has also been documented at KPg boundary marine sections worldwide (e.g., Hsü et al., 1982; Keller and Lindiger, 1989; Zachos et al., 1992; D'Hondt et al., 1998). The negative excursion is attributed to a brief but sudden decrease in primary produc-

tivity in the surface ocean, resulting in the homogenization of the marine surface-to-deep water carbon isotope gradient, which is normally positive (D'Hondt et al., 1998; Hsü et al., 1982). In normal conditions, photosynthetic plankton use ^{12}C preferentially, enriching dissolved inorganic carbon in the surface ocean in ^{13}C compared to deeper strata. Mortality and extinction of photosynthetic plankton following the KPg catastrophe would have obliterated the difference between surface and deep waters normally present (D'Hond't et al., 1998). However, addition of ^{12}C to the surface ocean-atmosphere reservoir would also have been required to produce the observed negative shift (Kump, 1991).

2.3.6 Sulfur stable isotopes

Only a few studies have investigated sulfur stable isotopes at the KPg boundary. One of the earliest published records of sulfur stable isotope measurements at a KPg section concerns metal-rich pyrite spherules, found in abundance in the Fish Clay of the marine Stevns Klint KPg section of Denmark (Schmitz et al., 1988). A $\delta^{34}S$ value of -32‰ was measured in these spherules and argued to be the product of sulfate reduction by anaerobic bacteria during early diagenesis of the boundary sediments. We identified only three more in-depth studies of sulfur stable isotopes across the boundary: one in marine KPg boundary sections, and two in North American terrestrial sections.

At the marine section of Kawaruppu, in the Katsuhira Formation, eastern Hokkaido, Japan, the sedimentary sequence was found to record a sudden and drastic increase in bulk $^{34}S/^{32}S$ ratios immediately at the boundary (Kajiwara and Kaiho, 1992). This increase began at the KPg boundary (bottom of claystone layer) and continued upward for a few tens of centimetres before adopting a gradual re-equilibration trend over approximately 4 metres of continuous sediment. The authors interpreted the ≈20‰ increase at the boundary to result from the advent of anoxic conditions beginning at

the end of the Cretaceous and continuing for ≈70 000 years. They noted that because the high $\delta^{34}S$ persisted for some distance above the boundary, and because the majority of sulfur was found in the form of framboidal pyrite - typically of biogenic origin, the sudden increase in $\delta^{34}S$ at the boundary could not result from the direct input from extra-terrestrial or mantle-derived sulfur. Because of the significant difference in resolution, it is difficult to compare their results with those from the Knudsen's Coulee and Knudsen's Farm sections of Alberta (Chapter 4), but it is interesting to note that the Kawaruppu section records an increase in sulfur content of the sediments at approximately 55 ky and 140 ky, which correspond approximately in time to what we interpret as the maxima of two Deccan pulses after the impact.

In a study of the Dogie Creek and Brownie Butte terrestrial KPg section in Montana, an increase in the $\delta^{34}S$ values of the sulfur (bulk, acid-volatile and HCl-soluble) was observed immediately at the boundary (Maruoka et al., 2002). The ≈12‰ increase was attributed to the input of ^{34}S-enriched sulfur, presumably from the melt ejecta or acid rain resulting from the Chicxulub impact. The authors suggested that the higher $\delta^{34}S$ values measured above the boundary resulted from the development of anoxic conditions in the freshwater system, but provided no information on the duration of this episode.

The sudden increase in $\delta^{34}S$ values in these KPg boundary sections is mirrored in the coal-rich terrestrial section of Sugarite, New Mexico (Holmes and Bohor, 1994), where an increase in the $\delta^{34}S$ of bulk sulfur of ≈3.5‰ was measured immediately at the boundary. This was interpreted to result from input of volatilized sulfate minerals from the Chicxulub impact.

The research presented in Chapter 4 is the highest-resolution study of sulfur stable isotopes across any KPg section so far and the first to provide a means of identifying the relative timing of two key events in Earth history: a bolide impact with evaporite

terrane, and the eruption of the main phase of the Deccan continental flood basalts.

Chapter 3: Sulfur isotope fractionation during microbial sulfate reduction by acidophilic sulfate-reducing bacteria

3.1 Contributions

The candidate (MLC) developped the study design described in this study and conducted all the experimental steps, including the design and preparation of the growth media, the chemical and biological analyses, and the sulfur extraction and analysis. All analyses except stable isotope analyses were conducted at the University of Ottawa (Lab of Dr. Fortin, Dept. Earth Sciences). Sulfur stable isotope analyses were conducted at the Dept. of Earth and Planetary Sciences, McGill University (Lab of Dr. Boswell Wing) by the candidate. The data analysis and interpretation, as well as manuscript and figure preparation, were accomplished by the candidate.

Cousineau, M.L., Fortin, D., and Wing, B.A. In preparation.

3.2 Abstract

We investigated sulfur isotope fractionation during microbial sulfate reduction by two strains of acidophilic sulfate-reducing bacteria. These are the first measurements of fractionation for non-neutrophilic strains of sulfate reducers. We investigated whether pH influences fractionation. Our results suggest that two regimes of fractionation can be identified during the growth cycle of the strains studied. A first regime corresponds to growth during the exponential phase and is characterized by significant fractionation rapid growth and rapid sulfate depletion. Fractionation and cell-specific sulfate reduction rates during this regime were in the range of values known for incomplete oxidizers (≈4-12‰, $2.5X10^{-15}$ to $9.2X10^{-15}$ moles $cell^{-1}$ day^{-1}). A second regime of low but measurable fractionation (<1‰) was identified early in the growth cycle, before the onset of dissimilatory microbial sulfate reduction. Fractionation was not constant across the pH range measured in the experiments but the effect of pH may be related to changes in metabolic activity. The significant increase in pH observed during this fractionation regime cannot be attributed to microbial sulfate reduction and hints at the existence of a parallel mechanism. Internal sulfate accumulation accompanied by the uptake of protons concurrently with the sulfate ion may help explain our results, but further studies are needed to confirm this hypothesis.

3.3 Introduction

Microbial sulfate reduction (MSR), one of the earliest metabolisms to appear on Earth (Shen et al., 2001; Wacey et al., 2011), is a multi-step respiratory process by which some prokaryotes use sulfate as an electron donor to obtain energy. In addition to the key role played by MSR in the global cycling of sulfur, it is one of the major processes responsible for organic carbon mineralization on the seafloor (Canfield, 1993; Jørgensen, 1982). Whether the reduction of sulfate during MSR is coupled to the oxidation of

organic matter or hydrogen gas (Postgate, 1984), it results in the fractionation of sulfur stable isotopes, with the product sulfide having lower ^{34}S-^{32}S ratios than the reactant sulfate. Because sulfur isotope fractionation during MSR is influenced both by biological and environmental factors, the extent of fractionation in sulfides from ancient rocks has been widely used to probe environmental conditions and the presence of sulfate-reducing micro-organisms on the early Earth (e.g., Schidlowski et al., 1983; Shen et al., 2001)

In the majority of laboratory studies with pure cultures of sulfate reducers, the isotopic difference between the sulfate reactant and the product sulfide falls between of 2‰ and 46‰ (Chambers et al., 1975; Habicht and Canfield, 1997; Canfield 2001), with one study (Sim et al., 2011) significantly exceeding this upper threshold. While species-specific S isotope fractionation is clearly present (Detmers et al, 2001), fractionation is also strongly influenced by the physiological state of the microbial population. For example, sulfate-reducing microbes that oxidize organic carbon incompletely (incomplete oxidizers) generally fractionate sulfur isotopes to a lesser extent (2-19‰, average 9.5‰; Detmers et al. 2001) than sulfate-reducing microbes that completely oxidize organic carbon to CO_2 (15-42‰, average 25‰; Detmers et al. 2001). In non-limiting sulfate concentrations (>1 mM) with pure and enrichment cultures of sulfate reducers, MSR leads to high fractionations (up to ≈50‰; Harrison and Thode, 1958; Habicht & Canfield, 1997; Canfield et al., 2000; Canfield, 2001), whereas at limiting sulfate conditions (<1mM), fractionation is significantly suppressed (<<10‰; Habicht et al., 2002).

Most sulfate reducers isolated and studied so far operate in near-neutral pH conditions (6 to 8; Widdell, 1988; Hao et al., 1996). Acid-tolerant and acidophilic strains have only been recently isolated (pH ≈4.0; Sen and Johnson, 1999; Senko et al. 2009), but S isotope fractionation associated with these strains has not been investi-

gated. Because MSR is a proton-consuming reaction, acid-tolerant species possess an energetic advantage at low pH (Koschorrek 2008). Acidic conditions result in a natural proton gradient toward the cell, but sulfate reducers maintain an elevated pH in the cytosol, which requires energy (Martin, 1990; Lowe et al., 1993). In active cells of acidophilic sulfate reducers, cytoplasmic pH values between 5.5 and 6.6 have been measured, representing a transmembrane pH gradient of up to 3.6 units (Koschorreck 2008). At least some sulfate reducers are able to generate a transmembrane proton gradient by pumping protons across the cytoplasmic membrane (Fitz and Cypionka, 1989; 1991). In a closed system, this uptake of sulfate increases pH through the removal of protons from solution, even in the absence of sulfide production (freshwater species; Cypionka, 1987; 1989; Kreke and Cypionka, 1992).

This paper describes the results of a study on sulfur isotope fractionation during MSR for two strains of acidophilic sulfate-reducing bacteria. The specific objectives of our study were to provide the first measurements of sulfur isotope fractionation associated with acidophilic sulfate reducing-microorganisms, and to examine whether pH influences sulfur isotope fractionation during MSR. We hypothesized that any effect of pH on sulfur isotope fractionation would be magnified in experiments with acidophilic strains since their metabolic activity is acutely sensitive to changes in pH.

3.4 Methods

3.4.1 Bacterial cultures

We acid-washed and autoclaved all glassware and equipment before preparing the bacterial cultures and conducting the experiments. All manipulations of the bacterial cultures were conducted in a Coy Model 2000 Anaerobic Chamber with a 5% H_2 and 95% N_2 gas mix using standard sterile techniques. Growth media were prepared under anaerobic conditions and cells were grown in strictly anoxic conditions.

The *Desulfosporosinus sp.* GBSRB4.2 strain is a gram-positive, acid-tolerant, spore-forming, metal-reducing sulfate-reducing bacterium isolated from coal mine-derived acidic mine drainage sediments (pH 4.1; 1 mM SO_4^{2-}; Senko et al., 2009). This strain is most closely affiliated with *Desulfosporosinus sp. LauIII* (16s rRNA gene sequencing; Senko et al., 2009). It has an optimum growth pH of 4.2 (2.9-6.3 pH range) and incompletely oxidizes glucose to acetate and CO_2. When transferred to new, non-limiting, medium, it can remain in a lag phase for several days (Senko et al., 2009).

The *Desulfosporosinus sp*. M1 sulfate reducing-bacterium is a gram-positive obligate anaerobic spore-forming, acid-tolerant (optimal pH 4.0), sulfate-reducing strain isolated from acidic sediments at a geothermal site on Montserrat, West Indies (Sen, 2001). It incompletely oxidizes glycerol to acetic acid in stoichiometric amounts. Its closest identified relative is *Desulfosporosinus orientis* (94% sequence identity with 16S rRNA; Kimura et al., 2006).

3.4.2 Bacterial experiments

The strain GBSRB4.2 was grown in a medium modified from Senko et al. (2009), which includes glucose (5 mM) as an electron donor, trypticase soy broth (0.5 g/L), and vitamins and trace metals (Tanner, 1997). We replaced $MgSO_4$ and $FeSO_4$ by $(NH_4)_2SO_4$ (8 mM) and Na_2SO_4 (10 mM) to minimize the precipitation of sulfides. The pH of the medium was adjusted to 4.2 (optimal growth pH) using HCl.

The strain M1 was grown in a medium modified from Kimura et al. (2006), which includes 20 mL/L of a heterotrophic basal salts solution, 1mL/L trace elements solution, 5 mM glycerol as the carbon source, 0.02% w/v yeast extract. We replaced $ZnSO_4$ and $FeSO_4$ by K_2SO_4 (8 mM) and Na_2SO_4 (10 mM). The pH was adjusted to 4.0 (optimal pH) using HCl. The initial concentration of ≈18 mM of sulfate in the growth medium for both pure cultures was based on results from preliminary experiments, which showed

that ≈20-50% of the sulfate was used during one growth cycle.

Fresh growth medium was dispensed in 2-L Pyrex media bottles. The bottles were fitted with a silicone septum, sealed inside the anaerobic chamber, and autoclaved. Each treatment bottle had a final volume of 1.8 L. For the low carbon (LowC; ≈0.5 mM electron donor, M1 strain only) and high-carbon (HighC; ≈5 mM electron donor) treatments, this included 180 mL of inoculum, added through the septum after sterilization. We incubated the cultures in the anaerobic chamber at ≈25°C. We used an experimental design that allowed us to follow the same population of sulfate reducers through an entire growth cycle, with the advantage of allowing a better time resolution of metabolic processes.

We included a "sterile" control, containing the electron donor but not inoculated with the live cultures, in the experimental design. For the GBSRB4.2 experiments, we also included a "carbon-free" control consisting of inoculated media without an added electron donor (glucose or glycerol). The inoculum for each of the two strains was prepared by culturing cells for 6-10 days in Fe^{2+}-free medium to eliminate Fe from the original culture. After three passes in this medium, the cultures were transferred into a series of sterile 50-mL "Falcon" tubes and spun down at 2500 rpm for 10-15 minutes into a pellet, decanted and reconstituted using the same volume (≈800 mL) of fresh sulfide-free experimental media. This culture was used as the inoculum. All experimental bottles were sampled at approximately daily intervals and more frequently during the exponential growth phase. The bottles were shaken lightly but thoroughly before sampling to homogenize the suspension. Growth of the bacterial cultures was deemed complete when no change in sulfide, sulfate or protein concentration could be observed, indicating that sulfate reduction was no longer occurring. Bacterial experiments and sample preparation for isotopic analyses were conducted at the University of Ottawa, Dept. of Earth Sciences in Ottawa, Ontario, Canada.

Average cell-specific sulfate reduction rates (fmol $cell^{-1}$ day^{-1}) during the log growth phase were calculated graphically for each experiment using the equation given by Detmers et al. (2001) [Figure 3.3b].

3.4.3 Chemical analyses

In the anaerobic chamber, we first removed 18-20 mL of solution from each of the experiment bottles. Approximately 2 mL were used to measure pH using an Orion Ross Ultra Semi-Micro pH electrode. Sulfide concentration was determined spectrophotometrically (Ultrospec 1100 Pro) on triplicate 1.5-mL samples with the methylene blue method (Cline, 1969). We set aside triplicate 1-mL samples for the determination, outside the glovebox, of protein concentration with the Coomassie Plus (Bradford, 1976) Assay kit (ThermoScientific) using an Ultrospec 1100 pro spectrophotometer. Protein concentration was used as a proxy for cell growth. To the remaining solution, we then added 20% zinc acetate solution to precipitate S(-II) as ZnS and terminate growth. Remaining chemical analyses were performed outside the anaerobic chamber. The $\delta^{3X}S$ values of the sulfate in the growth medium was determined at the initiation of each experiment.

We filtered ≈6 mL of culture solution with 47-mm diameter 0.45-µm pore size PVDF Durapore membrane filters. The filtrate was then separated into two samples: ≈1.5 mL were set aside for sulfate concentration determination (ion chromatography, Thionex ICS-2100); to the rest we added $BaCl_2$ (1 M) to precipitate the sulfate as $BaSO_4$. This $BaSO_4$ was then filtered on a 0.45 µm PVDF Durapore membrane filter, dried, and weighed before conversion to H_2S using a reduction solution (Thode et al., 1961). The sulfide was trapped via an acidified zinc acetate solution (3% v/v glacial acetic acid, 4% w/v zinc acetate dihydrate) to produce ZnS. This ZnS was then converted to Ag_2S by addition of ≈1 mL of 0.1 M $AgNO_3$, filtered, rinsed with Milli-Q water, and dried overnight at 60°C.

3.4.4 Isotope analysis

Approximately 3 mg of the samples in Ag_2S form were loaded into sample pockets made with aluminum foil soaked overnight in methanol. The silver sulfide was reacted with excess F_2 for 8 hours at 250°C in a Ni reaction vessel for conversion to SF_6. When the reaction was completed, this SF_6 was separated from the residual F_2 using a liquid nitrogen trap and the F_2 passivated on a KBr trap. The SF_6 was then heated to -120°C, volatilizing the SF_6 and trapping condensable contaminants. The volatilized SF_6 was then transferred to the injection loop of a gas chromatograph (GC) and cooled to -177°C using liquid nitrogen. Purification of the SF_6 was accomplished by passage through a dual chromatographic column (6' Haysep Q and 6' Molsieve 5A). The isotopic composition ($^{33}S/^{32}S$, $^{34}S/^{32}S$, $^{36}S/^{32}S$) of the SF_6 was determined via dual-inlet isotope ratio mass spectrometry on a Thermo Scientific MAT 253. Isotope analyses were conducted at the McGill University Stable Isotope Laboratory in Montréal, Québec, Canada.

Sulfur isotopic compositions are expressed on a per mil (‰) basis relative to the Vienna Cañon Diablo Standard (V-CDT) using standard notation ($\delta^{34}S$, $\Delta^{33}S$, $\Delta^{36}S$), where $\delta^{3X}S = (^{3X}S/^{32}S_{sample}/^{3X}S/^{32}S_{standard} - 1)$ X 1000 and X=33, 34 or 36, $\Delta^{33}S=\delta^{33}S-1000x((1+\delta^{34}S/1000)^{0.515}-1)$ and $\Delta^{36}S=\delta^{36}S-1000x((1+\delta^{34}S/1000)^{1.90}-1)$. On the V-CDT scale, the international silver sulfide standard IAEA-S1 has a $\delta^{34}S$ value defined as –0.3‰ (Ding et al 2001). We take the $\Delta^{33}S$ value of IAEA-S-1 to be 0.094‰ V-CDT. $\Delta^{33}S$ is a proxy for mass-independent fractionation. The uncertainty on measurements (1σ) was determined from multiple analyses of reference materials and is estimated to be better than 0.1‰ for $\delta^{34}S$, 0.01‰ for $\Delta^{33}S$, and 0.2‰ for $\Delta^{36}S$. Given the analytical uncertainty on $\delta^{36}S$ values, the variations measured in $\delta^{34}S$ values were too small for these to provide additional constraints on sulfur isotope fractionation. As a result, measured $\delta^{36}S$ values are not reported here but were all consistent with mass-

dependent fractionation.

Fractionation factors ($\varepsilon^{34}S$) were determined graphically for each regime using the relationship epsilon = $\delta^{34}S/\ln(f)$ and the change in $\delta^{34}S$ values and the sulfate fraction f (Figure 3.3a). Mass-dependent fractionation between $^{33}S/^{32}S$ and $^{34}S/^{32}S$ is described by the triple isotope fractionation coefficient $^{33}\lambda = \ln[1+^{\delta 3}3S/1000]/\ln[1+\delta^{34}S/1000]$. The $^{33}\lambda$ values were calculated for each of the two regimes identified in the experiments using a bootstrap method with 2000 iterations.

3.5 Results

3.5.1 Growth of cultures

Experiments were terminated when no measurable change in protein concentration has been observed for three consecutive days. Because of accumulated errors in sulfide measurements from repeated dilutions, we do not consider sulfide measurements past the end of the exponential growth phase in our interpretation.

For the GBSRB4.2 strain, no growth was observed in either of the two control experiments. We observed growth in two of the three high-carbon (≈5 mM, “HighC”) experiments, but in one of these only after re-inoculation (18 days after initiation). In the two high-carbon experiments where growth occurred, protein concentrations increased exponentially after an initial lag phase and subsequently stabilized, approaching zero increase in the stationary phase (Figure 3.1). The pH of the medium increased after 3 and 8 days after inoculation, but the exponential growth phase (as indicated by an increase in protein and sulfide concentrations) was delayed for another 3 and 4 days, respectively (Figure 3.1). The initial pH of the solution was 4.2 and increased to 5.8 at the end of the exponential growth phase, continuing to increase slowly to 6.0 until the experiment was terminated. Sulfate concentrations remained stable or decreased

slowly until the beginning of the exponential growth phase, when they dropped rapidly before stabilizing in the stationary phase. Approximately 50-55% of the available sulfate from the initial concentration of ≈18 mM (Figure 3.2b,f) was utilized. Average cell-specific sulfate reduction rates (Figure 3.3b) in the exponential phase were $4.8X10^{-15}$ mol $cell^{-1}$ day^{-1} and $2.5X10^{-15}$ mol $cell^{-1}$ day^{-1} for experiments HighC-1 and HighC-2, respectively. Results were similar for the two high-carbon experiments with this strain: Figure 3.1 shows a representative curve for this strain.

For the M1 strain, growth was observed in all three high-carbon experiments: we present data for only two of these, but results were similar. No growth was observed in the sterile control experiment. There was limited growth in the low-carbon experiment, but it did not proceed to a full-fledged exponential growth phase. The initial pH of 4.0 increased to ≈6.5 in the high-carbon experiments, and to ≈5.8 in the low-carbon experiment. The beginning of the exponential growth phase (increase in protein and sulfide concentrations) took place 3-7 days after inoculation, and ≈2.5 days after the initial rise in pH. The end of the exponential growth phase was reached at 8.9 and 11 days. Sulfate concentrations remained stable or decreased slowly until the beginning of the exponential growth phase, when they dropped rapidly before stabilizing in the stationary phase. Between 13% and 18% of the available sulfate was used (Figure 3.2). Average cell-specific sulfate reduction rates (Figure 3.3b) in the exponential phase were $7.3X10^{-15}$ mol $cell^{-1}$ day^{-1}, and $9.2X10^{-15}$ mol $cell^{-1}$ day^{-1}, and $8.0X10^{-15}$ mol $cell^{-1}$ day^{-1} for experiments High-C1, HighC-2, and LowC, respectively. Results were similar for the two high-carbon experiments for this strain: Figure 3.1 shows a representative growth curve for this strain.

We compared protein concentration, sulfate consumption (remaining sulfate fraction, f), $\delta^{34}S$ and $\Delta^{33}S$ to pH to explore whether these parameters changed as a function of changing pH (Figure 3.2). In the GBSRB4.2 experiments, protein concentrations and

$\delta^{34}S$ values increased slowly until pH reached a value of 5.5, when they increased rapidly until the maximum pH was reached and the experiments were terminated (Figure 3.2a,b). The response was reversed for sulfate concentration and $\Delta^{33}S$, which decreased slowly until pH reached 5.5, before decreasing rapidly (Figure 3.2c,d). Results were similar for the M1 experiments, but the pH at which the switch to a different regime occurred was 5.8 for the high-carbon experiments, while in the low-carbon experiment the second regime was never reached (Figure 3.2e, f, g, h).

Under high-carbon conditions, the growth cycle for both strains studied here was thus characterized by two distinct regimes. In the first regime, pH increased significantly, $\delta^{34}S$ values and protein concentrations remained low, and sulfate and $\Delta^{33}S$ values remained high. For each strain, the switch to the second regime, where pH and protein concentration increased rapidly while sulfate and $\Delta^{33}S$ values decreased, occurred at the same pH value.

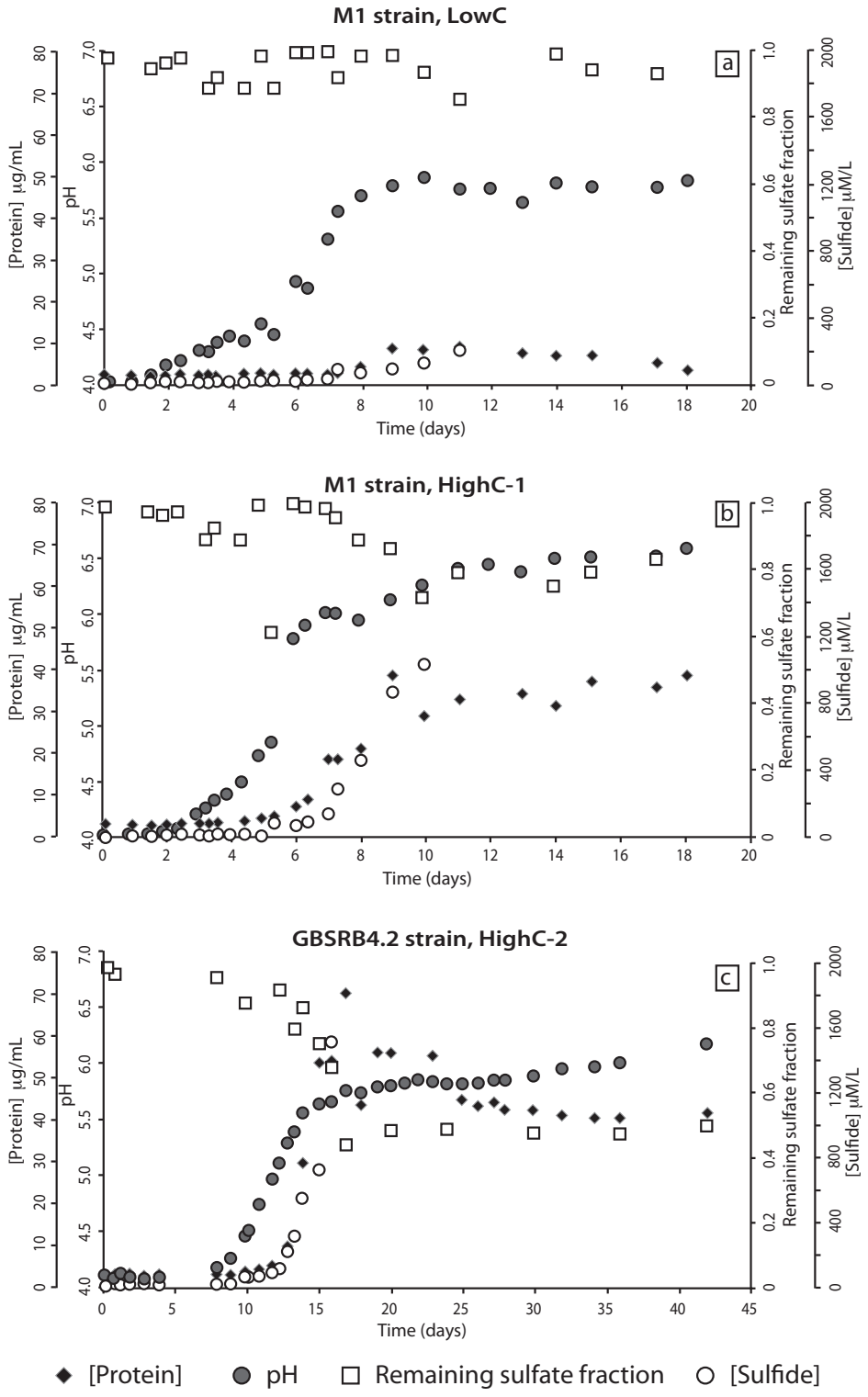

Figure 3.1: Representative growth curves for each strain and experiment (HighC, LowC) showing protein concentration, sulfate concentration, sulfide concentration and pH as a function of time. Sulfide measurements are shown only for the lag and exponential phases, due to errors arising from repeated dilutions.

3.5.2 Stable isotopes

For both strains studied, sulfur isotopic compositions ($\delta^{34}S$, $\Delta^{33}S$) remained virtually unchanged during the first regime, with $\delta^{34}S$ values centered near -1‰ and $\Delta^{33}S$ values centered near -0.02‰ and +0.04‰ (Figure 3.2d,h). In the second regime, $\delta^{34}S$ values increased rapidly while $\Delta^{33}S$ values quickly dropped suddenly (Figure 3.2d,h). For the strain GBSRB4.2, fractionation ($\varepsilon^{34}S$) during the first regime was measurable, but low (<-0.9‰, Table 3.1). During the second regime, $\varepsilon^{34}S$ values were between -10‰ and -11.5‰ (Table 3.1). For the M1 strain, fractionation was <-0.7‰ during the first regime and between 3.7‰ and 5‰ during the second regime (Table 3.1). When each growth regime is considered independently, fractionation was constant across the pH range covered.

We combined data from both M1 experiments to allow for the calculation of $^{33}\lambda$ values using a bootstrap method: results from the GBSRB4.2 strain show that this has little effect on the overall results (Table 3.1). Minor isotope relationships between ^{33}S and ^{34}S were marginally different between the two regimes, with the first regime described by slightly higher $^{33}\lambda$ values. However, there was no significant difference within one standard error (Table 3.1). $^{33}\lambda$ values measured for the M1 strain were significantly greater than those for the GBSRB4.2 strain.

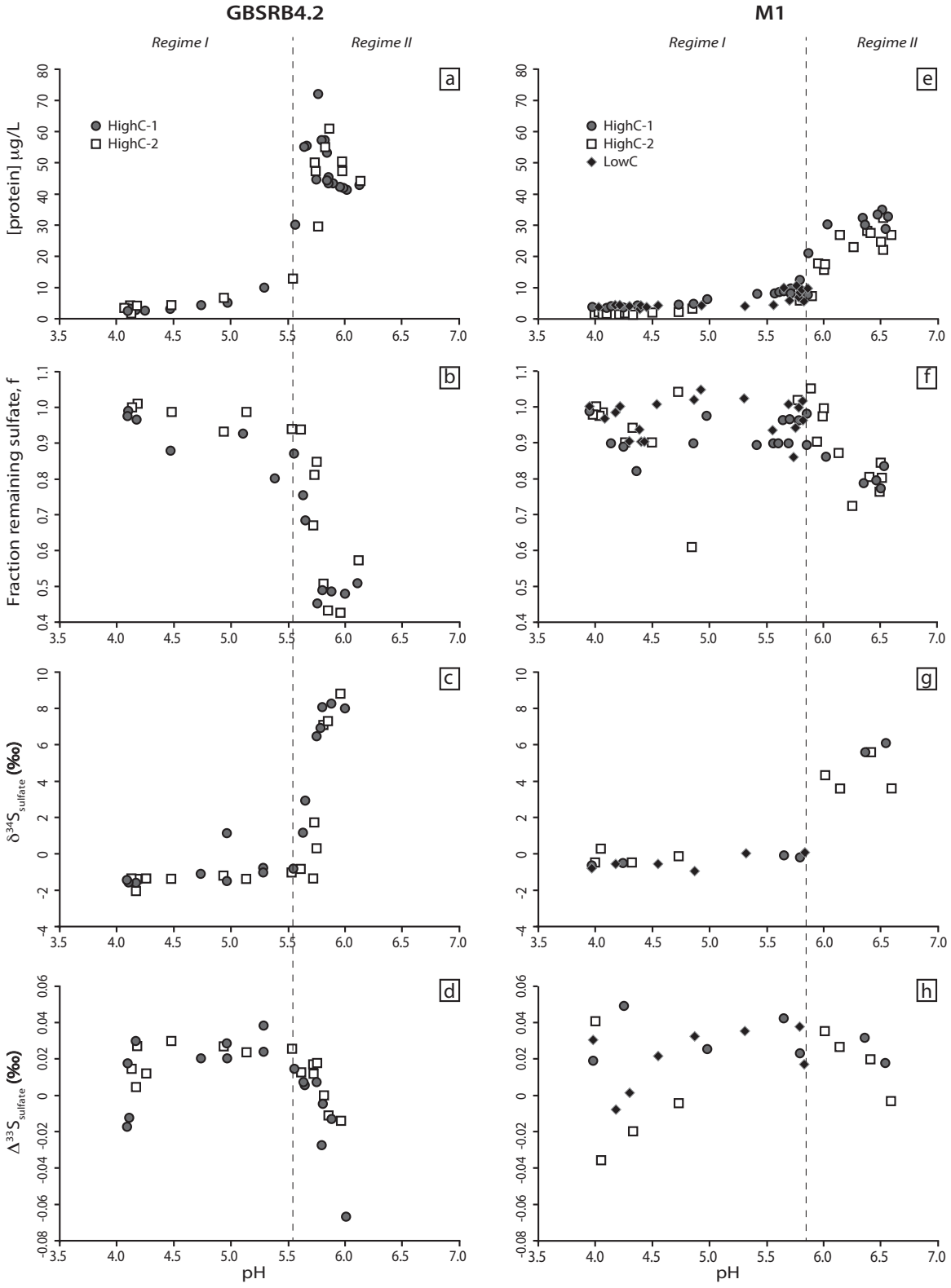

Figure 3.2: Protein concentration, remaining sulfate fraction f, $\delta^{34}S$, and $\Delta^{33}S$ as a function of pH. The two different fractionation regimes identified in the experiments are shown.

Table 3.1: Sulfur isotope effects during the growth of M1 and GBSRB4.2. The errors on $^{33}\lambda$ values were calculated using a bootstrap method. $\varepsilon^{34}S$ values were determined graphically (see Methods).

		Fractionation Regime I		Fractionation Regime II	
Strain	**Treatment**	$^{33}\lambda$	$\varepsilon^{34}S$ (‰)	$^{33}\lambda$	$\varepsilon^{34}S$ (‰)
GBSRB4.2	HighC-1	0.5239±0.0552	-0.5	0.5118±0.0025	-9.8
	HighC-2	0.5256±0.0157	-0.9	0.5101±0.0146	-11.5
M1	LowC	0.5265±0.0626	-0.7	NA	NA
	HighC*	0.4960±0.0555	-0.4	0.5185±0.0134	-3.7, -5.0

**Results from the two experiments combined*

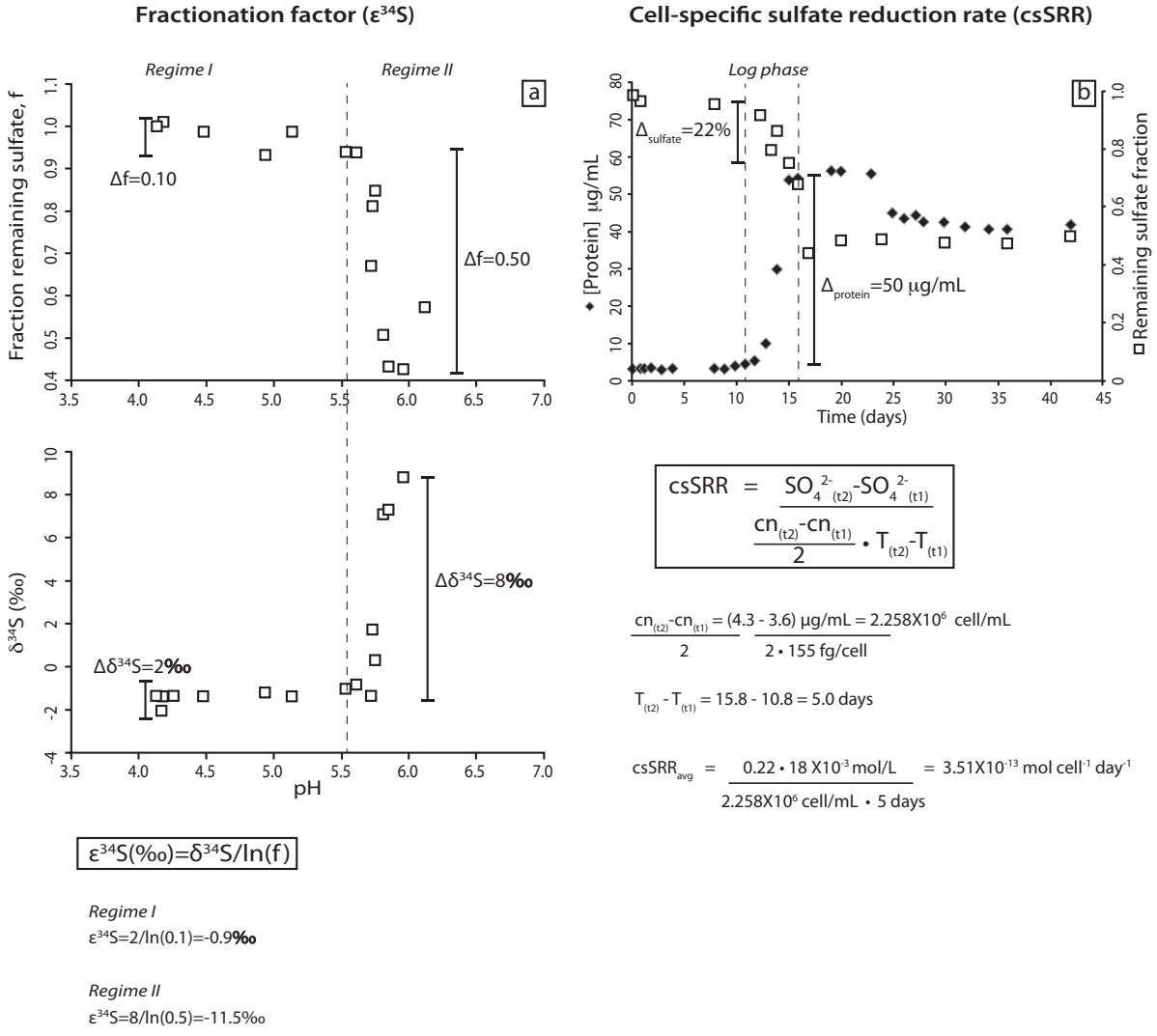

Figure 3.3: Graphical method used to calculate the fractionation factors ($\varepsilon^{34}S$, a) and cell-specific sulfate reduction rates (csSRR, b).

3.6 Discussion

A key objective of our study was to investigate the effect of pH on sulfur isotope fractionation during MSR. In a closed system where the conversion of the sulfate to sulfide is incomplete and fractionation is constant, a plot of $\delta^{34}S_{reactant}$ against the remaining sulfate fraction f yields a straight line (Rayleigh distillation effect; Mariotti et al., 1981). Our investigation of sulfur fractionation during MSR for two acidophilic strains of sulfate-reducers shows that fractionation was not constant across the pH range of the experiments. Two distinct regimes of fractionation were identified.

One fractionation regime (regime II) corresponds to the exponential growth and stationary phases of the microbial growth cycle and is consistent with the results of previous studies investigating sulfur isotope fractionation during microbial sulfate reduction. This regime is characterized by rapid growth accompanied by rapid sulfate depletion and significant sulfur isotope fractionation. Fractionation during this phase (4-12‰), as measured using the enrichment factor $\varepsilon^{34}S$, is consistent with previous measurements of fractionation during MSR by incomplete oxidizers (2-19‰; Detmers et al., 2001), as is the mass-dependent relationship between ^{33}S and ^{34}S, described by $^{33}\lambda$ (Farquhar and Wing, 2003; Johnson et al., 2005; Johnson et al., 2007; Sim et al., 2011). There was no evidence, as expected, of mass-independent fractionation, as indicated by the $\Delta^{33}S$ values near zero. Cell-specific sulfate reduction rates were also in the range reported for incomplete oxidation of carbon during MSR (fmoles $cell^{-1}$ day^{-1}) [Detmers et al., 2001; Sim et al., 2011].

Where our results depart from those of previous studies is in the identification of a distinct fractionation regime associated to the portion of the growth cycle taking place during the lag phase, before the initiation of exponential growth and sulfate reduction. This regime features a large increase in pH that is not accompanied by significant microbial growth or substantial sulfur isotope fractionation. It also displays a decou-

pling between the initiation of a change in pH, the production of sulfide (signaling the initiation of active sulfate reduction), and the increase in protein concentration (proxy for cell growth). This decoupling is more apparent for the GBSRB4.2 strain, which has a notably long lag phase, lasting up to several days (Senko et al., 2009). The shift to the second regime appears to coincide with the beginning of the exponential growth phase, as indicated by a rapid increase in protein concentration. This hints at a parallel mechanism contributing to the increase of pH in the growth environment, one not linked to the oxidation of carbon during MSR and the production of HCO_3^-, which increases pH. Fractionation during this first regime is small, but measurable, with $\varepsilon^{34}S$ values < 0.9‰. Most studies of sulfur isotope fractionation during sulfate reduction by bacteria have used near-neutral pH strains that typically have relatively short growth cycles (a few days at most): this may explain why fractionation during the lag phase of the growth cycle has apparently not been measured previously.

A possible explanation for the change in pH prior to the initiation of microbial sulfate reduction is internal sulfate accumulation coupled to the uptake of protons from the solution. Significant accumulation of sulfate by sulfate-reducing bacteria has been identified previously (Cypionka 1987; 1989). In most freshwater species, this process is accomplished with the concurrent uptake of two or three protons via a symport (Cypionka, 1987; 1989; Warthmann and Cypionka, 1990). Cells in the lag phase may have been accumulating internal sulfate concurrently with the uptake of protons from the growth environment, increasing pH, prior to the initiation of sulfate reduction. Fractionation during this initial regime is measurable and in the same direction as that measured during the exponential growth phase: lighter isotopes are favored, resulting in enrichment in ^{34}S of the remaining sulfate. If an accumulation process is responsible for the increase in pH prior to the initiation of sulfate reduction, our results could represent the first successful measurement of the fractionation associated to the first step of the sulfate reduction metabolism; the uptake of sulfate from the growth

environment. It should be noted that the fractionation factor measured for the first regime is in the same order of magnitude but goes in the opposite direction of that proposed in sulfate reduction models (e.g., Rees 1973). Further experimentation with strains characterized by long growth cycles and lag phases are needed to test this hypothesis.

A central objective of this study was to determine whether pH exerts an effect on fractionation of sulfur during microbial sulfate reduction. We speculated that a change in the proton gradient between the growth environment and the cytoplasm could affect sulfur fractionation. Our results indicate that fractionation is not constant across the pH range observed in our experiments, but it is unclear as to what mechanism is specifically responsible. If fractionation during the first phase results mostly from internal accumulation of sulfate unaccompanied by sulfate reduction, then it is possible that the switch to the second phase of fractionation at what appears to be a specific pH for each strain is related to the transmembrane proton gradient (ΔpH). Studies of internal sulfate accumulation by sulfate-reduction bacteria indicate that this parameter exerts an effect on alkalinisation and sulfide production and drives the uptake of sulfate from the growth medium (Cypionka 1987; 1989), suggesting that accumulation is enhanced at high transmembrane pH gradients, but inhibited when the environmental pH is close to or greater than the internal pH (Warthmann and Cypionka 1990). The switch to a different fractionation regime at a specific pH for each strain may indicate a change in metabolic activity related to the transmembrane pH.

Our results suggest that pH exerts an effect on fractionation of sulfur isotopes insofar as it plays a role in determining when the initiation of the bacterial sulfate reduction process takes place: if the growth cycle of the two strains studied here is considered in two distinct phases, then for each phase the extent of fractionation ($\varepsilon^{34}S$) and the mass-dependent relationship between ^{33}S and ^{34}S is constant. Our results suggest

that this effect of pH on fractionation is related to a change in metabolic activity and is not gradual or progressive as pH in the growth environment is changing.

3.7 Conclusion

Our results represent the first measurement of sulfur isotope fractionation for acidophilic sulfate reducers. We identified two regimes of fractionation that appear to be related to a change metabolic activity. The regime corresponding to the exponential and stationary growth phases is consistent with that identified in previous studies and is associated with significant isotope fractionation. The regime corresponding to the lag phase and associated to minimal sulfate reduction has to our knowledge not been identified previously. The switch to the second fractionation regime occurred at a specific pH for each strain and suggests that the initiation of active sulfate reduction is linked to the transmembrane pH gradient. The increase in pH during the first regime, prior to the initiation of sulfate reduction, may be associated to internal sulfate accumulation, with the uptake of protons concurrently with the sulfate ion leading to an increase in pH.

3.8 Acknowledgements

We extend our thanks to John Senko (University of Akron) and D. Barrie Johnson (Bangor University) for providing the pure cultures of acidophilic sulfate-reducing bacteria. We also thank John Senko and Alexandre Poulain (University of Ottawa) for helpful discussions, and Marc-André Cyr, Kizil Reder, André Pelletier, Thi Hao Bui and Grant Cox for lab assistance. Funding for this study was provided through NSERC Discovery Grants (DF and BW) and an NSERC Post-Graduate Scholarship (MLC).

Chapter 4 : Sulfur isotopes reveal that peak of Deccan volcanism post-dates the Cretaceous-Paleogene mass extinction

4.1 Contributions

The samples used in this study were collected by François Therrien and colleagues from the Royal Tyrell Museum of Paleontology (Drumheller, Alberta) for the purposes of investigating the stable carbon isotope and pollen records of the two KPg boundary sections featured in this study (Therrien et al., 2007). The candidate prepared and analysed the samples for sulfur concentration and sulfur stable isotope composition, in collaboration with Teruyuki Maruoka at the University of Tsukuba, Tsukuba, Japan (Graduate School of Life and Environmental Sciences), during a research internship under the auspices of the NSERC Japan Summer Program (2010). The data analysis and interpretation, and the preparation of the manuscript and figures were a joint effort between the candidate and Boswell Wing (Dept. Earth and Planetary Sciences, McGill University). François Therrien, Teruyuki Maruoka and Danielle Fortin commented on an earlier version of the manuscript.

Cousineau, M.L., Therrien, F., Maruoka, T., Fortin, D., and Wing, B.A. In preparation

4.2 Abstract

The mass extinction at the Cretaceous-Paleogene (KPg) boundary decimated marine and terrestrial species around the globe. Two major geologic events, the Chicxulub bolide impact and the eruption of the Deccan continental flood basalts, coincide with the KPg boundary and have been identified as possible triggers for the extinction, but their relative timing remains unresolved. From measurements of sulfur abundance and isotope composition at an exceptionally well-preserved terrestrial KPg boundary section in Alberta, Canada, we demonstrate that the peak of Deccan volcanism postdates the Chicxulub impact and the associated abrupt KPg mass extinction. The late occurrence of Deccan volcanism precludes a direct causal relationship with the mass extinction, but sheds light on underlying causes for the delayed recovery of ecosystems in the early Paleogene.

4.3 Main Text

The Cretaceous-Paleogene (KPg) boundary marks one of the most significant biotic turnovers in Earth history (1, 2), leaving an evolutionary imprint that can still be seen in the modern biota (3). The KPg mass extinction selectively reshaped marine and terrestrial ecosystems (4-7) and ultimately led to the demise of dinosaurs and subsequent radiation of mammals (2, 5, 8). Despite more than thirty years of research, the hypothesis of an extraterrestrial cause for the KPg extinctions (9), with dust from a bolide impact shading Earth's surface and leading to the catastrophic collapse of global food webs, still causes controversy (10-14). The primary competing hypothesis to an impact-driven mass extinction links the emplacement of the Deccan Traps – continental flood basalts that cover a surface area of ≈500 000 km^2 in western India (15) – to the KPg biotic crisis, either as a sole actor or against a backdrop of falling sea levels and fluctuating global temperatures (10-14, 16). Although impact- and vol-

canism-driven extinction scenarios predict different extinction patterns (5, 17, 18), the establishment of causal relationships relies fundamentally on the relative timing of extinction triggers across the KPg boundary. Radiometric and magnetostratigraphic age measurements show that the largest Deccan eruptions and the Chicxulub impact were roughly contemporaneous across the KPg boundary (16, 19), but are too uncertain to determine the relative timing of these events.

A common feature of both proposed triggers is the associated atmospheric release of massive amounts of sulfur (20, 21). In an oxidizing atmosphere, enhanced atmospheric S input is expected to increase the atmospheric burden of sulfate aerosols, disrupting Earth's radiative balance (22). The climatic effects of this S, along with dust, halogens, and CO_2, are a critical component of extinction scenarios accompanying the Chicxulub impact and Deccan eruptions (10-14). Injection of sulfur, dust and ash particles into the stratosphere, where global dispersion can occur rapidly, has been directly observed for volcanic events many orders of magnitude less energetic than the Chicxulub impact (22). For example, global climatic change followed the 1991 eruption of Mount Pinatubo (23), which explosively introduced 9 Teragrams of S (Tg S) (24) on top of a natural background volcanic S flux of 9 – 46 Tg S per year (25). Estimates of atmospheric S injections from the Chicxulub impact dwarf these numbers: ≈0.4 to 5.6×10^5 Tg S may have been released almost instantaneously into the atmosphere (21). In comparison, the S released over the full eruptive history of the Deccan Traps could have ranged from ≈1.7 to 3.5×10^6 Tg S (20, 26), with atmospheric S loadings from the largest single eruptive events potentially comparable to that from the Chicxulub impact (26).

Sulfur released by the Chicxulub impact would have primarily been derived from late Maastrichtian seawater and the ≈3-km-thick sequence of Cretaceous evaporite- and carbonate-bearing target rocks present at the impact site (27), whereas sulfur released

by Deccan volcanism would have an igneous origin. Maastrichtian seawater, Upper Cretaceous evaporites, and Chicxulub target evaporites have $\delta^{34}S$ values centered around ≈18‰ (28-30) while sulfate aerosols collected at active basaltic vents are characterized by much lower $\delta^{34}S$ values [≈8‰ (31)]. Consequently, in KPg stratigraphic sections characterized by low sulfur content, such as those deposited in terrestrial settings, S isotope profiles should reflect the relative contributions of impact- versus volcanism-derived S (32).

The Knudsen's Coulee Section (KCS) and Knudsen's Farm Section (KFS), located near the town of Drumheller, Alberta, Canada (Fig. 4.S1), are among the most complete and best-preserved terrestrial KPg sections in North America's Western Interior. These sections features lithological, paleontological, and geochemical markers indicative of the terrestrial KPg boundary including, at KCS, a three-part boundary claystone layer representing the initial ballistic melt ejecta, an early-formed 'fireball' layer of condensed vapor from the impactor and target rocks, and a later-formed layer of fine particles rich in Ir and sulfate aerosols (33). In order to constrain the relative timing of the Chicxulub impact and Deccan volcanism, we measured whole-rock S content and isotopic composition ($\delta^{34}S$) at an ultrahigh stratigraphic resolution (2 cm or less) at these sections. We focus our discussion on the KCS because it is exceptionally well preserved (33).

Sulfur contents and $\delta^{34}S$ values show similar behavior at the KCS (Fig. 4.1A, 4.1B). Below the KPg boundary claystone, S contents are extremely low, generally less than 0.2 wt%, while $\delta^{34}S$ values vary mildly (±2‰) around a mean value of ≈6.5‰. These features provide a favorable backdrop for monitoring ^{34}S-rich S addition to the sulfur-poor KCS sedimentary system. Within the three-part boundary claystone, S contents stay below 0.1 wt% in the first two subunits (hackly and satiny layers) but increase dramatically to ≈0.7 wt% in the uppermost subunit (laminated shale). Bulk $\delta^{34}S$ values

in the boundary claystone rise from ≈4‰ in the hackly layer to ≈16‰ in the laminated shale, the highest value measured at the KCS. High S contents persist over a ≈5 cm-interval above the boundary claystone before returning to <0.1 wt% by ≈10 cm. Over this same distance, $\delta^{34}S$ values decrease more steadily and bottom out at <2‰. Both S contents and $\delta^{34}S$ values exhibit second smaller peaks centered at ≈20 cm above the boundary claystone, where sulfur contents reach ≈0.5 wt % and $\delta^{34}S$ values rise to ≈10‰. The $\delta^{34}S$ peak is broader than the S content peak, spanning ≈15 cm rather than ≈10 cm.

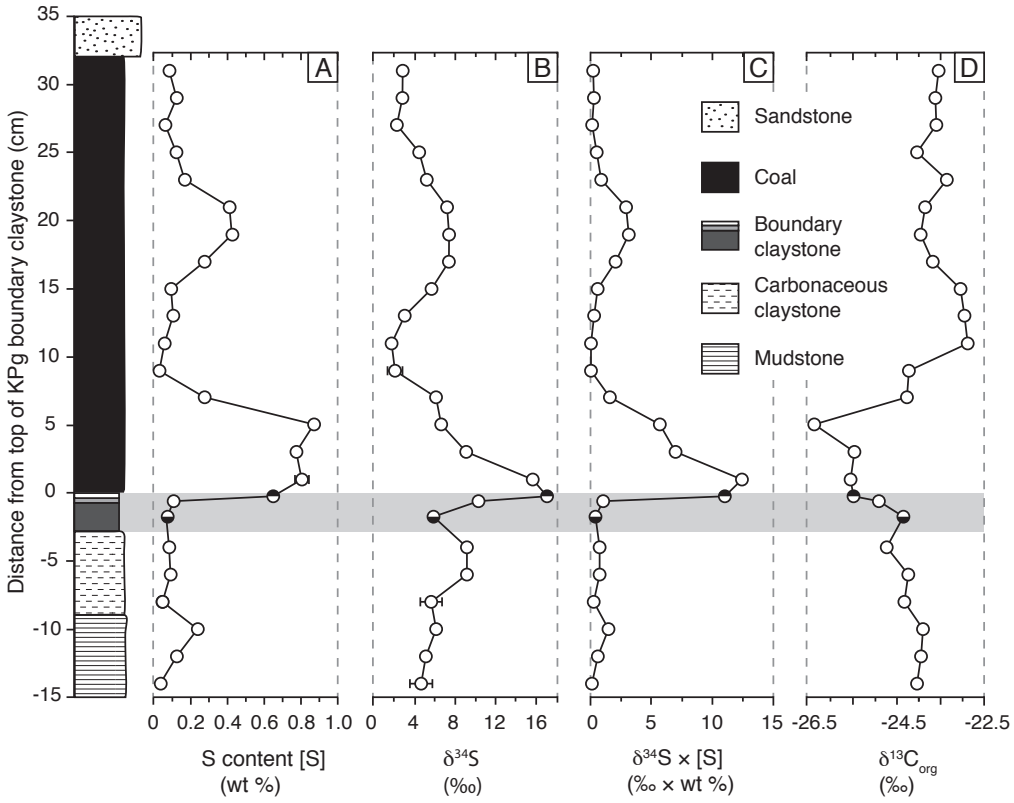

Fig. 4.1: Whole-rock S content [S] (A) and $\delta^{34}S$ values (B) at the Knudsen's Coulee KPg section. Data points represent 2 cm-thick sample intervals, except in the boundary claystone where samples were taken at higher resolution (in each subunit). Symbols are plotted at the midpoints of sample intervals. Error bars on S content and $\delta^{34}S$ values indicate standard deviation from the mean of three measurements. Where error bars are not visible, they are smaller than the symbols used. (C) Plot of $\delta^{34}S \times [S]$ representing the amount of ^{34}S-rich S added to the sediment. (D) Bulk $\delta^{13}C_{org}$ values from (38). Peaks in ^{34}S-rich S addition coincide with negative $\delta^{13}C$ excursions. The shaded area indicates the boundary claystone, which is divided into a three-part microstratigraphy of a hackly layer (gray), satiny layer (white), and laminated shale (black). Upper-half filled symbol reflects the sample from the hackly layer, while lower-half filled symbol reflects the sample from the laminated shale.

The close correspondence between increases in S contents ([S]) and $\delta^{34}S$ values throughout the KCS section suggests that addition of ^{34}S-rich S occurred across the KPg boundary. This hypothesis is corroborated by variations in $\delta^{34}S \times [S]$, a quantity that provides an estimate of the amount of ^{34}S-rich S in the system and emphasizes changes in ^{34}S-rich S relative to background conditions (Fig. 4.1C). The $\delta^{34}S \times [S]$ profile shows little deviation from background values except for two distinct peaks: an asymmetrical peak, starting in the upper boundary claystone and irregularly declining over the next 10 cm, and a second, more moderate and symmetrical peak situated 17-23 cm above the boundary claystone. These peaks indicate that addition of ^{34}S-rich sulfur took place during two discrete time intervals in the early Paleogene.

This ^{34}S-rich sulfur was added to a S-poor and low-$\delta^{34}S$ background population at the KCS, defined by a cluster of ≈10 points on a cross-plot of $\delta^{34}S$ values and [S] (Fig. 4.2). With increasing S content, one array of measurements extends from this background population to a plateau around $\delta^{34}S$ values approaching ≈8‰ (Fig. 4.2). A second array of measurements rises more rapidly, and levels out around a much higher $\delta^{34}S$ value approaching ≈18‰ (Fig. 4.2). The hyperbolic forms of these arrays are consistent with addition of sulfur from two distinct ^{34}S-rich S sources (33). The $\delta^{34}S$ value for the end-member of the lower array of samples is similar to sulfate aerosols from volcanogenic S oxidized at active sites of basaltic degassing (Fig. 4.2; (31)), whereas that of the end-member of the upper array of samples is comparable to Chicxulub target rocks, Upper Cretaceous evaporites and Maastrichtian seawater (Fig. 4.2; (28-30)). The lack of volcanic detritus in the ^{34}S-rich S parts of the KCS suggests a distal source for the volcanic sulfur identified here. Accordingly, we propose that the KCS section contains ^{34}S-rich S derived from Deccan volcanism and the Chicxulub impact. Our high-resolution sampling at the KCS has permitted, for the first time, recognition of the S isotope signatures of both terminal Cretaceous events at a single location.

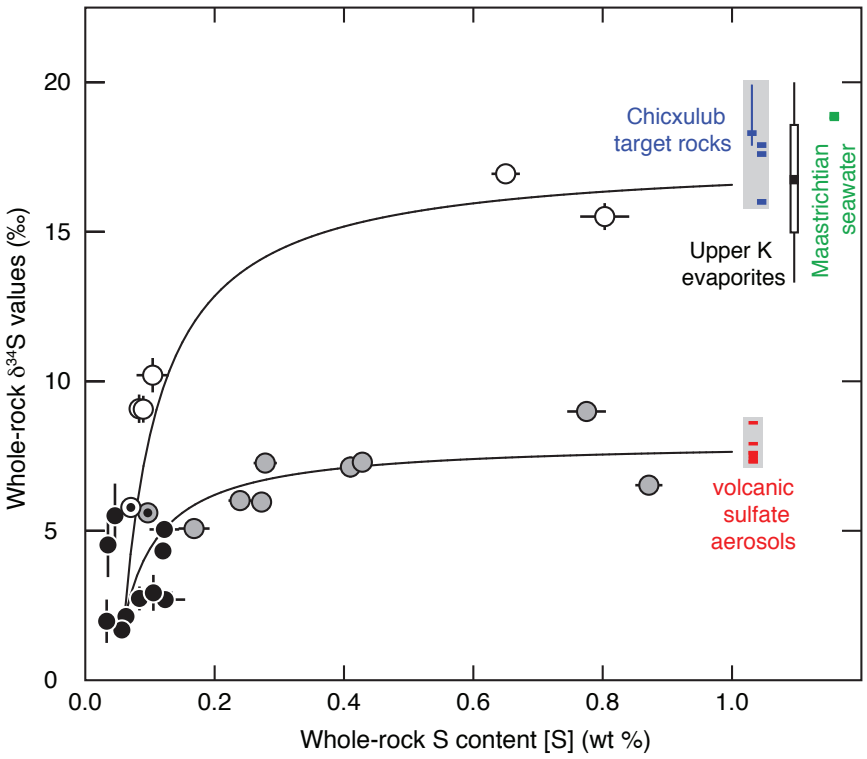

Fig. 4.2: Cross plot of whole-rock S contents and $\delta^{34}S$ values measured at the Knudsen's Coulee KPg section. The upper array is consistent with addition of S from Chicxulub target rocks and end-Cretaceous seawater and evaporites. The lower array is consistent with addition of S from oxidized volcanic SO_2. Hyberbolic curves show the calculated results of mixing S characterized by $\delta^{34}S$ = 17.5‰ (upper curve) and $\delta^{34}S$ = 8‰ (lower curve) into a background S pool characterized by [S] = 0.06 wt % and $\delta^{34}S$ = 2 ‰. White circles show samples incorporating impact S, gray circles show samples incorporating volcanic S, and black circles show samples that make up the background population.

To determine the relative timing of sulfur input derived from the Chicxulub impact and Deccan volcanism, we mapped the proposed sources of ^{34}S-rich S onto the $\delta^{34}S \times [S]$ profile (Fig. 4.3) and searched for the minimum number of Gaussian pulses needed to reproduce the measured variations (33). The profile modeling requires ^{34}S rich sulfur addition to have occurred in three pulses at the KCS: a pair of overlapping pulses originating at the KPg boundary and a second pulse centered ≈20 cm above the boundary claystone (Figs. 4.3, 4S4, 4S5). One of the overlapping pulses is brief and intense, restricted to the first centimeter above the KPg boundary claystone, whereas

the other is wider and more moderate, spanning a 10-cm interval above the boundary claystone. Based on the inferred ^{34}S-rich S source of each sample, we conclude that the spike at the KPg boundary is derived from the injection of impact-derived sulfate aerosols while the two broad pulses record addition of Deccan volcanic sulfate. These results reveal that the Chicxulub bolide impact coincided with the beginning of a Deccan volcanic eruptive phase at the KPg boundary (Fig. 4.3).

Recent high-resolution measurements of ^{187}Os/^{188}Os values from marine sediments are seemingly in conflict with this proposal. They show an initial decline at the start of magnetic polarity chron C29r (≈300 kyrs before the KPg boundary), followed by a brief plateau of unchanging values, and then a sharp decrease coinciding with Ir maxima (34, 35). This record is interpreted as an initial input of Deccan volcanic Os preceding the impact-induced isotopic signal at the KPg boundary. However, mass balance calculations suggest that the initial decline in ^{187}Os/^{188}Os values is too large to be strictly the result of an increased input of non-radiogenic Os from the Deccan basalts; removal of a source of radiogenic Os is also necessary (34, 35). Low-volume, early-erupted Deccan flows, if they covered Archean crust, would have had the required effect (35). The pre-KPg boundary ^{187}Os/^{188}Os record may only signal the initiation of main-phase Deccan volcanism (34), while the S isotope record instead reflects the intensity, duration, and frequency of the full Deccan eruptive history. In addition, seismic reflection, magnetic, and gravity data reveal a substantial pre-Deccan (Campanian-Maastrichtian) volcanostratigraphic province off the Western shore of India, with a minimum estimated volume ≈20-25% of the Deccan continental flood basalts (36). The submarine nature of this pre-Deccan eruption would lead to a direct transfer of volcanic Os to the oceanic environment, suggesting that it could have caused the marine ^{187}Os/^{188}Os drop prior to the KPg boundary. Any S emissions accompanying a submarine volcanic eruption, however, would be unlikely to leave an S isotope signal in terrestrial sediments. Given these viable explanations for the apparent discrepancy

between the S and Os isotope chemostratigraphies, we use the new record at KCS to examine the intensity and duration of S input from the Chicxulub impact and Deccan volcanism.

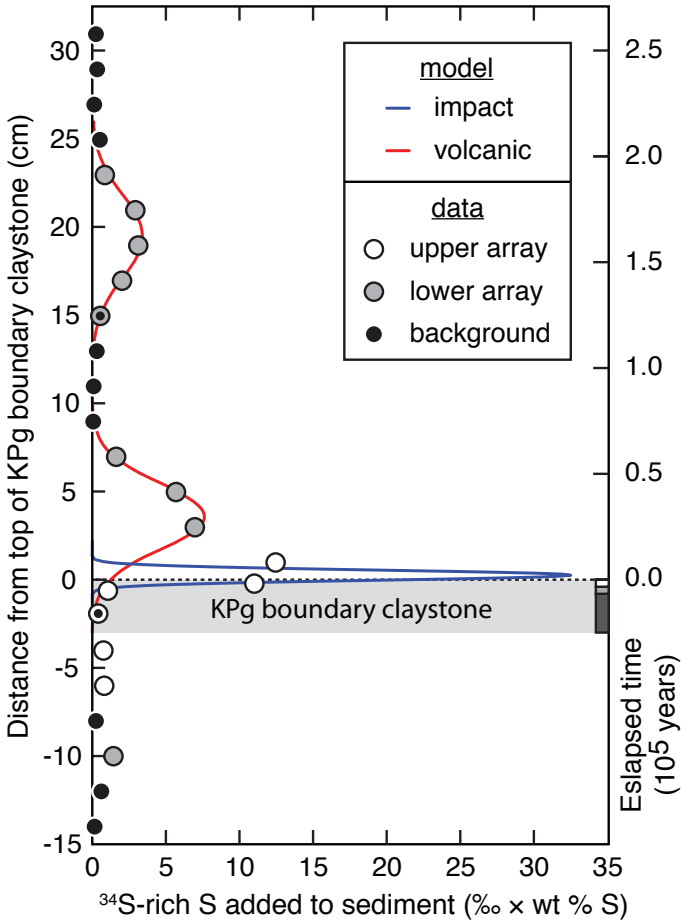

Fig. 4.3: Gaussian model of S addition to the Knudsen's Coulee KPg sedimentary environment. The timescale is derived from a chronological calibration of sediment thicknesses at this section (29). Symbols reflect the origin of ^{34}S-rich S added to the system (Fig. 4.2). The isotopic composition of the two samples immediately below the boundary claystone appears to be influenced by minute amounts of impact-derived S that percolated into the underlying strata in the post-impact acidic weathering environment. The boundary claystone microstratigraphy is represented as in Fig. 4.1.

By comparing the relative areas under the impact and volcanic S pulses at the terrestrial Knudsen's Coulee section (Fig. 4.3), we calculate that Chicxulub-derived S

accounts for ≈16% of the total amount of sulfur added to the KCS sedimentary environment (33). The volcanic pulse at the boundary accounts for ≈54% of the added S, while the second volcanic pulse accounts for ≈30% (33). This yields a ratio of ≈5.5:1 for sulfur derived from Deccan volcanism relative to the Chicxulub impact, in line with independent published estimates, which range from 3:1 to 88:1 (see above). The second volcanic pulse, although recorded over a similar length interval to the first eruptive pulse, represents only about half of its intensity in terms of S addition to the KCS sedimentary environment. This is consistent with estimates of S fluxes for the two later phases of Deccan volcanism (26).

The duration of the volcanic pulses can be estimated based on the chronological calibration of sediment thicknesses at KCS (33). Any estimate of the duration of the impact-derived sulfur pulse would be overestimated, due to the integrated nature of our sampling method. The first pulse of S input from Deccan volcanism, which began at the KPg boundary, ended ≈90 kyrs after the impact. A second, more moderate, pulse of volcanic S addition began approximately 30 kyrs later and lasted for ≈90 kyrs. Aside from a minor, geographically-restricted early phase of volcanism occurring ≈2-3 million years prior to the KPg boundary (26), current interpretations call on two brief, intense, and closely spaced phases of Deccan eruptions lasting 200-300 kyrs (19, 26), consistent with our environmental scenario.

Where our environmental scenario departs significantly from previous interpretations of the KPg transition is in the relative timing of the two proposed extinction triggers. Some stratigraphic examinations of the relationship between impact and volcanism suggest that the impact emplacement of the Ir-rich KPg claystone layer took place at the end of a major volcanic phase (16, 34, 37). In a recent paleomagnetic and geochronological reconstruction of Deccan eruptions, the major volcanic phase was positioned as starting before the KPg boundary and ending precisely at the boundary,

followed by a less intense phase of eruptions (19). However, an internally-consistent reconstruction of absolute ages across the KPg boundary shows that many of the stratigraphically-controlled main phase Deccan flows could have erupted after the impact defining the KPg boundary (Fig. 4.S7). The KCS S isotope profile, in fact, demonstrates that this is the case. The Chicxulub impact coincided with the beginning of the main Deccan volcanic eruptive phase at the KPg boundary, this main phase lasted for ≈90 kyrs, and the secondary eruptive phase started ≈30 kyrs after the main phase ended, lasting for another ≈90 kyrs (Fig. 4.3).

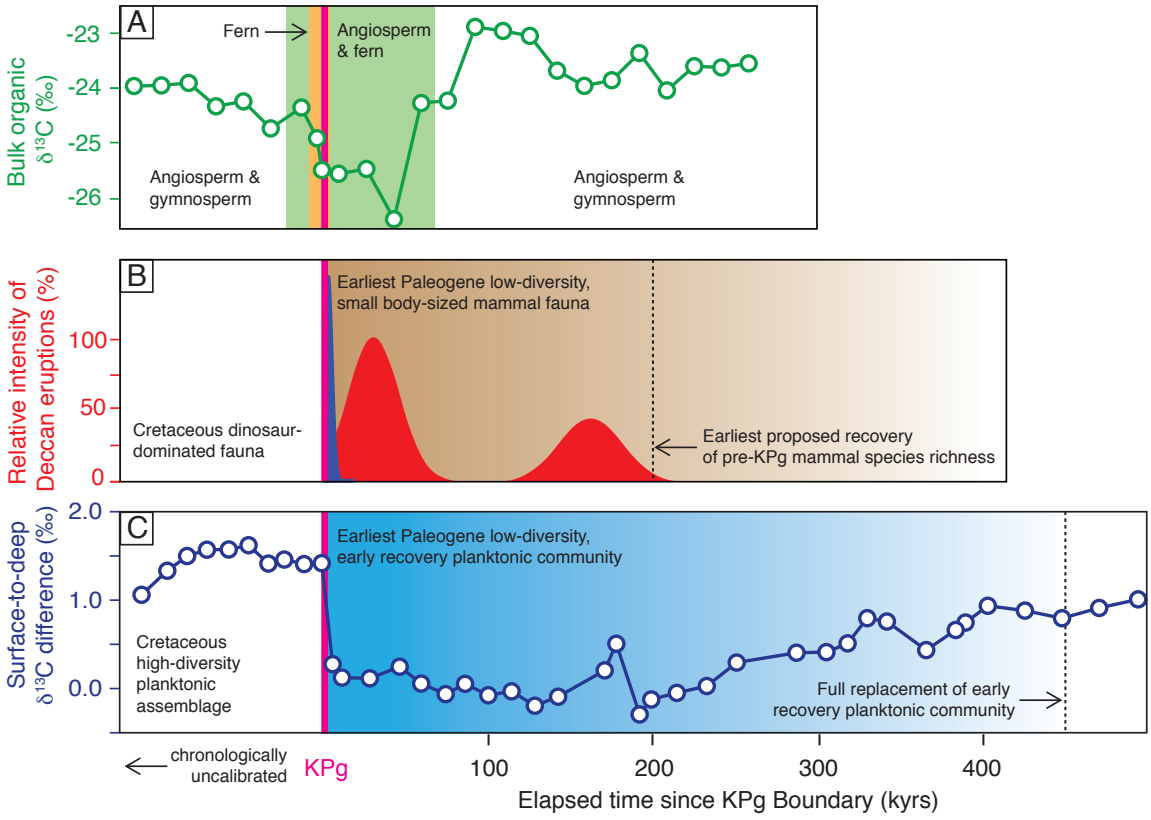

Fig. 4.4 Chronology of environmental and biological events across the KPg boundary in the Northern Hemisphere. Records prior to the KPg boundary are not chronologically calibrated but are included for reference. (A) Ecological recovery in terrestrial floras as monitored by $\delta^{13}C_{org}$ values and dominant floral assemblages at Knudsen's Coulee KPg section (29). (B) Relative timing of KPg boundary, Chicxulub impact S input (shown in blue, unscaled), and the two major phases of Deccan volcanism (shown in red). Recovery dynamics of terrestrial faunas from the Western Interior are superimposed (39). (C) Early ecological recovery in the pelagic marine environment as monitored by surface-to-deep $\delta^{13}C$ gradients and community structure from ODP hole 1209, Shatsky Rise, North Pacific (43).

Our new high-resolution environmental chronology indicates that the Chicxulub impact was the primary trigger for the KPg mass extinction, and argues against a causal relationship between Deccan volcanism and the extinctions. However, the massive amounts of sulfur released by the Deccan eruptions must have had deleterious ecological consequences (12, 20), raising the possibility that Deccan eruptions could have led to the delayed recovery of Paleogene ecosystems. Patterns of ^{34}S-rich S addition and $\delta^{13}C$ values in terrestrial organic matter show a clear inverse correlation throughout the KCS and KFS (Figs. 4.1, 4.S3). Minimum $\delta^{13}C_{org}$ values are reached during the peak of the major Deccan eruptive phase while pre-boundary $\delta^{13}C_{org}$ values and floral compositions return right after the first volcanic phase ended, ≈100 kyrs into the Paleogene ((38); Fig. 4.4A, 4.4B). In the Western Interior, depauperate and small-sized terrestrial vertebrate faunas characteristic of the earliest Paleogene began their recovery between ≈200 and 400 kyrs after the KPg boundary ((39, 40); Fig. 4.4B), in general coincidence with the end of the secondary Deccan eruptive phase. Surface-to-deep $\delta^{13}C$ profiles through deep sea sediments show that marine ecosystems experienced longer-lasting perturbations ((41); Fig. 4.4C), perhaps initially resulting from volcanically-induced metal poisoning (18) or ocean acidification (42). Early communities of bloom and disaster taxa dominated pelagic ecosystems for ≈450 kyrs in the North Pacific ((43); Fig. 4.4C), suggesting that the initiation of marine ecosystem recovery was delayed until after the complete cessation of Deccan eruptions. Although the Chicxulub impact may have triggered the KPg boundary mass extinction, the major eruptive phases of the Deccan Traps appear to have paced the tempo of marine and terrestrial ecosystem recovery into the brave new Paleogene world.

4.4 References and Notes

1. J. Alroy, Dynamics of origination and extinction in the marine fossil record. Proceedings of the National Academy of Sciences of the United States of America 105, 11536-11542 (2008).

2. R. Meredith et al., Impacts of the Cretaceous terrestrial revolution and KPg extinction on mammal diversification. Science 334, 521-524 (2011).

3. A. Krug, D. Jablonski, J. Valentine, Signature of the End-Cretaceous mass extinction in the Modern Biota. Science 323, 767-771 (2009).

4. D. J. Nichols, K. R. Johnson, Plants and the K-T Boundary (Cambridge University Press, Cambridge, 2008), p. 280.

5. J. D. Archibald, Extinction and radiation: How the fall of dinosaurs led to the rise of mammals (The Johns Hopkins University Press, Baltimore, 2011), p. 108.

6. S. D'Hondt, Consequences of the cretaceous/paleogene mass extinction for marine ecosystems. Annual Review of Ecology Evolution and Systematics 36, 295-317 (2005).

7. P. Sheehan, D. Fastovsky, Major extinctions of land-dwelling vertebrates at the Cretaceous-Tertiary Boundary, Eastern Montana. Geology 20, 556-560 (1992).

8. F. Smith et al., The evolution of maximum body size of terrestrial mammals. Science 330, 1216-1219 (2010).

9. L. W. Alvarez, W. Alvarez, F. Asaro, H. V. Michel, Extraterrestrial cause for the Cretaceous-Tertiary extinction - Experimental results and theoretical interpretation. Science 208, 1095-1108 (1980).

10. P. Schulte et al., The Chicxulub asteroid impact and mass extinction at the Creta-

ceous-Paleogene Boundary. Science 327, 1214-1218 (2010).

11. J. Archibald et al., Cretaceous Extinctions: Multiple Causes. Science 328, 973 (2010).

12. V. Courtillot, F. Fluteau, Cretaceous extinctions: The volcanic hypothesis. Science 328, 973-974 (2010).

13. G. Keller et al., Cretaceous extinctions: Evidence overlooked. Science 328, 974-975 (2010).

14. P. Schulte et al., Response - Cretaceous extinctions. Science 328, 975-976 (2010).

15. A. Jay, M. Widdowson, Stratigraphy, structure and volcanology of the SE Deccan continental flood basalt province: implications for eruptive extent and volumes. Journal of the Geological Society 165, 177-188 (2008).

16. G. Keller, T. Adatte, S. Gardin, A. Bartolini, S. Bajpai, Main Deccan volcanism phase ends near the K-T boundary: Evidence from the Krishna-Godavari Basin, SE India. Earth and Planetary Science Letters 268, 293-311 (2008).

17. V. Vajda, J. Raine, C. Hollis, Indication of global deforestation at the Cretaceous-Tertiary boundary by New Zealand fern spike. Science 294, 1700-1702 (2001).

18. S. Jiang, T. Bralower, M. Patzkowsky, L. Kump, J. Schueth, Geographic controls on nannoplankton extinction across the Cretaceous/Palaeogene boundary. Nature Geoscience 3, 280-285 (2010).

19. A. Chenet, X. Quidelleur, F. Fluteau, V. Courtillot, S. Bajpai, ^{40}K-^{40}Ar dating of the Main Deccan large igneous province: Further evidence of KTB age and short duration. Earth and Planetary Science Letters 263, 1-15 (2007).

20. S. Self, S. Blake, K. Sharma, M. Widdowson, S. Sephton, Sulfur and chlorine in

Late Cretaceous Deccan magmas and eruptive gas release. Science 319, 1654-1657 (2008).

21. E. Pierazzo, D. Kring, H. Melosh, Hydrocode simulation of the Chicxulub impact event and the production of climatically active gases. Journal of Geophysical Research-Planets 103, 28607-28625 (1998).

22. O. Toon, K. Zahnle, D. Morrison, R. Turco, C. Covey, Environmental perturbations caused by the impacts of asteroids and comets. Reviews of Geophysics 35, 41-78 (1997).

23. P. Minnis et al., Radiative climate forcing by the Mount-Pinatubo eruption. Science 259, 1411-1415 (1993).

24. S. Guo, G. Bluth, W. Rose, I. Watson, A. Prata, Re-evaluation of SO_2 release of the 15 June 1991 Pinatubo eruption using ultraviolet and infrared satellite sensors. Geochemistry Geophysics Geosystems 5, 1525-2027 (2004).

25. C. Oppenheimer, B. Scaillet, R. Martin, Sulfur degassing from volcanoes: Source conditions, surveillance, plume chemistry and Earth system impacts. Reviews in Mineralogy and Geochemistry 73, 363-421 (2011).

26. A. Chenet et al., Determination of rapid Deccan eruptions across the Cretaceous-Tertiary boundary using paleomagnetic secular variation: 2. Constraints from analysis of eight new sections and synthesis for a 3500-m-thick composite section. Journal of Geophysical Research-Solid Earth 114, 38 pp., B06103, doi:10.1029/2008JB005644 (2009).

27. H. Sigurdsson et al., Geochemical constraints on source region of Cretaceous Tertiary impact glasses. Nature 353, 839-842 (1991).

28. A. Paytan, M. Kastner, D. Campbell, M. H. Thiemens, Seawater sulfur isotope

fluctuations in the Cretaceous. Science 304, 1663-1665 (2004).

29. C. Koeberl, Chicxulub crater, Yucatan - Tektites, impact glasses, and the geochemistry of target rocks and breccias. Geology 21, 211-214 (1993).

30. G. E. Claypool, W. T. Holser, I. R. Kaplan, H. Sakai, I. Zak, The age curves of sulfur and oxygen isotopes in marine sulfate and their mutual interpretation. Chemical Geology 28, 199-260 (1980).

31. T. Mather et al., Oxygen and sulfur isotopic composition of volcanic sulfate aerosol at the point of emission. Journal of Geophysical Research-Atmospheres 111, 9 pp., D18205, doi:10.1029/2005JD006584 (2006).

32. E. C. Perry, D. J. Winter, B. Sagar, B. Wu, The Chicxulub structure: Surface manifestation and possible sulfur isotope signature, Lunar and Planetary Institute Science Conference Abstracts, 23, p. 1057 (1992).

33. Supplementary Online Material.

34. N. Robinson, G. Ravizza, R. Coccioni, B. Peucker-Ehrenbrink, R. Norris, A high-resolution marine $^{187}Os/^{188}Os$ record for the late Maastrichtian: Distinguishing the chemical fingerprints of Deccan volcanism and the KP impact event. Earth and Planetary Science Letters 281, 159-168 (2009).

35. G. Ravizza, B. Peucker-Ehrenbrink, Chemostratigraphic evidence of Deccan volcanism from the marine osmium isotope record. Science 302, 1392-1395 (2003).

36. G. Calves et al., Seismic volcanostratigraphy of the western Indian rifted margin: The pre-Deccan igneous province. Journal of Geophysical Research-Solid Earth 116, 28 pp., B01101, doi:10.1029/2010JB000862 (2011).

37. V. Courtillot et al., Cosmic markers, $^{40}Ar/^{39}Ar$ dating and paleomagnetism of the KT

sections in the Anjar Area of the Deccan large igneous province. Earth and Planetary Science Letters 182, 137-156 (2000).

38. F. Therrien, D. Eberth, D. Braman, D. Zelenitsky, High-resolution organic carbon isotope record across the Cretaceous-Tertiary boundary in south-central Alberta: Implications for the post-impact recovery rate of terrestrial ecosystems and use of $\delta^{13}C$ as a boundary marker. Canadian Journal of Earth Sciences 44, 529-542 (2007).

39. W. A. Clemens, Evolution of the mammalian fauna across the Cretaceous-Tertiary boundary in northeastern Montana and other areas of the Western Interior. 361, 217-245 (2002).

40. J. A. Lillegraven, J. J. Eberle, Vertebrate faunal changes through Lancian and Puercan time in southern Wyoming. Journal of Paleontology 73, 691-710 (1999).

41. S. D'Hondt, P. Donaghay, J. Zachos, D. Luttenberg, M. Lindinger, Organic carbon fluxes and ecological recovery from the Cretaceous-Tertiary mass extinction. Science 282, 276-279 (1998).

42. L. Alegret, E. Thomas, K. Lohmann, End-Cretaceous marine mass extinction not caused by productivity collapse. Proceedings of the National Academy of Sciences of the United States of America 109, 728-732 (2012).

43. P. Hull, R. Norris, T. Bralower, J. Schueth, A role for chance in marine recovery from the end-Cretaceous extinction. Nature Geoscience 4, 856-860 (2011).

4.5 Acknowledgements

Data measured for this study are available in the Supporting Online Materials. This study was made possible by a fellowship from the Japan Society for the Promotion of Science to MLC, and by the National Science and Engineering Research Council of Canada, through fellowships to MLC and FT and Discovery grants to DF and BAW. We thank Kent and Marian Knudsen for allowing free access to their property, Dennis Braman for assistance in sampling, Craig Scott for fruitful discussions, and Pincelli Hull for providing $\delta^{13}C$ data from ODP Hole 1209.

4.6 Supplementary Materials:

4.6.1 Detailed geology

The Knudsen's Coulee (KCS, 51°53'15''N; 113°01'46''W) and Knudsen's Farm (KFS, 51°54'32''N; 113°02'59''W) Cretaceous-Paleogene (KPg) boundary sections are located 2.5 km apart on the Knudsen's *T. rex* Ranch, in the valley of the Red Deer River, north of the town of Drumheller, Alberta, Canada (Fig. 4.S1). Both sections preserve excellent exposures of the Scollard Formation (Edmonton Group), which consists mostly in drab-coloured mudstones and sandstones deposited in an alluvial plain developed in response to the Cordilleran Orogeny (Richardson et al., 1988; Catuneanu and Sweet, 1999). The age of the Scollard Formation has been constrained to the late Maastrichtian through the early Paleocene using radiometric, biostratigraphic and magnetostratigraphic methods (Srivasta, 1970; Lerbekmo and Coulter, 1985; Lerbekmo and Braman, 2002). The lower portion of the Scollard Formation is equivalent in age to the Hell Creek Formation of Montana and South Dakota, the Lance Formation of Wyoming, and the Frenchman Formation of Saskatchewan. Typical Late Cretaceous vertebrate fossil remains, including those of Tyrannosaurus and Triceratops, can be found in strata below the KPg boundary at both localities. Palynofloral successions across the KPg boundary are also comparable at both sections (Lerbekmo et al., 1987; Sweet and Braman, 1992).

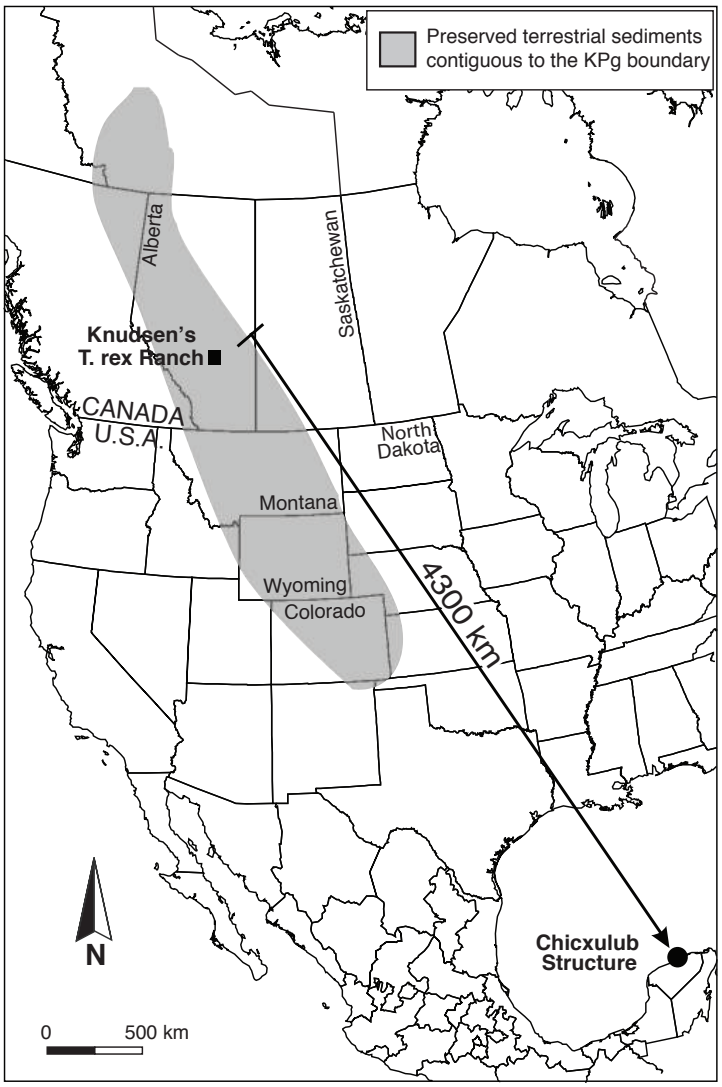

Fig. 4.S1: Location of the Knudsen's *T. rex* Ranch near Drumheller, Alberta, Canada. The Knudsen's Coulee and Knudsen's Farm KPg sections are 2.5 km apart on this property. The KPg sections on the Knudsen's property represent the farthest known extent the hackly ejecta layer. Figure modified from Sweet and Braman (2001).

4.6.1.1 Knudsen's Coulee Section

At the Knudsen's Coulee Section, the KPg boundary is exposed continuously over 50 m and discontinuously over 150 m of the Scollard Formation. The lowermost stratum of the section consists in gray mudstone, which contains root traces and is interpreted to represent the Bg horizon of a hydromorphic paleosol (Fig. 4.1). It is overlain

by 6 cm of carbonaceous claystone forming the base of the Nevis coal (#13; Gibson, 1977). The 3.0-cm thick boundary claystone is overlain by 32 cm of Nevis coal, the top of which is truncated by a 48 cm-thick sandstone body. At this locality, the composite claystone layer recognized as the KPg boundary claystone (Hildebrand and Boynton, 1988b) can be subdivided into three subunits (Fig. 4.S2) [Sweet et al., 1999]. The lowermost unit, the “hackly claystone” layer, is a 2.2-cm thick layer of light brownish grey claystone that represents weathered micro-spherules and micro-tecktites (Hildebrand, 1993). The middle 0.4-cm thick layer of “satiny claystone” is pinkish brown with a satiny luster. It contains “graupen” pellets, is gradational in texture with the overlying laminated shale and contains abundant shocked quartz (Lerbekmo et al., 1999). The topmost dark-brown “laminated shale” layer is 0.4-cm thick and contains 10-20 claystone laminae separated primarily by organic debris. It includes abundant shocked quartz and is easily distinguished from the hackly and satiny layers by its fissile nature. The hackly claystone, satiny claystone, and laminated shale microstratigraphy of the boundary claystone at the KCS are thought to represent, respectively, the ejecta layer, the fireball layer, and the layer of sulfur aerosols and condensate from the vaporized target and impacting body (Sweet et al, 1999). Iridium abundance profiles show maximum abundance within the boundary claystone in the satiny claystone and laminated shale layers (9.62 ± 0.06 and 9.27 ± 0.11 ppb, respectively; Lerbekmo et al., 1996). In a high-resolution study of carbon isotopes at the KCS and KFS, Therrien et al. (2007) found a 1.8 to 2.3‰ excursion starting in the satiny claystone layer. They used the carbon isotope and carbon content profiles, combined with palynofloral information, at both these sections to show that the post-impact recovery in the terrestrial environment of the Red Deer Valley took approximately ≈100 kyrs. Detailed palynological work (e.g. Sweet et al., 1999) shows, starting in the satiny layer of the boundary, the fern-spore abundance spike characteristic of many KPg sections (Nichols and Johnson, 2008).

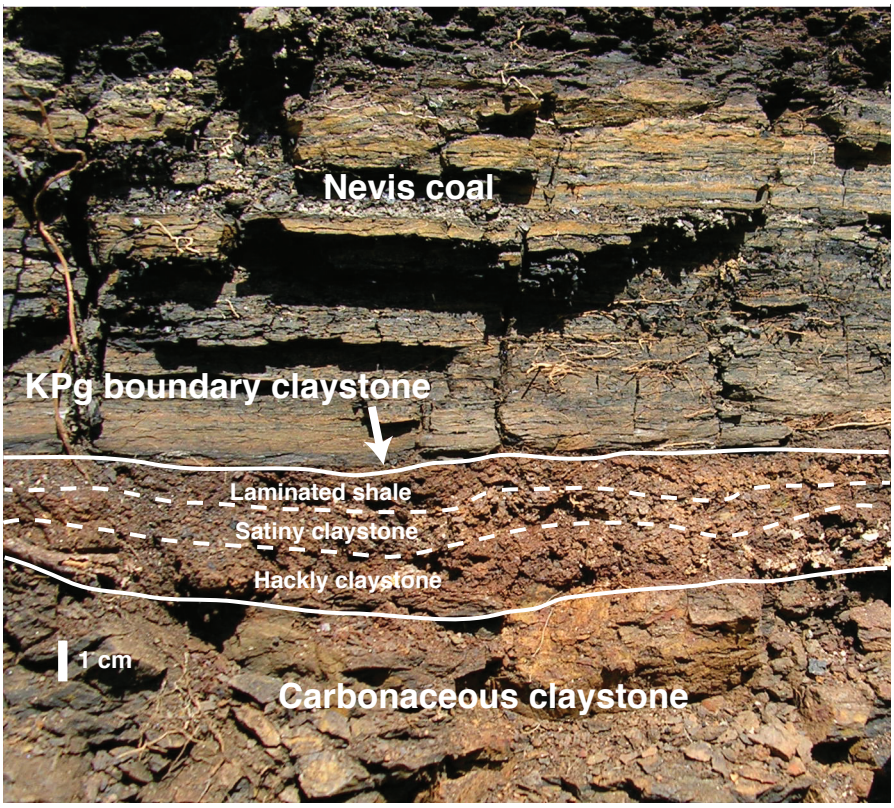

Fig. 4.S2: KPg boundary at the Knudsen's Coulee Section, at the base of the Nevis coal, overlying carbonaceous mudstone. The KPg boundary claystone includes three-part microlithostratigraphy. Figure modified from Therrien et al. (2007).

4.6.1.2 Knudsen's Farm

The Knudsen's Coulee and Knudsen's Farm (KFS) KPg sections preserve many of the same lithological, geological and palynological features, but at the Knudsen's Farm Section, groundwater movement has resulted in homogenization of the boundary claystone layer. At this locality, the 2 cm-thick boundary claystone is underlain by 30 40 cm of gray mudstone (see above) and overlain by 38 cm of Nevis coal (Fig. 4.S3). However, where a sandstone body truncates the Nevis coal at the KCS, at the KFS it is conformably overlain by a whitish 10 cm-thick bentonite dated to 65.68 ± 0.23 Ma (McWilliams et al., 1991, 1992; revised from an unpublished age of 64.71 ± 0.09 Ma, see discussion below), which we use to calculate a sedimentation rate for the coal

overlying the KPg boundary, in the Scollard Formation. A maximum Ir abundance of 3.36 ± 0.04 ppb is reported for this section (Lerbekmo et al., 1987). The boundary claystone contains microdiamonds at this location (Carlisle and Braman, 1991)

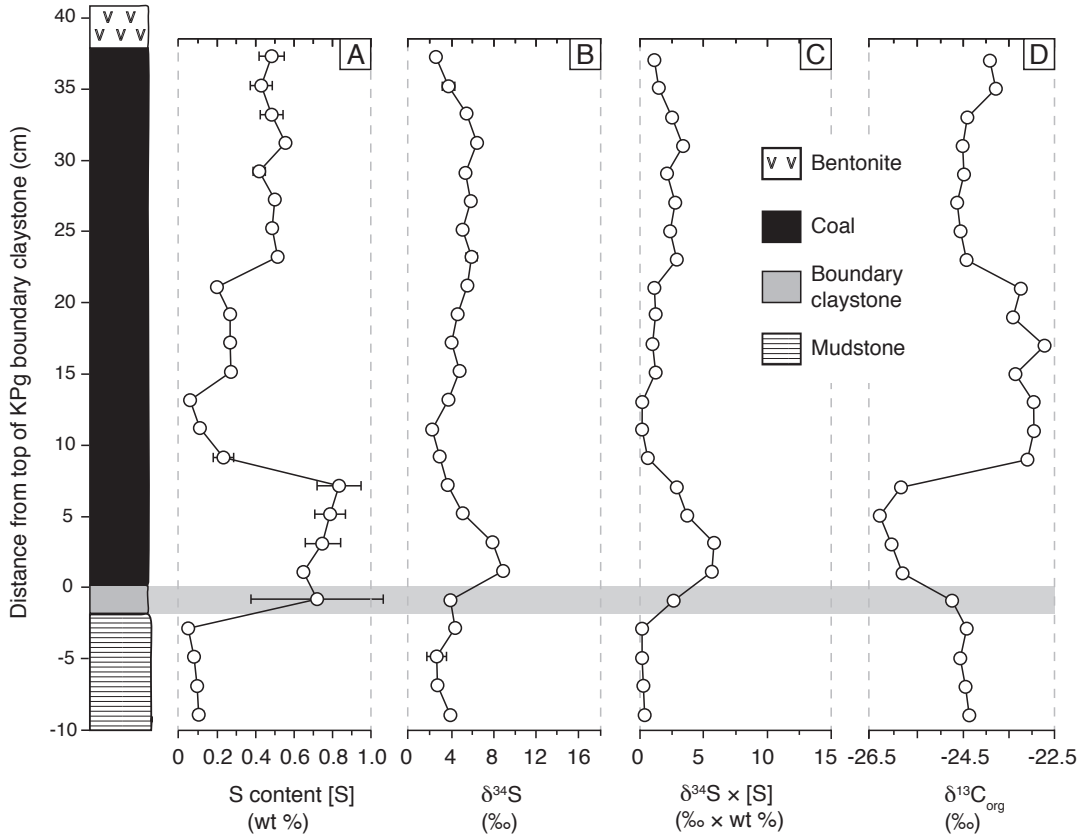

Fig. 4.S3: (A) Whole-rock S content and (B) whole-rock $\delta^{34}S$ values at the Knudsen's Farm KPg section. Error bars on [S] and $\delta^{34}S$ values indicate one standard deviation from the mean of three measurements. (C) The quantity $\delta^{34}S \times [S]$ indicates the amount of enriched S added to the sediment. (D) Carbon isotope compositions ($\delta^{13}C$) were reported previously in Therrien et al. (2007). Peaks in ^{34}S-rich S addition are matched by negative $\delta^{13}C$ excursions. The shaded area indicates the boundary claystone, which is divided into a three-part microstratigraphy of a hackly layer (gray), satiny layer (white), and laminated shale layer (black).

4.6.2 Detailed analytical methods

The sampling procedure used is described in Therrien et al. (2007). Samples were crushed to a fine powder using an agate mortar and pestle. We cleaned the mortar and pestle between each sample using concentrated hydrochloric acid and by repeated cycles (3 cycles) of crushing of high-purity quartz powder to abrade the sur-

face and remove any remaining traces of the previous sample. Ultrapure water was used for rinsing steps. Sulfur content (wt%) and isotopic composition ($\delta^{34}S$, ‰) were measured directly in the crushed samples using a helium-gas continuous flow isotopic ratio mass spectrometer (CF-IR-MS; Isoprime-EA, Isoprime Ltd.) at the University of Tsukuba, Tsukuba, Ibaraki, Japan. Three- to 10-mg samples (1-10 µg S) were weighted into 12X5 mm tin capsules with ≈0.3 mg of vanadium pentoxide to promote complete combustion (Yanagisawa and Sakai, 1983). Sulfur isotopic compositions are expressed in terms of $\delta^{34}S$ (‰) relative to V-CDT (Vienna-Canyon Diablo Troilite). The IAEA (International Atomic Energy Agency) silver sulfide standards S-1 (-0.3‰) and S-2, (+21.8‰) [Mayer and Krouse, 2004] were used to constrain the $\delta^{34}S$ values and to calibrate S content. Precision (1σ) for isotopic composition measurements was ±0.3‰ for samples with 10 µg S and ±1‰ for samples with 1 µg S. Sulfur content was determined with a precision of ±5 rel % for 10 µg S and ±30 rel % for 1 µg S. Sulfur content and $\delta^{34}S$ values reported in this paper are the mean values of three repeated measurements, with the error given by one standard deviation (1SD) from the mean.

4.6.3 Detailed modeling

In order to quantify the addition of ^{34}S-rich S at the Knudsen's Coulee section, we fit Gaussian functions to the $\delta^{34}S \times [S]$ profile (Fig. 4.1C). We chose to use Gaussian functions for two reasons. First, our measurements do not reflect discrete points in the KCS stratigraphy but complete sedimentary intervals of 2 cm or less. This sampling procedure means that our measurements are physical averages, and should be inherently more Gaussian than the underlying discrete profile. Second, atmospheric transport of sulfur from impact and volcanic sources leads to a dispersed pattern of transit times and deposition (Waugh and Hall, 2002), even if production is effectively instantaneous. Gaussian pulses are a straightforward way to capture this phenomenon. Each function has three free parameters: (1) the $\delta^{34}S \times [S]$ value at the peak of

the Gaussian function; (2) the width of the Gaussian function; and (3) the vertical position of the peak of the Gaussian function. We varied these parameters in order to minimize the squared difference between the measured $\delta^{34}S\times[S]$ values and the integrated area under the Gaussian curve over the same interval. When overlapping peaks were required (Fig. 4.3), we used a sum of Gaussian functions. This process reproduced the $\delta^{34}S\times[S]$ peak just above the top of KPg boundary claystone (Fig. 4. S4) as well as the peak centered ≈25 cm above the top of the boundary claystone (Fig. 4.S5). We estimated the relative S added to the KCS environment for each of the three S pulses by integrating the area under each model curve and dividing by the $\delta^{34}S$ of the appropriate source.

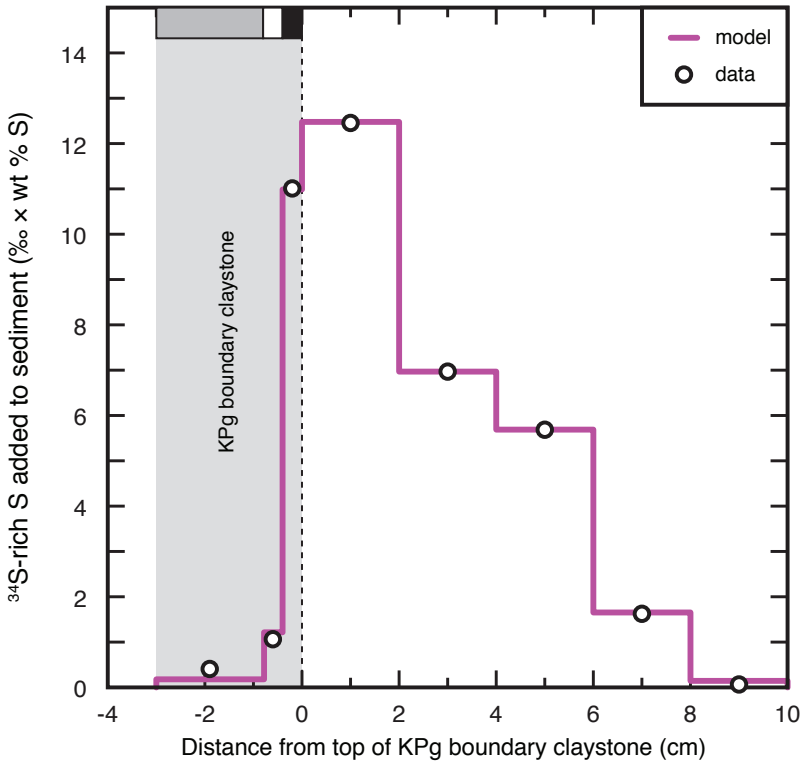

Fig. 4.S4: Model-data comparison for ^{34}S-rich S peak just above the KPg boundary claystone. White circles indicate the measured $\delta^{34}S\times[S]$ values, and are centered in each sampling interval. Purple line indicates the average value of the sum of two Gaussian model functions over each sampling interval. The Gaussian pulses producing this integrated signal are shown in blue (impact-derived S) and red (volcanic S) on Fig. 4.3. The shaded area indicates the boundary claystone, which is divided into a three-part microstratigraphy of a hackly layer (gray), satiny layer (white), and laminated shale layer (black).

We note that the linearized forms of the mixing equations, as shown in a cross plot of $\delta^{34}S$ and 1/[S] (Fig. 4.S6), are consistent with our addition hypothesis. The intercept for the lower array is at $\delta^{34}S$ = 7.8‰, similar to sulfate aerosols from volcanogenic SO_2. The upper array has an intercept at $\delta^{34}S$ = 15.8‰, comparable to Chicxulub target rocks, Upper Cretaceous evaporites and Maastrichtian seawater. The origin of the sulfur peaks at the KCS suggested by the linearized mixing equations (Fig. 4.S6) is in agreement with our proposed environmental scenario (Fig. 4.3).

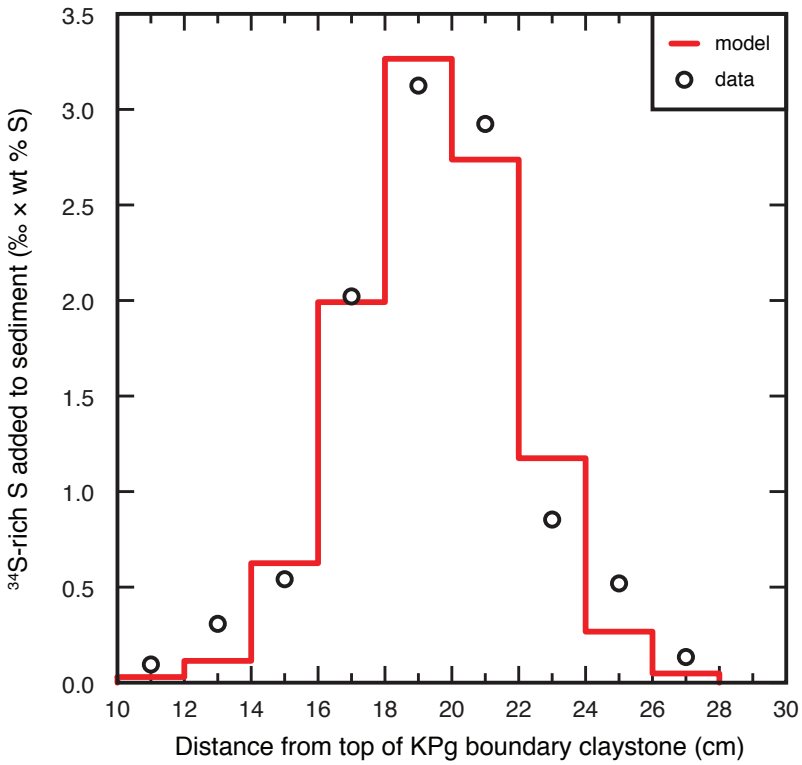

Fig. 4.S5. Model-data comparison for ^{34}S-rich S peak centered ≈20 cm above the KPg boundary claystone. White circles indicate the measured $\delta^{34}S \times [S]$ values, and are centered in each sampling interval. Red line indicates the average value of Gaussian model function over each sampling interval. The Gaussian pulse producing this integrated signal is shown in red (volcanic S) on Fig. 4.3.

The linearized analysis highlights potential origins of the background sulfur. For example, the measurement for the hackly layer of the boundary claystone falls between these two linearized mixing arrays and could reflect a combination of volcanogenic sulfur and from Chicxulub evaporitic target rocks. An intriguing possibility is

that this sample includes a component of meteoritic sulfur ($\delta^{34}S$ = 0‰), which would pull the $\delta^{34}S$ value off of upper evaporitic array. As is apparent in the mixing analysis presented in the text (Fig. 4.2), there is a hint of volcanically-derived sulfur in samples below the boundary claystone, possibly reflecting contribution from a minor early phase of Deccan volcanism prior to the KPg boundary.

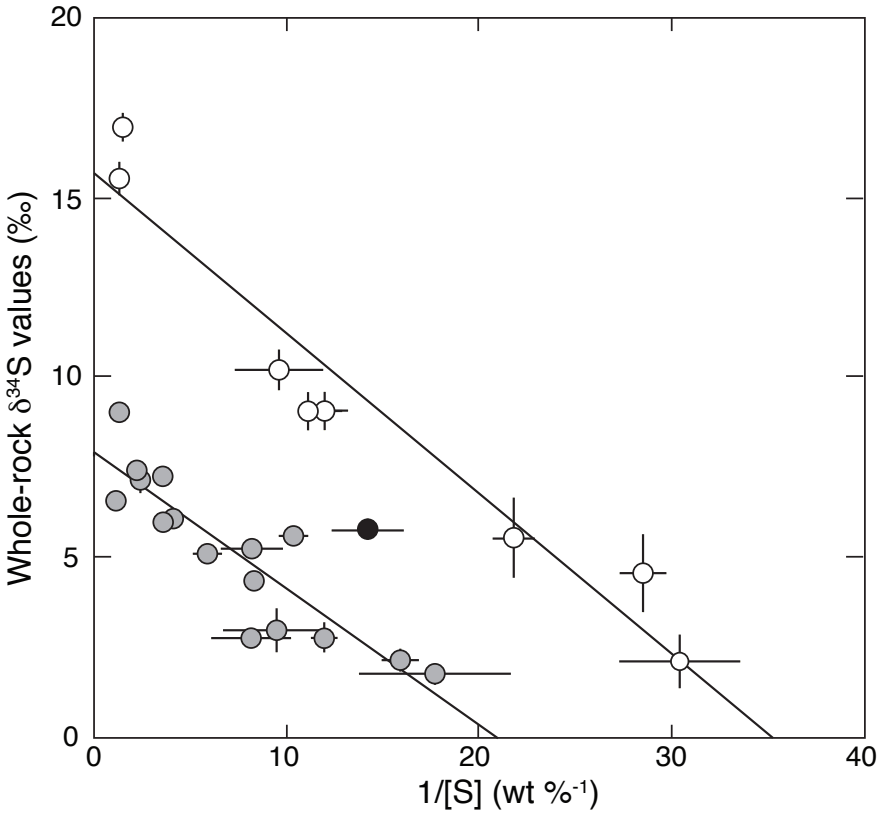

Fig. 4.S6: Linearized cross plot of $\delta^{34}S$ values and the inverse of whole-rock S contents (1/[S]) measured at the Knudsen's Coulee Section. The upper mixing array is consistent with S from Chicxulub target rocks and end-Cretaceous seawater and evaporites (white circles). The lower mixing array is consistent with S from oxidized volcanic SO_2 (gray circles). The measurement for the lowermost unit of the boundary claystone, the hackly layer (black cirle), falls between these two arrays and could reflect mixing between various sources of S, including meteoritic S ($\delta^{34}S$ = 0‰), volcanogenic S and S from the Maastrichtian evaporitic target rocks. Error bars indicate standard deviation from the mean of three measurements. Where these are not visible, they are smaller than the symbols used.

4.6.4 KFS discussion

Although the Knudsen's Farm KPg Section (KFS) preserves many of the same lithological, palynological and geochemical features as the Knudsen's Coulee Section, the KFS boundary claystone is completely homogenized and its constituent subunits cannot be recognized. Apparently, groundwater movement has resulted in the loss of any microlithostratigraphy that was originally present. Because of the clear post-depositional chemical mobility, we do not quantitatively interpret the S isotope systematics at KFS. However, the S content, $\delta^{34}S$ and ^{34}S-rich S profiles for the KFS are broadly comparable to those for the KCS (Figs. 4.1, 4.S3). For example, S content and $\delta^{34}S$ profiles are closely correlated around the boundary claystone (Fig. 4.S3A, B) leading to a peak of ^{34}S-rich S extending to >10 cm above the claystone (Fig. 4.S3C). This peak is not as sharp as the corresponding feature in the KCS profile. Similarly, while a distinct second peak of ^{34}S-rich S is centered about 20 cm above the boundary claystone in the KCS profile, the upper KFS profile shows a much more subdued pattern of ^{34}S addition. Within a broad region that persists over the remainder of the section, levels of ^{34}S-rich S are only slightly above background values (Fig. 4.S3C). This pattern likely reflects S mobilization by groundwater flow through the sediment as both the S contents and $\delta^{34}S$ values are spread out over a similar vertical distance (Fig. 4.S3A, B). In summary, we expect that profiles of S content, $\delta^{34}S$ values, and ^{34}S-rich S at the KFS originally resembled those at the KCS. However, post-depositional S transport acted as a broadband filter, destroying comparable chronologic information at the KFS. We note that this does not seem to be the case for $\delta^{13}C$ values in organic matter (cf. Fig. 4.1D, Fig. 4.S3D). The C content of the Nevis Coal is much greater than its S content, thereby making the organic $\delta^{13}C$ record much more resistant to resetting than the $\delta^{34}S$ record. Both the KCS and KFS preserve $\delta^{13}C$ minima at ≈5 cm above the boundary claystone, supporting our application of stratigraphic timescales calculated for KFS to the KCS.

4.6.5 Absolute KPg chronology

In order to compare our proposed relative environmental chronology to absolute timing of events across the KPg boundary, we compiled age estimates of the KPg boundary, Chicxulub impactites, bentonites in Western Interior sedimentary basins, and the continental flood basalts of the main Deccan traps. Age estimates from $^{40}Ar/^{39}Ar$ measurements were recalculated to a common age standard in order to construct a consistent chronology (Fig. 4.S7). Here we present detailed descriptions of the components of this chronology, explore potential pitfalls associated with the chronology, and use it to derive a chronological calibration for the Scollard Formation in the area of Knudsen's *T. rex* Ranch.

4.6.5.1 KPg boundary

Marine paleomagnetic measurements indicate that the KPg boundary falls in the middle the 29r magnetic polarity chron (Cande and Kent, 1995). The latest consensus geologic time scale places the KPg boundary at 65.50 ± 0.30 Ma (Gradstein et al, 2004). Cross-calibrations of orbitally tuned sedimentary cycles with high-precision $^{40}Ar/^{39}Ar$ age determinations produced a slightly older, and significantly more precise, estimate of 65.957 ± 0.043 Ma for the KPg boundary (uncertainty is 2 standard error [SE] on the mean; Kuiper et al., 2008; Fig. 4.S7A). A recent astronomical calibration of Maastrichtian marine cyclostratigraphic datasets (magnetic susceptibility and grayscale measurements from Ocean Drilling Project and Deep Sea Drilling Project cores) returned an equivalent age for the KPg boundary of 66.00 ± 0.07 Ma (Husson et al., 2011; Fig. 4.S7A). These estimates, and consistent ages for magnetic polarity chron boundaries (C30n/C29r - 66.30 ± 0.08 Ma, Husson et al., 2011; C29r/C29n - 65.724 ± 0.055 Ma [2SE], Kuiper et al., 2008), provide a chronological framework for examining the absolute ages of environmental events across the KPg boundary. The 65.957 ± 0.043 Ma age for the KPg boundary is cross calibrated to an age of

28.201 Ma for sanidine from the Fish Canyon Tuff (FCT), widely used as an standard for $^{40}Ar/^{39}Ar$ age determinations (Kuiper et al., 2008). Therefore we recalculated $^{40}Ar/^{39}Ar$ ages from the literature to be consistent with an FCT age of 28.201 Ma when necessary.

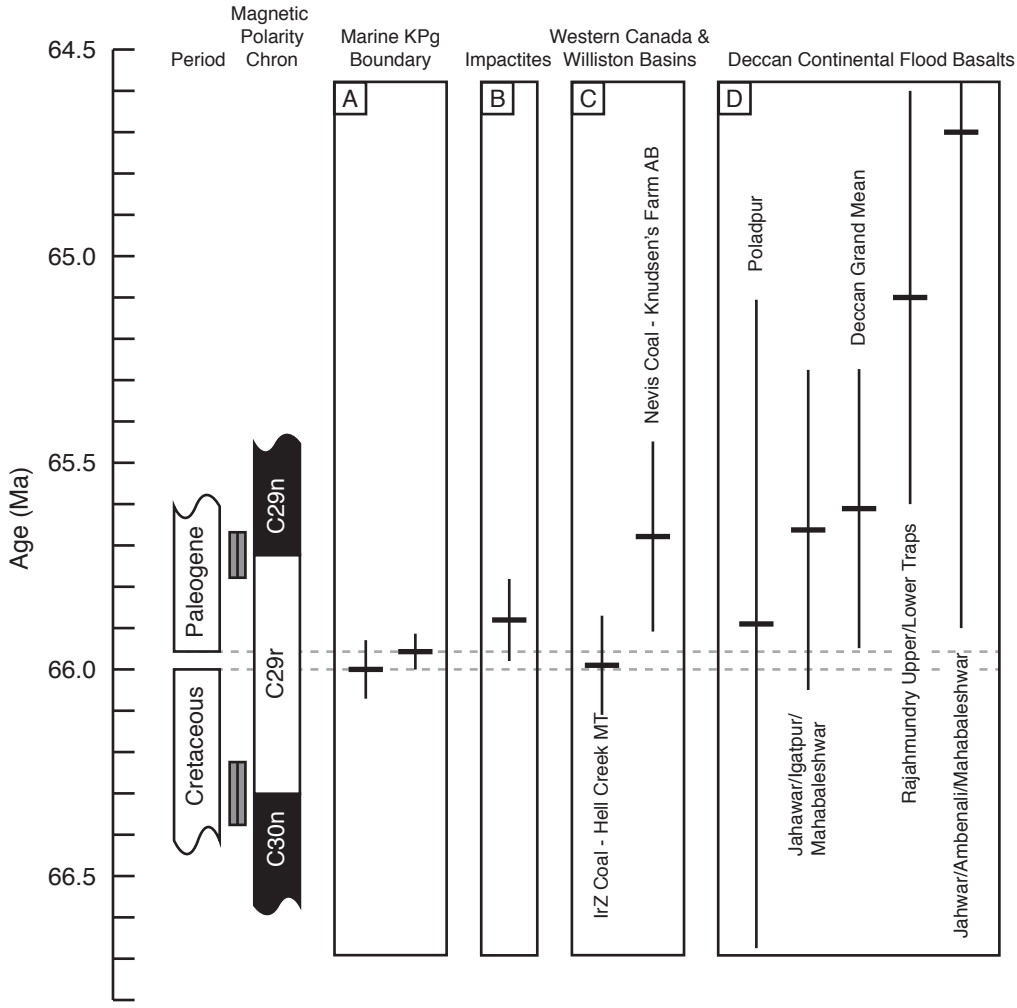

Fig. 4.S7: Comparison of absolute age determinations for environmental events and markers around the Cretaceous-Paleogene (KPg) boundary. Ages shown as thick horizontal lines, while reported thin vertical lines indicate age uncertainties. (A) Recent age determinations for the marine KPg boundary. Cross-calibration between cyclostratigraphy and $^{40}Ar/^{39}Ar$ geochronology returns an age of 65.957 ± 0.043 Ma (2SE; Kuiper et al., 2008). Orbital tuning of marine cyclostratigraphic datasets returns an equivalent age of 66.0 ± 0.07 Ma (Husson et al., 2011). The agreement between these two KPg boundary age determinations allows their independent determinations of the surrounding magnetic polarity chron transitions to be used without introducing substantial bias (C30r/C29n - 66.30 ± 0.08 Ma, Husson et al., 2011; C29n/C29r - 65.724 ± 0.055 Ma, Kuiper et al., 2008). Gray bands to the left of the magnetic polarity chron boundaries reflect their reported age uncertainties. (B) Recent recalculations of $^{40}Ar/^{39}Ar$ age determinations of KPg impactites. Reported determinations (Kuiper et al.,

2008) are all consistent with a grand mean of 65.88 ± 0.10 Ma (2SE). (C) Recalculation of terrestrial KPg boundary ages from Western Interior of North America. The lowest coal in the Williston Basin (IrZ Coal) is enriched in Ir (Swisher et al., 1993). Bentonite beds within the IrZ Coal return $^{40}Ar/^{39}Ar$ ages on sanidine of 65.99 ± 0.12 Ma (2SE; Swisher et al., 1993 as recalculated in Kuiper et al., 2008). The first coal seam above the KPg boundary clay in the Western Canada Sedimentary Basin of Alberta (Nevis Coal) contains a bentonite bed characterized by a $^{40}Ar/^{39}Ar$ age of 65.68 ± 0.23 Ma (as estimated from data in McWilliams et al, 1991, 1992; Kuiper et al., 2008). (D) Recent and recalculated age determinations for Deccan Traps volcanism. Seven $^{40}Ar/^{39}Ar$ age determinations on mineral separates from samples of the Jahwar, Igatpuri, and Mahabaleshwar Formations are consistent with a single mean age of 65.66 ± 0.39 Ma (95% CI [1SE = 0.16 Ma]; recalculated from Hoffman et al., 2000). Three $^{40}Ar/^{39}Ar$ age on plagioclase mineral separates from samples of the Poladpur Formation are consistent with a single mean age of 65.89 ± 0.79 Ma (95% CI [1SE = 0.18 Ma]; recalculated from Hooper et al., 2010). Upper and lower Rajahmundry Traps are characterized by a single mean age of 65.1 ± 0.5 Ma (95 CI; recalculated from mean age of 12 analyses of 8 samples reported in Knight et al., 2003). Ages determined with the $^{40}K/^{40}Ar$ method on seven samples from the Jahwar, Igatpuri, Ambenali, and Mahabaleshwar Formations are consistent with a single mean value of 64.7 ± 1.2 Ma (2SE; Chenet et al., 2007). Uncertainty was assigned under the assumption that 1σ values reported for these samples refer to the standard error on the reported mean values (Chenet et al., 2007).

4.6.5.2 Impactites

Relative to an FCT age of 28.201 Ma, impactites associated with the KPg impact event (tektites from Beloc Haiti [Izett et al., 1991; Swisher et al., 1992; Dalyrymple et al., 1993], microtektites from Arroyo el Mimbral, Mexico [Swisher et al., 1992], and glassy melt rock C-1 from Chicxulub crater [Swisher et al., 1992]) yield a sample distribution of $^{40}Ar/^{39}Ar$ ages that are consistent with a single mean value (Kuiper et al., 2008). The grand mean of these ages is 65.88 ± 0.10 Ma (Fig. 4.S7B), where the uncertainty is calculated as the 95% confidence interval (CI) on the mean accounting for the effects of small-number statistics (Mahon, 1996). The associated SE is 0.04 Ma.

4.6.5.3 Western Interior sedimentary basins

Abundant and well-studied pollen, plant, and vertebrate fossils constrain the paleontological expression of the terrestrial KPg boundary in sedimentary strata of the North American midcontinent (Nichols and Johnson, 2008; Archibald, 2011). Sedimentary

basins of the North American midcontinent also preserve a broadly distributed, distinctive stratigraphic horizon at the KPg boundary – the 'boundary claystone' – that is taken to represent fallout from a KPg impact event (Bohor et al., 1984). A consistent three-part microstratigraphy is often found within the boundary claystone (Sweet et al., 1999), and is well illustrated by the boundary clay found in the Knudsen's Coulee section in the Scollard Formation, AB (Fig. 4.S2). Paleomagnetic measurements indicate that the KPg boundary in these sections occurs within magnetic polarity chron 29r (Swisher et al., 1993), consistent with the marine magnetostratigraphic record.

Widespread coals with interbedded bentonites enable a highly resolved absolute chronology for Western Interior sedimentary basins (Swisher et al., 1993). A maximum age for the terrestrial KPg boundary is constrained by a $^{40}Ar/^{39}Ar$ age of 65.99 ± 0.12 Ma (2SE; Swisher et al., 1993, recalculated based on a FCT age of 28.201 Ma in Kuiper et al., 2008; Fig. 4.S7C) measured on sanidine from bentonites within the IrZ coal (Williston Basin, Hell Creek, Montana). Unpublished high-precision $^{40}Ar/^{39}Ar$ ages from the first bentonite above the boundary clay (conformably overlying the Nevis Coal) at Knudsen's Farm, AB are 0.20 ± 0.15 Ma older than Beloc tektites from Haiti (uncertainty is 2SE on the difference between two mean values; McWilliams et al., 1991, 1992). Taking the grand mean of impactite $^{40}Ar/^{39}Ar$ ages (65.88 ± 0.10 Ma [95% CI; 1SE = 0.04 Ma], as described in the preceding section) to reflect the age of the Beloc tektites, the relative timing suggests that the bentonite overlying the Nevis Coal formed at 65.68 ± 0.23 Ma (2SE; Fig. 4.S7C).

4.6.5.4 Deccan Traps continental flood basalts

The Deccan Traps preserve a limited number of magnetic reversals, long hinting at a rapid eruption history (McElhinny, 1968; Wensink and Klootwijk, 1971). Paleontological and geochronological observations suggest that the Deccan eruptions span the KPg boundary, indicating that transition between magnetic polarity chrons C29r

and C29n is the most likely candidate for the major magnetic reversal recorded in the Deccan magnetostratigraphy (Courtillot et al., 1986). Early syntheses of geological, paleontological, geochronological and paleomagnetic datasets concluded that a dominant majority of the Deccan eruptions took place within magnetic polarity chron C29r (Vandamme et al., 1991), a result supported by recent detailed interdisciplinary reexaminations (Fig. 4.S8; Chenet et al., 2009; Jaye et al., 2009). Aside from a minor, geographically restricted early phase of volcanism occurring around the transition between magnetic polarity chrons C30r and C30n, current interpretations call on two brief, intense, and closely paced pulses of Deccan eruptions (Chenet et al., 2009). Much of this main Deccan eruptive phase occurs during magnetic polarity chron C29r, with the transition between magnetic polarity chrons C29r and C29n occurring during the emplacement of the Mahabaleshwar Formation (Fig. 4.S8; Chenet et al., 2009; Jaye et al., 2009). In fact, eruptive accounting suggests that more than 85% of the main Deccan eruptive phase occurred during magnetic polarity chron C29r (Self et al., 2006), which lasts 0.576 ± 0.097 (2SE) Myrs within the chronological framework used here (Fig. 4.S7).

This timing is supported by recent age determinations on stratigraphically controlled Deccan Trap flows and their possible far-field equivalents. Three samples of the Poladpur Formation (Fig. 4.S8), at the base of the uppermost and most voluminous collection of Deccan flows (the Wai subgroup; Self et al., 2006), are consistent with a single mean $^{40}Ar/^{39}Ar$ age of 65.89 ± 0.79 Ma (95% CI [1SE = 0.18 Ma]; Hooper et al., 2010, recalculated ages based on an age of GA1550 = 99.416 Ma relative to FCT = 28.201 Ma; Kuiper et al., 2008; Fig. 4.S7D). This temporal consistency appears to extend through the Deccan Traps as a whole. Samples from the lower and upper main Traps (Jahwar/Igatpuri/Mahabaleshwar Formations; Fig. 4.S8) are consistent with a single mean $^{40}Ar/^{39}Ar$ age of 65.66 ± 0.39 (95% CI [1SE = 0.16 Ma]; Hofmann et al., 2000, recalculated ages based on an age of Hb3gr = 1079.23 Ma relative to

FCT = 28.201 Ma; Kuiper et al., 2008; Fig. 4.S7D). Far-field flows from the Rajahmundry Traps are consistent with a mean $^{40}Ar/^{39}Ar$ age of 65.1 ± 0.5 Ma (2SE; Knight et al., 2003, recalculated ages based on an age of FCT = 28.201 Ma; Kuiper et al., 2008; Fig. 4.S7D), in line with their interpreted geochemical and paleomagnetic equivalence to the Ambenali and Mahabaleshwar Formations nearly 400 km away (Fig. 4.S8; Vandamme and Courtillot, 1992; Self et al., 2006). Independent radiometric techniques also confirm Deccan age homogeneity, although with slightly greater uncertainty, with samples from the lower and upper Traps (Jahwar/Igatpuri/Ambenali/Mahabaleshwar Formations; Fig. 4.S8) consistent with a mean $^{40}K/^{40}Ar$ age of 64.7 ± 1.2 Ma (2SE; Chenet et al., 2007; Fig. 4.S7D). Taken together, these measurements are all consistent with a single mean age of 65.61 ± 0.34 Ma (95% CI [1SE = 0.11 Ma]; Fig. 4.S7D) for the main Deccan Trap eruptions.

4.6.5.5 Synthesis

The chronological framework described here is consistent with the sequence of KPg environmental events inferred from the high-resolution S isotope data discussed in the main text (Fig. 4.3). While the uncertainty of the absolute ages is too large to fully distinguish the relative order of events, the absolute age distribution does emphasize the well-known temporal coincidence of the KPg boundary, the Chicxulub impact, and eruption of the main phase of the Deccan Traps (Fig. 4.S7; Courtillot et al., 1986). Most recent environmental histories do not highlight the apparent prevalence of Deccan eruptions after the KPg boundary however (Chenet et al., 2009; Robinson et al., 2009; Schulte et al., 2010), although this possibility has been acknowledged previously (Knight et al., 2003; Keller et al., 2008).

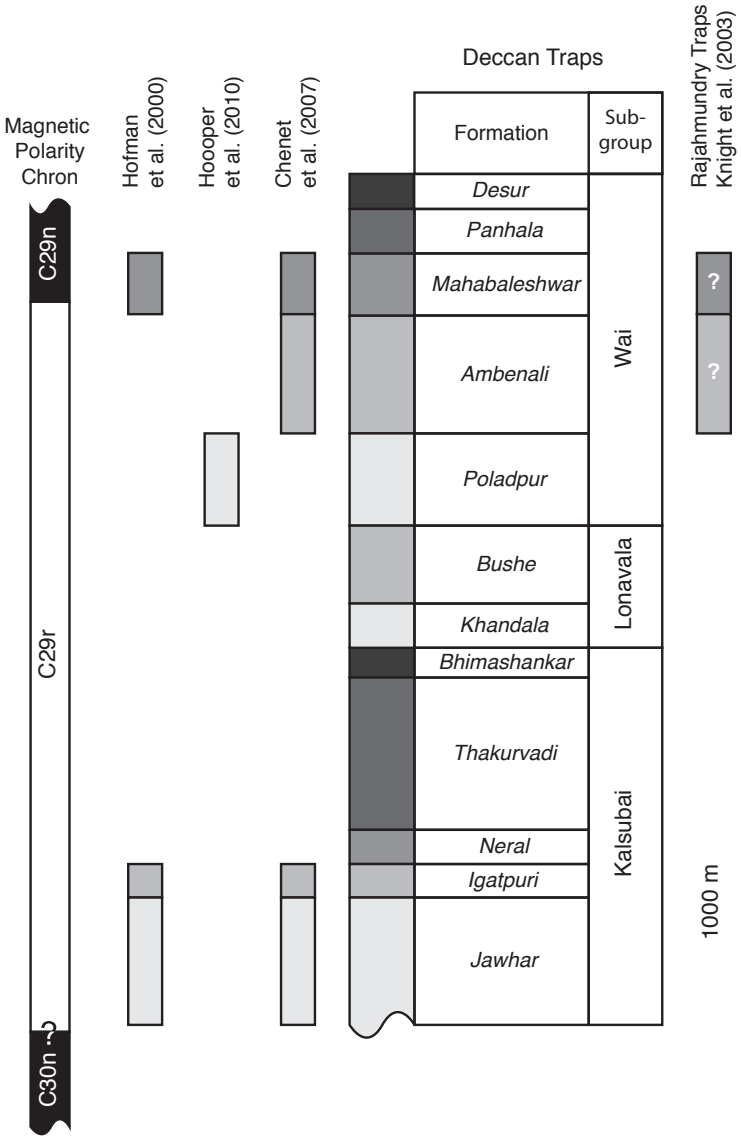

Fig. 4.S8: Sampling coverage of main Deccan Traps stratigraphy for radiometric age determinations. Discontinuous stacks of vertical columns indicate sampled formations. Division of the main Deccan Traps into formations and sub-groups is based on geochemical differences (Beane et al., 1986; Devey and Lightfoot, 1986). The composite stratigraphic column shown here is taken from Jaye and Widdowson (2008), with height of the formations illustrating their maximum cumulative thicknesses. High-resolution magnetostratigraphy pins the C29r/C29n magnetic polarity transition to the lower part of the Mahableshwar Formation (Chenet et al., 2009; Jaye et al., 2009), while the location of the magnetic polarity transition between magnetic polarity chrons C30n and C29r is less well defined. A transition from a reversed to normal magnetic polarity has been documented in three stratigraphically controlled samples from the Rajahmundry Traps (Vandamme and Courtillot, 1992). Along with geochemical comparisons to main Deccan chemotypes, this observation has been used to correlate the Lower and Upper Rajahmundry Traps to the Ambenali and Mahabaleshwar Formations over an exposure gap of ≈400 km (Vandamme and Courtillot, 1992; Self et al., 2008).

The relationship between the KPg boundary and the $^{40}Ar/^{39}Ar$ ages of the main Deccan eruptions presented here depends on the chosen chronological calibration for the KPg boundary and on the accepted age of the FCT. Strengths of the framework used here include: (1) chronological consistency between the astronomical calibration of the KPg boundary and the age of the FCT (Kuiper et al., 2008); (2) independent cyclostratigraphic derivations of an equivalent age for the KPg boundary (Husson et al, 2011; Westerhold et al., 2008); (3) recalibrated $^{40}Ar/^{39}Ar$ ages for terrestrial KPg bentonites from the Western Interior of North America as well as for impactites that match the KPg boundary age; and (4) broad agreement between the Deccan $^{40}Ar/^{39}Ar$ ages recalculated here and $^{40}K/^{39}Ar$ ages from similar samples (Chenet et al., 2007). A potential weakness of the framework is the relatively young age recalculated for the Rajahmundry Traps (Fig. 4.S7D).

4.6.5.6 Rajahmundry Traps

The Rajahmundry Traps have had an outsized influence on the evolution of geological thought about the relationship between the Deccan Traps eruptions and the KPg mass extinction (Vandamme and Courtillot, 1992; Knight et al., 2003; Self et al., 2008; Keller et al., 2008). They are few in number, thin (maximum thicknesses of ≈150 m; Knight et al., 2003), and occupy an exposed area that is more than 4 orders of magnitude smaller than that associated with the Deccan Traps (Knight et al., 2003; Jaye and Widdowson, 2008). They are ≈400 km from the nearest Deccan exposure, and >900 km from proposed Deccan vent sites (Self et al., 2008). Geochemical, paleomagnetic, and geochronological similarities have been used to correlate the lower and upper Rajahmundry Traps to the Ambenali and Mahabaleshwar Formations of the upper Deccan Wai Subgroup (Self et al., 2008). This correlation is acknowledged to be non-unique both because of geochemical variations within Deccan chemotypes (Self et al., 2008) and Rajahmundry flows (Knight et al.,2005) and permissive radiometric

age constraints on the observed R/N magnetic polarity transition (Knight et al., 2005). The Rajahmundry-Deccan correlation appears to be critical, however, to current interpretations that the first pulse of main phase Deccan volcanism ended 'precisely' at the KPg boundary (Chenet et al., 2009). This perspective depends on recent location of the KPg boundary within the Rajahmundry Traps (Keller et al., 2008).

The sedimentary record co-existing within the Deccan Traps flows is fragmentary and scarce. Intertrappean evidence for the KPg boundary Ir spike is rare, and complicated by a low signal-to-noise ratio (Courtillot et al., 2000). Paleontological observations from intertrap sediments of the main Deccan flows offer broad constraints on the location of the KPg boundary (Jaeger et al., 1989). However, a complex spectrum of planktic foraminiferal remains in sediments between the Upper and Lower Rajahmundry Traps suggest that the upper flows were deposited after the early Danian while the lower flows were deposited before the early Danian (Keller et al., 2008). The Danian age lasted from ≈66.00 to 62.35 Ma within the chronological framework used here (Kuiper et al., 2008). The time interval between the KPg boundary and the deposition of the Rajahmundry intertrap sediments is ≈0.06 to 0.1 Myr based on estimates of the duration of the interpreted intertrap biozones (P0 and P1a; Keller et al., 1995). The estimated depositional duration of the full intertrap sedimentary package is ≈0.2 Myr (Keller et al., 2008). Despite the loose constraints these features provide for the timing of the lower Rajahmundry Traps (Keller, et al., 2008), they have been correlated back to the main Deccan field in order to locate the KPg boundary near the top of the Ambenali Formation (Chenet et al., 2009), thereby separating the main phase of Deccan volcanism into two discrete pulses, one before and one after the KPg boundary.

Within the chronological framework used here – which places the KPg boundary at 66.00 to 65.957 Ma – the recalculated age estimate for the Rajahmundry Traps (65.1 ± 0.5 Ma) seems to be only marginally consistent with this scenario. In fact, the

recalculated age suggests that the proposed R/N magnetic polarity transition in the Rajahmundry Traps reflects the C28r/C28n transition (64.698 ± 0.055 Ma; Kuiper et al., 2008) rather than the C29r/C29n transitions of the main Deccan field. This suggestion is not new (Knight et al., 2005). However even the existence of a major polarity transition must be a tentative interpretation given the limited number of stratigraphically controlled paleomagnetic measurements from the Rajahmundry Traps (3 samples; Vandamme and Courtillot, 1992). Although a younger age of the Rajahmundry Traps is not supported by the biostratigraphic interpretations discussed in the preceding paragraph, alternative planktic foraminiferal zonation schemes exist (Arenillas et al., 2006; Molina et al., 2009). Within these schemes, some of the index species within the Rajahmundry intertrap sediments apparently have non-overlapping stratigraphic ranges. The resulting interpretation would be that much of the Rajahmundry intertrap planktic foraminiferal record is reworked and potentially younger than early Danian. A reworked component of the Rajahmundry intertrap planktic foraminiferal population has been identified (Keller et al., 2008).

Clearly the relationships among the Rajahumundry Traps, the Deccan Traps, and environmental events across the KPg boundary are complex and unsettled though the statistical synchroneity of the Rajahumundry and Deccan eruptions (Fig. 4.S7D) does place limits on the timeframe over which these relationships must play out.

4.6.5.7 Implications

Aside from the broad implications of the coincidence among the Chicxulub impact, eruption of the Deccan Traps, and the biotic turnover indicated by the KPg boundary, the chronological framework discussed here has specific implications for the timing of these events as represented in the Knudsen's Coulee (AB) section.

Like many of terrestrial KPg boundaries in the North American mid-continent (Nichols

and Johnson, 2008), the KPg boundary at Knudsen's Coulee is defined by a boundary claystone with a well-defined microstratigraphy, coincident with Ir enrichment and a spike in fern spore abundances (Sweet et al., 1999). The Nevis Coal overlies the boundary claystone at Knudsen's Coulee (Sweet et al., 1999). Paleomagnetic compilations from various KPg sections across the Western Canada sedimentary basin in Alberta indicate that the KPg boundary here occurs within magnetic polarity chron C29r (Lerbekmo and Braman, 2002). Like many terrestrial and marine KPg sections (e.g., Lerbekmo, 1999; Westerhold et al., 2008; Husson et al., 2011), the distance from the KPg boundary to the C29r/C29n magnetic polarity transition is less than the distance from the C30n/C29r magnetic polarity transition to the KPg boundary (Lerbekmo and Coulter, 1985). Condensed intervals after the KPg boundary are not uncommon in marine sections (Westerhold et al., 2008), and may represent a unique sedimentary response to the KPg boundary event. Conformable contacts across the KPg boundary at Knudsen's Coulee (Therrien et al, 2007) imply that this youngwards shift results from lower sedimentation rates towards the end of magnetic polarity chron C29r, rather than from any missing depositional intervals. Together with the synchronous deposition of the KPg boundary claystone throughout the Western Interior, these features suggest that the best estimate of the age of the KPg boundary at Knudsen's Coulee is the 65.99 ± 0.12 Ma age of the IrZ Coal from the Hell Creek area, Montana (Swisher et al., 1993 as recalculated in Kuiper et al., 2008).

There are no direct age measurements from the Knudsen's Coulee section. However, a nearby section (Knudsen's Farm, 2.5 km away) preserves many of the same geological, paleontological, and geochemical features as Knudsen's Coulee (Therrien et al., 2007). A bentonite in the Nevis Coal here has a $^{40}Ar/^{39}Ar$ age of 65.68 ± 0.23 Ma (McWilliams et al., 1991, 1992; estimated as described previously). This implies that the 38 cm of sedimentary rock (Therrien et al., 2007) between the top of boundary claystone and the first bentonite in the Nevis Coal represents 0.31 ± 0.26 Myr (2SE).

The stratigraphic chronological calibration at Knudsen's Farm is 0.12 ± 0.10 cm/kyr (2SE). Although $\delta^{13}C_{org}$ profiles at Knudsen's Farm are slightly more dispersed than at Knudsen's Coulee, in keeping with the greater amount of diagenetic alteration seen at Knudsen's Farm, the minimum in both profiles occurs within the sample taken from 4-6 cm above the top of the boundary claystone (Therrien et al., 2007). This implies that sedimentation rates at the two sites were equivalent, and we take 0.12 ± 0.10 cm/kyr as our best estimate of the stratigraphic chronological calibration at Knudsen's Coulee. The 30 cm of sedimentary rock in our section above the boundary claystone at Knudsen's Coulee therefore represents ≈245 ± 205 kyr (2SE). We use this estimate to provide a timescale for the environmental events revealed by our S isotope profile.

Table 4.S1: S content (wt. %) and $\delta^{34}S$ (‰) measurements at the Knudsen's Coulee (A) and Knusden's Farm (B) KPg sections near Drumheller, Alberta.

Table 4.S1A. Knudsen's Coulee Section

Sample	Stratigraphic position relative to top of boundary claystone (cm)	Sulfur content ±1SD[1] (wt %)	$\delta^{34}S$ ±1SD[1] (‰)
KC-top	30-32	0.0838±0.0040	2.74 ± 0.41
KC-01	28-30	0.1235 ± 0.0313	2.70 ± 0.22
KC-02	26-28	0.0629 ±0.0038	2.13 ± 0.27
KC-03	24-26	0.1201 ± 0.0033	4.33 ± 0.22
KC-04	22-24	0.1682 ± 0.0239	5.08 ± 0.19
KC-05	20-22	0.4100 ± 0.0123	7.13 ± 0.36
KC-06	18-20	0.4284 ± 0.0024	7.29 ± 0.20
KC-07	16-18	0.2782 ± 0.0181	7.27 ± 0.22
KC-08	14-16	0.0967 ± 0.0065	5.60 ± 0.18
KC-09	12-14	0.1053 ± 0.0308	2.93 ± 0.59
KC-10	10-12	0.0565 ± 0.0126	1.68 ± 0.25
KC-11	8-10	0.0330 ± 0.0034	1.98 ± 0.74
KC-12	6-8	0.2725 ± 0.0043	5.96 ± 0.16
KC-13	4-6	0.8714 ± 0.0206	6.52 ± 0.18
KC-14	2-4	0.7751 ± 0.0296	8.99 ± 0.20
KC-15	0-2	0.8031 ± 0.0383	15.51 ± 0.45
KC-lam[3]	(−0.4)-0	0.6500 ± 0.0222	16.94 ± 0.31
K-sat	(−0.8)-(−0.4)	0.1042 ± 0.0249	10.20 ± 0.57
K-bound	(−3)-(−0.8)	0.0704 ± 0.0093	5.78 ± 0.31
KC-19	(−5)-(−3)	0.0832 ± 0.0071	9.08 ± 0.47
KC-20	(−7)-(−5)	0.0897 ± 0.0040	9.07 ± 0.44
KC-21	(−9)-(−7)	0.0459 ± 0.0022	5.50 ± 1.08
KC-22	(−11)-(−9)	0.2394 ± 0.0175	6.01 ± 0.16
KC-23	(−13)-(−11)	0.1223 ± 0.0243	5.05 ± 0.24
KC-24	(−15)-(−13)	0.0351 ± 0.0014	4.53 ± 1.08

1. Mean and standard deviation on three replicates.

2. The second decimal is retained to avoid rounding-off errors.

3. K-lam is the laminated subunit of the boundary claystone, K-sat is the satiny subunit, and K-bound is the hackly subunit. We retain these sample labels for consistency with earlier studies.

Table 4.S1B. Knudsen's Farm Section

Sample	Stratigraphic position relative to top of boundary claystone (cm)	Sulfur content ±1SD[1] (wt %)	$\delta^{34}S$ ±1SD[1] (‰)
KF-01	36-38	0.4808 ± 0.0642	2.43 ± 0.31
KF-02	34-36	0.4290 ± 0.0543	3.55 ± 0.58
KF-03	32-34	0.4799 ± 0.0602	5.32 ± 0.30
KF-04	30-32	0.5568 ± 0.0144	6.25 ± 0.22
KF-05	28-30	0.4175 ± 0.0292	5.21 ± 0.34
KF-06	26-28	0.5027 ± 0.0100	5.69 ± 0.27
KF-07	25-26	0.4880 ± 0.0234	4.95 ± 0.38
KF-08	22-24	0.5190 ± 0.0195	5.73 ± 0.48
KF-09	20-22	0.2004 ± 0.0075	5.33 ± 0.20
KF-10	18-20	0.2689 ± 0.0202	4.50 ± 0.23
KF-11	16-18	0.2680 ± 0.0227	3.83 ± 0.27
KF-12	14-16	0.2736 ± 0.0165	4.69 ± 0.26
KF-13	12-14	0.0623 ± 0.0020	3.62 ± 0.26
KF-14	10-12	0.1113 ± 0.0095	2.19 ± 0.17
KF-15	8-10	0.2350 ± 0.0545	2.74 ± 0.23
KF-16	6-8	0.8364 ± 0.1128	3.55 ± 0.17
KF-17	4-6	0.7882 ± 0.0789	4.90 ± 0.31
KF-18	2-4	0.7514 ± 0.0903	7.78 ± 0.23
KF-19	0-2	0.6514 ± 0.0246	8.68 ± 0.27
KF-20[3]	(−2)-0	0.7139 ± 0.3361	3.81 ± 0.21
KF-21	(−4)-(−2)	0.0519 ± 0.0012	4.20 ± 0.34
KF-22	(−9)-(−4)	0.0832 ± 0.0244	2.46 ± 0.86
KF-23	(−8)-(−6)	0.1005 ± 0.0151	2.54 ± 0.33
KF-24	(−10)-(−8)	0.1045 ± 0.0218	3.73 ± 0.28

1. Mean and standard deviation on three replicates.
2. The second decimal is retained to avoid rounding-off errors.
3. KF-20 is the homogenized boundary claystone.

References

Achenbach-Richter, L., Stetter, K.O., and Woese, C.R. 1987. A possible biochemical missing link among archaebacteria. *Nature*, 327: 348-349.

Alexander, P.O. 1976. Age and duration of Deccan volcanism. K-Ar evidence. *Geological Society of India Memoir*, 3: 244-258.

Alt, D., Sears, J.M., and Hyndman, D.W. 1988. Terrestrial Maria: The origins of large basalt plateaus, hotspot tracks and spreading ridges. *The Journal of Geology*, 96: 647-662.

Alvarez, L.W., Alvarez, W., Asaro, F., and Michel, H.V. 1980. Extraterrestrial cause for the Cretaceous-Tertiary extinction. *Science*, 208: 1095–1108.

Alvarez, L.W., Alvarez, W., Asaro, F. and Michel, H.V., 1982. Current status of the impact theory for the terminal Cretaceous extinction. *Geological Society of America Special Paper*, 190: 305-315.

Alvarez, W., Claeys, P., and Kieffer, S.W. 1995. Emplacement of Cretaceous-Tertiary boundary shocked quartz from Chicxulub Crater. *Science*, 269: 930-935.

Anbar, A.D., and Knoll, A.H. 2002. Proterozoic ocean chemistry and evolution: A bioinorganic bridge? *Science*, 297: 1137-1142.

Aneja, V.P., and Cooper, W.J. 1989. Biogenic sulfur emissions: A review. pp. 2-13 *In:* Saltzmann, E.S., and Cooper, W.J. (Eds.). Biogenic sulfur in the environment. ACS Symposium Series 393. American Chemical Society, Washington, D.C. 572 p.

Anderson, R.R., and Hartung, J. 1992. The Manson impact structure; Its contribution to impact materials at the Cretaceous/Tertiary Boundary. *Proceedings of Lunar and Planetary Science*, 22: 101-110.

Andreae, M.O., and Barnard, W.R. 1984. The marine chemistry of dimethylsulfide. *Marine Chemistry*, 14: 267-279.

Angert, A., Rachmilevitch, S., Barkan, E., Luz, B. 2003. Effects of photorespiration, the cytochrome pathway, and the alternative pathway on the triple isotopic composition of atmospheric O_2. *Global Biogeochemical Cycles*, 17. DOI:10.1029/2002GB001933.

Archibald, J.D. 2011. Extinction and radiation: how the fall of dinosaurs led to the rise of mammals. Johns Hopkins University Press, Baltimore. 108 p.

Arenillas, I., Arz, J., Grajales-Nishimura, J., Murillo-Muneton, G., Alvarez, W., Camargo-Zanoguera, A., Molina, E., and Rosales-Dominguez, C. 2006. Chicxulub impact event is Cretaceous/Paleogene boundary in age: New micropaleontological evidence. *Earth and Planetary Science Letters,* 249: 241-257.

Arens, N.C., and Jahren, A.H. 2000. Carbon isotopic excursion in atmospheric CO_2 at the Cretaceous-Tertiary boundary: Evidence from terrestrial sediments. *Palaios*, 15: 14-322.

Bajpai, S, and Prasad, G.V.R. 2000. Cretaceous age for Ir-rich Deccan intertrappean deposits: palaeontological evidence from Anjar, western India. *Journal of the Geological Society, London*, 157: 257-260.

Bak, F., and Pfennig, N. 1987. Chemolithotrophic growth of *Desulfovibrio-Sulfodismutans sp-nov* by disproportionation of inorganic sulfur compounds. *Archives of Microbiology*, 147: 184–189.

Beane, J.E., Turner, C.A., Hooper, P.R., Subbarao, K.V., and Walsh, J.N. 1986. Stratigraphy, composition and form of the Deccan basalts, Western Ghats, India. *Bulletin of Volcanology*, 48: 61-63.

Beaudoin, G., Taylor, B.E., Rumble III, D., and Thiemens, M. 1994. Variations in the

sulfur isotope composition of troilite from the Cañon Diablo iron meteorite. *Geochimica et Cosmochimica Acta*, 56: 2839.

Beerling, D.J., Lomax, B.H., Upchurch, G.R.Jr., Nichols, D.J., Pillmore, C.L., Handley, L.L., and Scrimgeour, C.M. 2001. Evidence for the recovery of terrestrial ecosystems ahead of marine primary production following a production biotic crisis at the Cretaceous-Tertiary boundary. *Journal of the Geological Society, London*, 158: 737-740.

Bekki, S. 1995. Oxidation of volcanic SO_2: A sink for stratospheric OH and H_2O. *Geophysical Research Letters*, 22: 913-916.

Berner, R.A. 1984. Sedimentary pyrite formation; An update. *Geochimica et Cosmochimica Acta*, 48: 605–615.

Bhandari, N., Shukla, P.N., Ghevariya, Z.G., and Sundaram, S.M. 1995. Impact did not trigger Deccan volcanism: Evidence from Anjar K/T boundary intertrappean sediments. *Geophysical Research Letters*, 22: 433-436.

Bigeleisen J. 1965. Chemistry of isotopes. *Science*, 147: 463-471.

Blum, J.D., and Chamberlain, C.P. 1992. Oxygen isotope constraints on the origin of impact glasses from the Cretaceous-Tertiary boundary. *Science*, 257: 1104-1107.

Bohor, B.F., Foord, E.E., Modreski, P.J., and Triplehorn, D.M. 1984. Mineralogic evidence for an impact event at the Cretaceous-Tertiary boundary. *Science*, 224: 867-869.

Bolliger, C., Schroth, M.H., Bernasconi, S.M., Kleikemper, J., and Zeyer, J. 2001. Sulfur isotope fractionation during microbial sulfate reduction by toluene-degrading bacteria. *Geochimica et Cosmochimica Acta*, 65: 3289-3298.

Bose, M.K. 1972. Deccan basalts. *Lithos*, 5:131–145

Bottomley, R. J., Grieve, R., York, D., and Masaitis, V. 1997. The age of the Popigai impact event and its relation to events at the Eocene/Oligocene boundary. *Nature*, 388: 365-368.

Bottomley, R. J., and York, D. 1989. The dating of impact melt rocks using the ^{40}Ar-^{39}Ar method. *Lunar and Planetary Science*, XX: 101-102.

Bottomley, R. J., York, D., and Grieve, R.A.F. 1993. Age of Popigai impact event using the ^{40}Ar-^{39}Ar method. *Lunar and Planetary Science XXIV*: p. 161.

Boudreau, B.P., and Westrich, J.T. 1984. The dependence of bacterial sulfate reduction on sulfate concentration in marine sediments. *Geochimica et Cosmochimca Acta*, 48: 2503–2516.

Bradford, M. 1976. A rapid and sensitive method for the quantitation of microgram quantities of protein utilizing the principle of protein-dye binding. *Analytical Biochemistry*, 72: 248-254.

Brasseur, G.P., Orlando, J.J. and Tyndall, G.S. (Editors). 1999. Atmospheric chemistry and global change. Oxford University Press, New York. 654 p.

Brimblecombe, P., Hammer, C., Rodhe, H., Ryaboshapko, A., and Boutron, C.F. 1989. Human influence on the sulphur cycle. pp. 77-121 *In*: Brimblecombe, P., and Lein, A.Y. (Eds.). Evolution of the global biogeochemical sulphur cycle. SCOPE 39. Wiley, Chichester. 241 pp.

Brüchert, V., Knoblauch, C., and Jørgensen, B.B. 2001. Controls on stable sulfur isotope fractionation during bacterial sulfate reduction in Arctic sediments. *Geochimica and Cosmochimica Acta*, 65: 763-776.

Brunner, B., and Bernasconi, S.M. 2005. A revised isotope fractionation model for dissimilatory sulfate reduction in sulfate reducing bacteria. *Geochimica and Cosmo-*

chimica Acta, 69: 4759-4771.

Brunner, B., Bernasconi, S.M., Kleikemper, J., and Schroth, M. H. 2005. A model for oxygen and sulfur isotope fractionation in sulfate during bacterial sulfate reduction processes. *Geochimica et Cosmochimica Acta*, 69: 4773-4785.

Buick, R., and Dunlop, J.S.R. 1990. Evaporitic sediments of early Archaean age from the Warrawoona group, North Pole. *Sedimentology*, 37: 247–277.

Cameron, E.M. 1982. Sulphate and sulphate reduction in early Precambrian oceans. *Nature*, 296: 145-148.

Cande, S.C., and Kent, D.V. 1995. Revised calibration of the geomagnetic polarity timescale for the Late Cretaceous and Cenozoic. *Journal of Geophysical Research,* 100: 6093-6096.

Canfield, D.E. 1993. Organic matter oxidation in marine sediments, pp. 333-363. *In*: Wollast, R., Mackenzie, F.T., and Chou, L. (Eds.) Interactions of C, N, P and S biogeochemical cycles. Springer, Berlin. 521 p.

Canfield, D.E. 2001. Isotope fractionation by natural populations of sulfate-reducing bacteria. *Geochimica et Cosmochimica Acta*, 65: 1117-1124.

Canfield, D.E., Habicht, K., and Thamdrup, B. 2000. The Archean sulphur cycle and the early history of atmospheric oxygen. *Science*, 288: 658-661.

Canfield, D.E., Olesen, C.A., and Cox, R.P. 2006. Temperature and its control of isotope fractionation by a sulfate-reducing bacterium. *Geochimica et Cosmochimica Acta*, 70: 548-561.

Canfield, D.E., and Raiswell, R. 1999. The evolution of the sulfur cycle. *American Journal of Science*, 299: 697–723.

Canfield, D.E., and Teske, A. 1996. Late Proterozoic rise in atmospheric oxygen concentration inferred from phylogenetic and sulphur-isotope studies. *Nature*, 382: 127-132.

Canfield, D.E., and Thamdrup, B. 1994. The production of ^{34}S-depleted sulfide during bacterial disproportionation of elemental sulfur. *Science*, 266: 1973-1975.

Carlisle, D. B. 1995. Dinosaurs, diamonds, and things from outer space. Stanford University Press, Stanford, California. 264 p.

Carlisle, D.B., and Braman, D.R. 1991. Nanometre-size diamonds in the Cretaceous/Tertiary boundary clay of Alberta. *Nature*, 352: 708-709.

Catuneanu, O., and Sweet, A.R. 1999. Maastrichtian-Paleocene foreland-basin stratigraphies, western Canada: a reciprocal sequence architecture. *Canadian Journal of Earth Sciences*, 36: 685-703.

Chambers, L.A., and Trudinger, P.A. 1975. Are thiosulfate and trithionate intermediates in dissimilatory sulfate reduction? *Journal of Bacteriology*, 123: 36-40.

Chambers, L.A., Trudinger, P.A., Smith, J.W., and Burns, M.S. 1975. Fractionation of sulfur isotopes by continuous cultures of *Desulfovibrio desulfuricans*. *Canadian Journal of Microbiology*, 21: 1602-1607.

Charlson, R.J., Lovelock, J.E., Andreae, M.O., and Warren, S.G. 1987. Oceanic phytoplankton, atmospheric sulphur, albedo and climate. *Nature*, 326: 655-661.

Chenet, A.-L., Courtillot, V., Fluteau, F., Gérard, M., Quidelleur, X., Khadri, S.F.R., Subbarao, K.V., and Thordarson, T. 2009. Determination of rapid Deccan eruptions across the Cretaceous-Tertiary boundary using paleomagnetic secular variation: 2. Constraints from analysis of eight new sections and synthesis for a 3500-m-thick composite section. *Journal of Geophysical Research*, 114: doi:10.1029/2008JB005644.

Chenet, A.-L., Fluteau, F., Courtillot, V., Gérard, M., and Subbarao, K.V. 2008. Determination of rapid Deccan eruptions across the Cretaceous-Tertiary boundary using paleomagnetic secular variation: Results from a 1200-m-thick section in the Mahabaleshwar escarpment. *Journal of Geophysical Research*, 113. doi:10.1029/2006JB004635

Chenet, A.-L., Quidelleur, X., Fluteau, F., Courtillot, V., and Bajpai, S. 2007. ^{40}K-^{40}Ar dating of the Main Deccan large igneous province: Further evidence of KTB age and short duration. *Earth and Planetary Science Letters*, 263: 1-15.

Clark, I.D., and Fritz, P. 1997. Environmental isotopes in hydrogeology. CRC Press, Boca Raton, Florida. 352 p.

Claypool, G.E., Holser, W.T., Kaplan, I.R., Sakai, H, and Zak, I. 1980. The age curves of sulfur and oxygen isotopes in marine sulfate and their mutual interpretation. *Chemical Geology*, 28: 199-260.

Cline, J.D. 1969. Spectrophotometric determination of hydrogen sulfide in natural waters. *Limnology and Oceanography*, 14: 454-458.

Clube, V., and Napier, B. 1990. The cosmic winter. Blackwell, Oxford. 307 p.

Colman, J.J., Xu, X.P., Thiemens, M.H., and Trogler, W.C. 1996. Photopolymerization and mass-independent sulphur isotope fractionations in carbon disulphide. *Science*, 273: 774-776.

Courtillot, V., Besse, J., Vandamme, D., Montigny, R., Jaeger, J.-J., and Capetta, H. 1986. Deccan flood basalts at the Cretaceous/Tertiary boundary? *Earth and Planetary Science Letters*, 80: 361-374.

Courtillot, V., Gallet, Y., Rocchia, R., Féraud, G., Robin, E., Hofmann, C., Bhandari, N., and Ghevariya, Z.G. 2000. Cosmic markers, $^{40}Ar/^{39}Ar$ dating and paleomagnetism of the KT sections in the Anjar Area of the Deccan large igneous province. *Earth and*

Planetary Science Letters, 182: 137-156.

Cox, R.A., and Sheppard, D. 1980. Reactions of OH radicals with gaseous sulphur compounds. *Nature*, 284: 330-331.

Craig, H. 1968. Isotope separation by carrier diffusion. *Science*, 159: 93-96.

Cropp, R.A., Gabric, A.J., McTainsh, G.H., Braddock, R.D., and Tindale, N. 2005. Coupling between ocean biota and atmospheric aerosols: Dust, dimethylsulphide, or artifact? *Global Biogeochemical cycles*, 19: doi:10.1029/2004GB002436

Cypionka, H. 1987. Uptake of sulphate, sulphite and thiosulphate by proton-anion symport in *Desulfovibrio desulphuricans*. *Archives of Microbiology*, 148: 144-149.

Cypionka, H. 1989. Characterization of sulphate transport in *Desulfovibrio desulphuricans. Archives of Microbiology,* 152: 237-243.

Cypionka, H. 1995. Solute transport and cell energetics, pp. 151-184. *In:* Barton, L.L. (Ed.) Sulfate-reducing bacteria, Volume 8. Plenum Press. 352 p.

Dalrymple, G. B., Izett, G. A., Snee, L. W., and Obradovich, J. D. 1993. $^{40}Ar/^{39}Ar$ age spectra and total-fusion ages of tektites from Cretaceous-Tertiary boundary sedimentary rocks in the Beloc Formation, Haiti. U. S. *Geological Survey Bulletin,* 2065: 20 p.

Deino, A. L., Garvin, J.B., and Montanari, S. 1991. K/T age for the Popigai impact event? *Lunar and Planetary Science*, XXII: 297-298.

Detmers, J., Brüchert, V., Habicht, K.S., and Kuever, J. 2001. Diversity of sulfur isotope fractionations by sulfate-reducing prokaryotes. *Applied and Environmental Microbiology*, 67: 888-894.

Devey, C.W., and Lightfoot, P.C. 1986. Volcanology and tectonic control of stratigraphy and structure in the western Deccan traps. *Bulletin of Volcanology*, 48: 195-207.

D'Hondt, S., Donaghay, P., Zachos, J.C., Luttenberg, D., and Lindinger, M. 1998. Organic carbon fluxes and ecological recovery from the Cretaceous-Tertiary mass extinction. *Science*, 282: 276–279.

Ding, T., Valkiers, Sl, Kipphardt, H., De Bievre, P., Taylor, P.D.P., Taylor, R., Gonfiantini, R., and Krouse, R. 2001. Calibrated sulphur isotope abundance ratios of three IAEA sulphur isotope reference materials and V-CDT with a reassessment of the atomic weight of sulphur. *Geochimica et Cosmochimica Acta*, 65: 2433-2437.

Duncan, R.A., and Pyle, D.G. 1988. Rapid eruption of the Deccan flood basalts at the Cretaceous-Tertiary boundary. *Nature*, 333: 841–843.

Farquhar, J., Canfield, D.E., Masterson, A., Bao, H., and Johnston, D. 2008. Sulfur and oxygen isotope study of sulfate reduction in experiments with natural populations from Fllestrand, Denmark. *Geochimica et Cosmochimica Acta*, 72: 2805-2821.

Farquhar, J., Johnston, D.T., Wing, B.A., Habicht, K.S., Canfield, D.E., Airieau, S., and Thiemens, M.H. 2003. Multiple sulphur isotopic interpretations of biosynthetic pathways: Implications for biological signatures in the sulphur isotope record. *Geobiology*, 1: 27-36.

Farquhar, J. Savarino, J., Airieau, S., and Thiemens, M.H. 2001. Observation of wavelength-sensitive mass-independent sulphur isotope effects during SO_2 photolysis: Implications for the early atmosphere. *Journal of Geophysical Research*, 106: 32829-32839

Farquhar, J., and Wing, B.A. 2003. Multiple sulfur isotopes and the evolution of the atmosphere. *Earth and Planetary Science Letters*, 213: 1-13.

Fastovsky, D.E., and Sheehan, P.M. 2005. The extinction of the dinosaurs in North America. *GSA today*, 15: 4–10.

Ferek, R.J., Chatfield, R.B., and Andreae, M.O. 1986. Vertical distribution of dimethylsulfide in the marine atmosphere: Implications for the atmospheric sulfur cycle. *Nature*, 320: 514—516.

Fitz, R.M., and Cypionka, H. 1989. A study on electron transport-driven proton translocation in *Desulfovibrio desulphuricans. Archives of Microbiology*, 152: 369-376.

Fitz, R.M., and Cypionka, H. 1990. Formation of thiosulfate and trithionate during sulfite reduction by washed cells of *Desulfovibrio desulfuricans*. *Archives of Microbiology*, 140: 400-406.

Fitz, R.M., and Cypionka, H. 1991. Generation of a proton gradient in *Desulfovibrio vulgaris. Archives of Microbiology*, 155: 444-448.

Fleming, R.F., and Nichols, D.J. 1990. The fern-spore abundance anomaly at the Cretaceous-Tertiary boundary - A regional bioevent in western North America. pp. 347-349 *In*: Kaufman, E.G., and Walliser, O.G. (Eds.) Extinction events in Earth history: Proceedings of the Project 216, Global Biological Events in Earth History. Lecture Notes in Earth Sciences. Springer-Verlag. 442 p.

Forrest, J., Klein, J.H., and Newman, L. 1973. Sulphur isotope ratios of some power plant flue gases: A method for collecting the sulphur-oxide. *Journal of Applied Chemistry and Biotechnology*, 23: 855-63.

French B.M. 1984. Impact event at the Cretaceous-Tertiary boundary - A possible site. *Science*, 226: 353.

Ganerød, M., Torsvik, T. H. , van Hinsbergen, D. J. J., Gaina, C., Corfu, F., Werner, S., Owen-Smith, T.M., Ashwal, L.D., Webb, S.J., and Hendriks, B.W.H. 2011. Paleoposition of the Seychelles microcontinent in relation to the Deccan Traps and the Plume Generation Zone in Late Cretaceous-Early Palaeogene time. *Geological Society, Lon-*

don, Special Publications, 357: 229-252

Gartner, S., and Keany, J. 1978. The terminal Cretaceous event: A geologic problem with an oceanographic solution. *Geology*, 6: 708.

Gibson, D.W. 1977. Upper Cretaceous and Tertiary coal-bearing strata in the Drumheller-Ardley region, Red Deer River Valley, Alberta. *Geological Survey of Canada, Paper*, 76-35: 1-41.

Glass, S.J., and Matteson, M.J. 1973. Ion enrichment in aerosols dispersed from bursting bubbles in aqueous salt solutions. *Tellus*, 25: 272-280.

Goodwin, A.M., Monster, J., and Thode, H.G. 1976. Carbon and sulphur isotope abundance in Archean Iron-Formations and early Precambrian life. *Economic Geology*, 71: 870-891.

Gradstein, F.M., Ogg, J.G., Smith, A.G., Bleeker, W., and Lourens, L.J. 2004. A new geologic time scale, with special reference to Precambrian and Neogene. *Episodes*, 27: 83-100.

Grassineau, N.V., Nisbet, E.G., Bickle, M.J., Fowler, C.M.R., Lowry, D., Mattrey, D.P., Abell, P., and Martin, A. 2000. Antiquity of the biological sulphur cycle: Evidence from sulphur and carbon isotopes in 2700 million-year-old rocks of the Blingwe Belt, Zimbabwe. *Proceedings of the Royal Society of London B*, 268: 113-119.

Grinenko, V.A., and Ivanov, M.V. 1983. Principal reactions of the global biogeochemical cycle of sulfur, pp. 1-24 *In:* Ivanov, M.V., and Freney, J.R. (Eds.) The global geochemical sulfur cycle. International Council of Scientific Unions. Scientific Committee on Problems of the Environment. Wiley, New York.470 p.

Grinenko, V.A., and Thode, H.G. 1970. Sulphur isotope effects in volcanic gas mixtures. *Canadian Journal of Earth Sciences*, 7: 1402-1409.

Gupta, M.L, and Gaur, V.K. 1984. Surface heat flow and probable evolution of Deccan volcanism. *Tectonophysics*, 105: 309-318.

Habicht, K.S., and Canfield, D.E., 1996. Sulphur isotope fractionation in modern microbial mats and the evolution of the sulphur cycle. *Nature*, 382: 342–343. doi:10.1038/382342a0

Habicht, K.S., and Canfield, D.E. 1997. Sulfur isotope fractionation during bacterial sulfate reduction in organic-rich sediments. *Geochimica et Cosmochimica Acta*, 61: 5351-5361.

Habicht, K.S., Canfield, D.E., and Rethmeier, J. 1998. Sulfur isotope fractionation during bacterial reduction and disproportionation of thiosulfate and sulfite. *Geochimica et Cosmochimica Acta*, 62: 2585–2595.

Habicht, K.S., Gade, M., Thamdrup, B., Berg, P., and Canfield, D.E. 2002. Calibration of sulfate levels in the Archean ocean. *Science,* 298: 2372-2374.

Habicht, K.S., Salling, L., Thamdrup, B., and Canfield, D.E. 2005. Effect of low sulfate concentrations on lactate oxidation and isotope fractionation during sulfate reduction by *Archeoglobus fulgidus* strain Z. *Applied and Environmental Microbiology*, 71: 3770-3777.

Hansen, T.A. 1993. Carbon metabolism of sulfate-reducing bacteria. p. 21-40. *In* Odom, J.M., and Singleton, R. (Editors). The sulfate-reducing bacteria: Contemporary perspectives. Springer-Verlag, New York. 289 pp.

Hansen, T.A. 1994. Metabolism of sulfate-reducing prokaryotes. *Antonie von Leeuwenhoek*, 66: 165-185.

Hao, O.J., Chen, J.M., Huang, L., and Buglass, R.L. 1996. Sulfate-reducing bacteria. *Critical Reviews in Environmental Science and Technology*, 26: 155–187.

Harrison, A.G., and Thode, H.G. 1957. The kinetic isotope effect in the chemical reduction of sulphate. *Transactions of the Faraday Society*, 53: 1648-1651.

Harrison, A.G., and Thode, H.G. 1958. Mechanism of the bacterial reduction of sulphate from isotope fractionation studies. *Transactions of the Faraday Society*, 54: 84-92.

Hartung, J.B., Kunk, M.J., and Anderson, R.R. 1990. Geology, geophysics, and geochronology of the Manson impact structure. pp. 207-221 *In* Sharpton, V.L., and Ward, P.D. (Eds.) Global catastrophes in Earth history: An interdisciplinary Conference on Impacts, Volcanism, and Mass Mortality. *Geological Society of America Special Papers*, 247.

Hattori, K., and Cameron, E. M. 1986. Archaean magmatic sulphate. *Nature*, 319: 45–47.

Hildebrand, A.R. 1993. The Cretaceous-Tertiary boundary impact (or the dinosaurs didn't have a chance*). Journal of the Royal Astronomical Society of Canada*, 87: 77-118.

Hildebrand, A.R., and Boynton, W.V. 1988. Provenance of the K/T boundary layers. *Lunar and Planetary Institute Contribution*, 673: 78-79.

Hildebrand, A.R., Penfield, G.T., Kring, D.A., Pilkington, M., Camargo Z.A., Jacobsen, S.B., and Boynton, W.V. 1991. Chicxulub Crater: A possible Cretaceous/Tertiary boundary impact crater on the Yucatán Peninsula, Mexico. *Geology*, 19: 867-871.

Hobbs, P.V., Radke, L.F., Lyons, J.H., Ferek, R.J., Coffman, D.J., and Casadevall, T.J. 1991. Airborne measurements of particle and gas emissions from the 1990 volcanic eruptions of Mount Redoubt. *Journal of Geophysical Research*, 96: 18,735-18,752. doi:10.1029/91JD01635

Hoefs, J. 1997. Stable isotope geochemistry. 4th edition. Springer Verlag. 201 p.

Hofmann, C., Féraud, G., and Courtillot, V. 2000. $^{40}Ar/^{39}Ar$ dating of mineral separates and whole rocks from the Western Ghats lava pile: Further constraints on duration and age of the Deccan traps. *Earth and Planetary Science Letters*, 180: 13-27.

Holland, H.D. 1978. The chemistry of the atmosphere and oceans. Wiley, New York. 351 p.

Holmes, C.W., and Bohor, B.F. 1994. Stable isotope (C,N,S) distributions in coals spanning the Cretaceous/Tertiary boundary in the Raton Basin, Colorado and New Mexico. (abs.) *U.S. Geological Survey Circular*, 1107: p. 141.

Holser, W.T., Maynard, J.B. and Cruikshank, K.M. 1989. Modelling the natural cycle of sulfur through phanerozoic time. pp. 21-56 *In:* Brimblecombe, P. and Lein A.Y. (Editors). Evolution of the global biogeochemical sulfur cycle. SCOPE 39. John Wiley and Sons, Chichester. 241 p.

Hooper, P., Widdowson, M., and Kelley, S. 2010. Tectonic setting and timing of the final Deccan flood basalt eruptions. *Geology*, 38: 839-842.

Hough, R.M., Wright, I.P., Pillinger, C.T., and Gilmour, L. 1995. Microdiamonds from the iridium-rich layer of the Arroyo El Mimbral K-T boundary outcrop, N.E., Mexico. *Abstracts of the Lunar and Planetary Science Conference*, 26: p. 629.

Hsü, K.J.,He, Q.,McKenzie, J.A.,Weissert, H., Perch-Nielsen K., Oberhänsli, H., Kelts, K., Labrecque, J., Tauxe, L., Krähenbühl, U., Percival, S.F. Jr, Wright, R., Karpoff, A.M., Petersen, N., Tucker, P., Poore, R.Z., Gombos, A.M., Pisciotto, K., Carman, M.F. Jr, and Schreiber, E. 1982. Mass mortality and its environmental and evolutionary consequences. *Science*, 216: 249–256.

Huber, B.T., Hodell, D.A., and Hamilton, C.P. 1995. Middle-Late Cretaceous climate

of the southern high latitudes: Stable isotopic evidence for minimum equator-to-pole thermal gradients. *Geological Society of America Bulletin*, 107: 1164-1191.

Hulston, J.R., and Thode, H.G. 1965. Variations in ^{33}S, ^{34}S and ^{36}S contents of meteorites and their relation to chemical and nuclear effects. *Journal of Geophysical Research*, 70: 3475-3484.

Husson, D., Galbrun, B., Laskar, J., Hinnov, L.A., Thibault, N., Gardin, S., and Locklair, R.E. 2011. Astronomical calibration of the Maastrichtian (Late Cretaceous). *Earth and Planetary Science Letters*, 305: 328-340.

International Atomic Energy Agency (IAEA), and United Nations Educational, Scientific and Cultural Organization. 2000. Environmental isotopes in the hydrological cycle. Principles and applications. Volume 1. Water Resources Programme. 164 p.

Iba, Y., Mutterlose, J., Tanabe, K., Sano, S., Misaki, A., and Terabe, K. 2011. Belemnite extinction and the origin of modern cephalopods 35 m.y. prior to the Cretaceous-Paleogene event. *Geology*, 39: 483-486.

Ingvorsen, K., and Jørgensen, B.B. 1984. Kinetics of sulfate uptake by freshwater and marine species of *Desulfovibrio*. *Archives of Microbiology*, 139: 61-66

Ingvorsen, K., Zehnder, A. J.B., and Jørgensen, B.B. 1984. Kinetics of sulfate and acetate uptake by *Desulfobacter postgatei*. *Applied and Environmental Microbiology*, 47: 403-408.

Isaksen, M.F., Bak, F., and Jørgensen, B.B. 1994. Thermophilic sulfate-reducing bacteria in cold marine sediment. *FEMS Microbiology and Ecology*, 14: 1-8.

Isaksen, M.F., and Jørgensen, B.B. 1996. Adaptation of psychrophilic and psychotrophic sulphate-reducing bacteria to permanently cold marine environments. *Applied and Environmental Microbiology*, 62: 408-414.

Ivany, L.C., and Salawitch, R.J. 1993. Carbon isotopic evidence for biomass burning at the K/T boundary. *Geology*, 21: 487–490.

Izett, G.A., Cobban, W.A., Obradovich, J.D., and Kunk, M.J. 1993. The Manson impact structure: $^{40}Ar/^{39}Ar$ Age and its distal impact ejecta in the Pierre Shale in Southeastern South Dakota. *Science*, 262: 729-32.

Izett, G.A., Dalrymple, G.B., and Snee, L.W. 1991. $^{40}Ar/^{39}Ar$ Age of Cretaceous-Tertiary Boundary tektites from Haiti. *Science*, 252: 1539-1542.

Jaeger, J.-J., Courtillot, V., and Tapponnier, P. 1989. Paleontological view of the ages of the Deccan Traps, the Cretacous/Tertiary boundary, and the India-Asia collision. *Geology*, 17: 316-319.

Jaye, A.E., and Widdowson, M. 2008. Stratigraphy, structure and volcanology of the SE Deccan continental flood basalt province: Implications for eruptive extent and volumes. *Journal of the Geological Society, London*, 165: 177-188.

Jaye, A.E., Mac Niocaill, C., Widdowson, M., Self, S., and Turner, W. 2009. New palaeomagnetic data from Mahabaleshwar Plateau, Deccan Flood Basalt Province, India: implications for the volcanostratigraphic architecture of continental flood basalt provinces. *Journal of the Geological Society, London*, 166: 13-24.

Johnson, D.B. 2000. Biological removal of sulfurous compounds from inorganic wastewaters. pp. 175-206 *In:* Lens, P., and Hulshoff-Pol, L. (Eds.) Environmental technologies to treat sulfur pollution: Principles and engineering. International Association of Water Quality, London. 547 p.

Johnston, D.T., Farquhar, J., and Canfield, D.E. 2007. Sulfur isotope insights into microbial sulfate reduction: When microbes meet models. *Geochimica et Cosmochimica Acta*, 71: 3929-3947.

Johnston, D.T., Farquhar, J., Wing, B.A., Kaufman, A.J., Canfield, D.E., and Habicht, K.S. 2005. Multiple sulfur isotope fractionations in biological systems: A case study with sulfate reducers and sulfur disproportionators. *American Journal of Science*, 305: 645-660.

Jørgensen, B.B. 1982. Mineralization of organic matter in the sea bed - the role of sulfate reduction. *Nature*, 296: 643-645.

Jørgensen, B.B., Isaksen, M.F., and Jannasch, H.W. 1992. Bacterial sulphate reduction above 100°C in deep-sea hydrothermal vent sediments. *Science*, 258: 1756-1757.

Kajiwara, Y., and Kaiho, K. 1992. Oceanic anoxia at the Cretaceous/tertiary boundary supported by the sulfur isotopic record. *Palaeogeography, Palaeoclimatology, Palaeoecology*, 99: 151–162.

Kakegawa, T., Kawai, H., and Ohmoto, H. 1999. Origins of pyrites in the ~2.5 Ga Mt. McRae Shale, the Hamersley District, western Australia. *Geochimica et Cosmochimica Acta*, 62: 3205-3220.

Kaminski, E., Chenet, A.-L., Jaupart, C., and Courtillot, V. 2011. Rise of volcanic plumes to the stratosphere aided by penetrative convection above. *Earth and Planetary Science Letters*, 301: 171–178.

Kaneoka, I. 1980. $^{40}Ar/^{39}Ar$ dating on volcanic rocks of the Deccan traps, India. *Earth and Planetary Science Letters*, 46: 233-243.

Kaplan, I.R., and Rittenberg, S.C. 1964. Microbiological fractionation of sulfur isotopes. *Journal of General Microbiology*, 34: 195-212.

Keller, G. 1989. Extended period of extinctions across the Cretaceous /Tertiary boundary in planktonic foraminifera of continental-shelf sections: Implications for impact

and volcanism theories. *Geological Society of America Bulletin*, 101: 1408-1419.

Keller, G., Adatte, T., Gardin, S., Bartolini, A., and Bajpai, S. 2008. Main Deccan volcanism phase ends near the K-T boundary: Evidence from the Krishna-Godavari Basin, SE India. *Earth and Planetary Science Letters*, 268: 293-311.

Keller, G., Li, L., and MacLeod, N. 1995. The Cretaceous/Tertiary boundary stratotype section at El Kef, tunisia: How catastrophic was the mass extinction? *Palaeogeography, Palaeoclimatology, Palaeoecology*, 119: 221-254.

Keller, G., and Lindiger, M. 1989. Stable isotope, TOC and $CaCO_3$ record across the Cretaceous/Tertiary boundary at El Kef, Tunisia. *Palaeogeography, Palaeoclimatology, Palaeoecology*, 73: 243–266.

Keller, G., Stinnesbeck, W., Adatte, T., and Stüben, D. 2003. Multiple impacts across the Cretaceous–Tertiary boundary. *Earth-Science Reviews*, 1283: 1–37.

Kellogg, W.W., Cadle, R.D., Allen, E.R., Lazrus, A.L., and Martell, E.A. 1972. The sulphur cycle. *Science*, 175: 587-596.

Kemp, A.L.W., and Thode, H.G. 1968. Mechanism of the bacterial reduction of sulphate from isotope fractionation studies. *Transactions of the Faraday Society*, 54: 84-92.

Kennedy, W.J. 1989. Thoughts on the evolution and extinction of Cretaceous ammonites. *Proceedings of the Geologists' Association*, 100: 251–279.

Kimura, S., Hallberg, K.B., and Johnson, D.B. 2006. Sulfidogenesis in low pH (3.8-4.2) media by a mixed population of acidophilic bacteria. *Biodegradation*, 17: 159-167. DOI 10.1007/s10532-005-3050-4

Knauth, L.P. 2005. Temperature and salinity history of the Precambrian ocean: Impli-

cations for the course of microbial evolution. *Palaeogeography, Palaeoclimatology, Palaeoecology,* 219: 53-69.

Knight, K.B., Renne, P.R., Baker, J., Waight, T., and White, N. 2005. Reply to '$^{40}Ar/^{39}Ar$ dating of the Rajahmundry Traps, Eastern India and their relationship to the Deccan Traps: Discussion. *Earth and Planetary Science Letters*, 239: 374-382.

Knight, K.B., Renne, P.R., Halkett, A., and White, N. 2003. $^{40}Ar/^{39}Ar$ dating of the Rajahmundry Traps, Eastern India and their relationship to the Deccan Traps. *Earth and Planetary Science Letters*, 208: 85-89.

Kobayashi, K., Seki, Y., and Ishimoto, M. 1974. Biochemical studies on sulfate-reducing bacteria. XIII. Sulfite reductase from *Desulfovibrio vulgaris* - Mechanism of trithionate, thiosulfate, and sulfide formation and enzymatic properties. *Journal of Biochemistry*, 75: 519-529.

Kolmert, A., and Johnson, D.B. 2001. Remediation of acidic waste waters using immobilised, acidophilic sulfate-reducing bacteria. *Journal of Chemical Technology and Biotechnology*, 76: 836-843.

Koschorreck, M. 2008. Microbial sulfate reduction at a low pH. *FEMS Microbiology and Ecology*, 64: 329-342.

Kreke, B. and Cypionka, H. 1992. Protonmotive force in freshwater sulphate-reducing bacteria, and its role in sulphate accumulation in *Desulfobulbus propionicus. Archives of Microbiology*, 158: 183-187.

Kreke, B., and Cypionka, H. 1995. Energetics of sulphate transport in *Desulfomicrobium baculatum*. *Archives of Microbiology*,163: 307-309.

Krishnan, M.S. 1960. Geology of India and Burma. Higginbothams, Madras, India. 553 p.

Krouse, H.R., Stewart, J.W.B., and Grinenko, V.A. 1991. Pedosphere and Biosphere. pp. 267-306 *In* Krouse, H.R., and Grinenko, V.A. (Editors). Stable isotopes: Natural and anthropogenic sulphur in the environment. SCOPE 43. John Wiley and Sons, Chichester. 440 p.

Kuiper, K.F., Deino, A., Hilgen, F.J., Krijgsman, W., Renne, P.R., and Wijbrans, J.R., 2008. Synchronizing rock clocks of Earth history. *Science*, 320: 500-504.

Kump, L. 1991. Interpreting carbon-isotope excursions: Strangelove oceans. *Geology*, 19: 299–302.

Kunk, M.J., Sutter, J.F., Izett, G.A., and Haugerud, R.A. 1989. ^{40}Ar-^{39}Ar dating of the Manson impact structure - A Cretaceous-Tertiary boundary crater candidate. *Science*, 244: 1565-1568.

Labandeira, C., Johnson, K., and Wilf, P. 2002. Impact of the terminal Cretaceous event on plant-insect associations. *Proceedings of the National Academy of Sciences of the United States of America*, 99: 2061-2066.

Lerbekmo, J.F. 1999. Magnetostratigraphy of the Canadian Continental Drilling Program Cretaceous-Tertiary (K-T) Boundary Project core holes, western Canada. *Canadian Journal of Earth Sciences*, 36: 705-715.

Lerbekmo, J.F., and Braman, D.R. 2002. Magnetostratigraphic and biostratigraphic correlation of late Campanian and Maastrichtian marine and continental strata from the Red Deer Valley to the Cypress Hills, Alberta, Canada. *Canadian Journal of Earth Science*, 39: 539-557.

Lerbekmo, J.F., and Coulter, K.C. 1985. Late Cretaceous to early Tertiary magnetostratigraphy of a continental sequence: Red Deer Valley, Alberta, Canada. *Canadian Journal of Earth Sciences*, 22: 567-583.

Lerbekmo, J.F., Sweet, A.R., and Davidson, R.A. 1999. Geochemistry of the Cretaceous-Tertiary (K-T) boundary interval: South-central Saskatchewan and Montana. *Canadian Journal of Earth Sciences*, 36: 717-724.

Lerbekmo, J.F., Sweet, A.R., and Duke, M.J.M. 1996. A normal polarity subchron which embraces the K-T boundary: A measure of sedimentary continuity across the boundary and synchroneity of boundary events. pp. 465-476 *In:* Ryder, G., Fastovsky, D., and Gartner, S. (Eds.) Cretaceous-Tertiary event and other catastrophes in earth history. *Geological Society of America, Special Paper*, 307.

Lerbekmo, J.F., Sweet, A.R., and St. Louis, R.M. 1987. The relationship between the iridium anomaly and palynological floral events at three Cretaceous-Tertiary boundary localities in western Canada. *Geological Society of America Bulletin*, 99: 325-330.

Lowe, S.E., Jain, M.K., and Zeikus, J.G. 1993. Biology, ecology, and biotechnological applications of anaerobic-bacteria adapted to environmental stresses in temperature, pH, salinity, or substrates. *Microbiological Reviews*, 57: 451–509.

Machel, H.G., Krouse, H.R., and Sassen, R. 1995. Products and distinguishing criteria of bacterial and thermochemical sulphate reduction. *Applied Geochemistry*, 10: 373-389.

MacIntyre, F. 1974. The top millimeter of the ocean. *Scientific American*, 230: 62-69.

Mahon, K.I. 1996. The New “York” regression: Application of an improved statistical method to geochemistry. *International Geology Review*, 38: 293-303.

Mangalo, M., Einsiedl, F., Meckenstock, R.U., and Stichler, W. 2008. Influence of the enzyme dissimilatory sulfite reductase on stable isotope fractionation during sulfate reduction. *Geochimica et Cosmochimica Acta*, 72: 1513-1520.

Mariotti, A., Germon, J.C., Hubert, P., Kaiser, P., Leto Ile, R.,Tardieux, A. and Tardieux,

P. 1981. Experimental determination of nitrogen kinetic isotope fractionation: Some principles; Illustration for the denitrification and nitrification processes. *Plant and Soil*, 62: 413-430.

Marshall, C.R. 1995. Distinguishing between sudden and gradual extinctions in the fossil record: Predicting the position of the Cretaceous-Tertiary iridium anomaly using the ammonite fossil record on Seymour Island, Antarctica. *Geology*, 23: 731-734.

Martin, A. 1990. Bioenergetic parameters and transport in obligate acidophiles. *Biochimica et Biophysica Acta*, 1018: 267–270.

Maruoka, T. Koeberl, C., Newton, J., Gilmour, I., and Bohor, B.F. 2002. Sulfur isotopic compositions across terrestrial Cretaceous-Tertiary boundary successions. *Geological Society of America Special Paper*, 356: 337-344.

Mather, T., McCabe, J.R., Rai, V.K., Thiemens, M.H., Pyle, D.M., Heaton, T.H.E., Sloane, H.J., and Fern, G.R. 2006. Oxygen and sulfur isotopic composition of volcanic sulfate aerosol at the point of emission. *Journal of Geophysical Research-Atmospheres*, 111: 9 p. D18205,doi:10.1029/2005JD006584.

Mayer, B., and Krouse, H.R. 2004. Procedures for sulfur isotope abundance studies. pp. 538-596 *In* de Groot, P. (Ed.). Handbook of Stable Isotope Analytical Techniques V. I. Elsevier, Amsterdam. 622 p.

McElhinny, M.W. 1968. Northward drift of India – Examination of recent palaeomagnetic results. *Nature*, 217: 342-344.

McLean, D.W. 1978. A terminal Mesozoic “greenhouse”: Lessons from the past. *Science*, 201: 401.

McLean, D.M. 1985. Deccan Traps mantle degassing in the Terminal Cretaceous marine extinctions. *Cretaceous Research*, 6: 235-259.

McWilliams, M.O. 1991. High-resolution $^{40}Ar/^{39}Ar$ ages from Cretaceous-Tertiary boundary bentonites in western North America. Event Markers in Earth history meeting. Calgary, Alberta, August 28-30, 1991: p. 53.

McWilliams, M.O., Baksi, A.K., Bohor, B.F., Izett, G.A., and Murali, A.V. 1992. High-precision relative ages of K/T boundary events in North America and Deccan Trap volcanism in India. *Eos, Transactions, American Geophysical Union,* 73: p. 363.

Meldahl, K.H. 1990. Sampling, species abundance, and the stratigraphic signature of mass extinction - a test using Holocene tidal flat mollusks. *Geology*, 18: 890-893.

Melosh, H.J., Schneider, N.M., Zahnle, K.J., and Latham, D. 1990. Ignition of global wildfires at the Cretaceous/Tertiary boundary. *Nature*, 343: 251-254.

Meschede, M., Myhrvold, C., and Tromp, J. 2011. Antipodal focusing of seismic waves due to large meteorite impacts on Earth. *Geophysical Journal International*, 187: 529-537.

Miller M.F. 2002. Isotopic fractionation and the quantification of ^{17}O anomalies in the three oxygen isotope system: An appraisal and geochemical significance. *Geochimica et Cosmochimica Acta*, 66: 1881-1889.

Minz, D., Flax, J.L., Green, S.J., Muyzer, G., Cohen, Y., Wagner, M., Rittmann, B.E., and Stahl, D.A. 1999. Diversity of sulfate-reducing bacteria in oxic and anoxic regions of a microbial mat characterized by comparative analysis of dissimilatory sulfite reductase genes. *Applied and Environmental Microbiology*, 65: 4666-4671.

Molina, E., Alegret, L., Arenillas, I., Arz, J., Gallala, N., Grajales-Nishimura, J., Murillo-Muneton, G., and Zaghbib-Turki, D. 2009. The Global Boundary Stratotype Section and Point for the base of the Danian Stage (Paleocene, Paleogene, “Tertiary”, Cenozoic): Auxiliary sections and correlation. *Episodes*, 32: 84-95.

Molina, E., Arenillas, I., and Arz, J.A. 1998. Mass extinction in planktic Foraminifera at the Cretaceous/Tertiary boundary in subtropical and temperate latitudes. *Bulletin de la Société géologique de France*, 169: 351-363.

Monster, J., Appel, P.W.U., Thode, H.G., Schidlowski, M., Carmichael, C.M., and Bridgewater, D. 1979. Sulfur isotope studies in early Archaean sediments from Isua, West Greenland: Implications for the antiquity of bacterial sulfate reduction. *Geochimica et Cosmochimica Acta*, 43: 405-413.

Morel, F.M.M., and Hering, J.G. 1993. Principles and applications of aquatic chemistry. Wiley, New York. 588 p.

Morgan, W.J. 1972. Deep mantle convection plumes and plate motion. *Bulletin of the American Association of Petroleum Geologists,* 56: 203-213.

Moss, M.R. 1978. Sources of sulfur in the environment: The global sulfur cycle. pp. 23-50 *In:* Nriagu, J.O. (Ed.). Sulfur in the environment. Part I: The atmospheric cycle. John Wiley and Sons, New York. 464 p.

Motani, R. 2009. The evolution of marine reptiles. *Evolution: Education and Outreach*, 2: 224–235. DOI 10.1007/s12052-009-0139-y

Negi, J.G., Agrawal, P.K., Pandey, O.P., and Singh, A.P. 1993. A possible K-T boundary bolide impact site offshore near Bombay and triggering of rapid Deccan volcanism. *Physics of the Earth and Planetary Interiors*, 76: 189–197.

Newman, L., Krouse, H.R., and Grinenko, V.A. 1991. Chapter 5. Sulphur isotope variations in the atmosphere. pp. 132-176 *In:* Krouse, H.R., and Grinenko, V.A. (Eds.) Stable isotopes: Natural and anthropogenic sulphur in the environment. SCOPE 43. Wiley and Sons. 440 p.

Nichols, D.J., and Johnson, K.R. 2008. Plants and the K-T Boundary. Cambridge Uni-

versity Press. 292 pp.

Nielsen, H. 1974. Isotopic composition of the major contributors to atmospheric sulphur. *Tellus*, 26: 213-221.

Nriagu, J.O., and Coker, R.D. 1978. Isotopic composition of sulfur in precipitation within the Great Lakes basin. *Tellus*, 30: 365-374.

Officer CB, and Drake CL. 1985. Terminal Cretaceous environmental events. *Science*, 227: 1161–1167.

Officer, C., and Page, J. 1996. The great dinosaur extinction controversy. Addison-Wesley, Reading, Massachusetts. 209 p.

Ohmoto, H. 1997. When did the Earth's atmosphere become oxic? *The Geochemical News*, 93: 12-13, 26-27.

Ohmoto, H., Kakegawa, T., and Lowe, D.R. 1993. 3.4-billion-year-old biogenic pyrites from Barberton, South Africa: Sulfur isotope evidence. *Science*, 262: 555-557.

O'Keefe, J.D., and Ahrens, T.J. 1989. Impact production of CO_2 by the Cretaceous/Tertiary extinction bolide and the resultant heating of the Earth. *Nature*, 338: 247-249.

Orth, C.J., Gilmore, J.S., Knight, J.D., Pillmore, C.L., Tschudy, R.H., and Fassett, J.E. 1981. An iridium abundance anomaly at the palynological Cretaceous-Tertiary boundary in northern New Mexico. *Science*, 214: 1341-1343.

Paytan, A., Kastner, M., Campbell, M., Thiemens, M.H. 1998. Sulfur isotopic composition of Cenozoic seawater sulfate. *Science*, 282: 1459-1462.

Penfield, G.T., and Camargo, Z.A. 1981. Definition of a major igneous zone in the central Yucatan platform with aeromagnetics and gravity. Annual Meeting Abstracts, Society Of Exploration Geophysicists, 51: p. 37.

Perry, E.C.Jr., Monster, J., and Reimer, T. 1971. Sulphur isotopes in Swaziland System barites and the evolution of the Earth's atmosphere. *Science*, 171: 1015-1016.

Polcyn, M.J., and Bell, G.L. Jr. 2005. *Russellosaurus coheni n. gen.,n. sp.,* a 92-million-year-old mosasaur from Texas (USA), and the definition of the parafamily Russellosaurina. *Netherlands Journal of Geosciences*, 84: 321–333.

Postgate, J.R. 1984. The sulphate-reducing bacteria. Cambridge University Press, Cambridge. 208 p.

Prahm, L.P., Torp, U., and Stern, R.M. 1975. Deposition and transformation rates of sulphur oxides during atmospheric transport over the Atlantic. *Tellus*, 28: 355-372.

Prinn, R. G., and Fegley, B. Jr. 1987. Bolide impacts, acid rain, and biospheric traumas at the Cretaceous-Tertiary boundary. *Earth and Planetary Science Letters*, 83: 1-15.

Rampino, M.R., and Stothers, R. 1988. Flood basalt volcanism during the past 250 million years. *Science*, 241: 663-668

Rees, C.E. 1973. A steady-state model for sulphur isotope fractionation in bacterial reduction processes. *Geochimica et Cosmochimica Acta*, 37: 1141-1162.

Richardson, R.J.H., Strobl, R.S., Macdonald, D.E., Nurkowski, J.R., McCabe P.J., and Bosman, A. 1988. An evaluation of the coal resources of the Ardley Coal Zone, to a depth of 400 m in the Alberta Plains area. Alberta Geological Survey, Open File Report 1988-02.

Robertson, D.S., McKenna, M.C., Toon, O.B., Hope, S., and Lillegraven, J.A. 2004. Survival in the first hours of the Cenozoic. *Geological Society of America Bulletin*, 116: 760-768.

Robin, E., Boclet, D., Bonté, P., Froget, L., Jéhanno, C., and Rocchia, R. 1991. The stratigraphic distribution of Ni-rich spinels in Cretaceous-Tertiary boundary rocks at El Kef (Tunisia), Caravaca (Spain), and Hole 761C (Leg 122). *Earth and Planetary Science Letters*, 107: 715–721.

Robinson, N., Ravizza, G., Coccioni, R., Peucker-Ehrenbrink, B., and Norris, R. 2009. A high-resolution marine $^{187}O/^{188}O$ record for the late Maastrichtian: Distinguishing the chemical fingerprints of Deccan volcanism and the KP impact event. *Earth and Planetary Science Letters*, 281: 159-168.

Robock, A., and Oppenheimer, C. (Eds.) 2003. Volcanism and the Earth's atmosphere. American Geophysical Union, Geophysical Monograph, 139. 360 p.

Roy, A.B. and Trudinger, P.A. 1970. The biochemistry of inorganic compounds of sulfur. Cambridge University Press, Cambridge. 400 p.

Rudnicki, M.D., Elderfield, H., and Spiro, B. 2001. Fractionation of sulfur isotopes during bacterial sulfate reduction in deep ocean sediments at elevated temperatures. *Geochimica et Cosmochimica Acta*, 65: 777-789.

Russell, D.A. 1967. Systematics and morphology of American mosasaurs (Reptilia, Sauria). *Peabody Museum of Natural History, Yale University, Bulletin,* 23: 1-241.

Russell, D., and Tucker, W. 1971. Supernovae and the extinction of the dinosaurs. *Nature*, 229: 553 - 554. doi:10.1038/229553a0

Ryaboshapko, A.G. 1983. The atmospheric sulphur cycle. pp. 203-296 *In:* Ivanov, M.V., and Freney, J.R. (Eds). The global biochemical sulphur cycle. SCOPE 19. John Wiley and Sons, Chichester. 470 p.

Sagemann, J., Jørgensen, B.B., and Greeff, O. 1998. Temperature dependence and rates of sulfate reduction in cold sediments of Svalbard, Arctic Ocean. *Geomicrobio-*

logy Journal, 15: 85-100.

Sakai, H., and Dickson, F.W. 1978. Experimental determination of the rate and equilibrium fractionation factors of sulphur isotope exchange between sulphate and sulphide in slightly acid solutions at 300°C and 1000 bars. E*arth and Planetary Science Letters*, 39: 151-161.

Scherer, S., and Neuhaus, K. 2002. Life at low temperatures. pp. 210-262 *In:* Balows, A., Trüper, H.G., Dworkin, M., Harder, W., and Schleifer, K.H. (Eds.) The prokaryotes: an evolving electronic resource for the microbiological community, 3rd edition. Springer, New York.

Schidlowski, M., Hayes, J.M., and Kaplan, I.R. 1983. Isotopic inferences of ancient biochemistries - Carbon, sulfur, hydrogen, and nitrogen. pp. 149-186 *In:* Schoopf, W. (Ed.) Earth's earliest biosphere: Its origin and evolution. Princeton, NJ, Princeton University Press. 610 p.

Schimmelmann, A., and DeNiro, M.J. 1984. Elemental and stable isotope variations of organic matter from a terrestrial sequence containing the Cretaceous/Tertiary boundary at York Canyon, New Mexico. *Earth and Planetary Science Letters*, 68: 392-398.

Schlesinger, W. H. 1991. Biogeochemistry: an analysis of global change. Academic Press Inc., London. 443 p.

Schmitz, B., Andersson, P., and Dahl, J., 1988, Iridium, sulfur isotopes and rare earth elements in the Cretaceous-Tertiary boundary clay at Stevns Klint, Denmark. *Geochimica et Cosmochimica Acta*, 52: 229–236.

Schneider, A. 1970. The sulfur isotope composition of basaltic rocks. *Contributions to mineralogy and petrology*, 25: 95-124. doi: 10.1007/BF00389779.

Schulte, P., Alegret, L., Arenillas, I., Arz, J.A., Barton, P.J., Bown, P.R., Bralower, T.J.,

Christeson, G.L., Claeys, P., Cockell, C.S., Collins, G.S., Deutsch, A., Goldin, T.J., Goto, K., Grajales-Nishimura, J.M., Grieve, R.A.F., Gulick, S.P.S., Johnson, K.R., Kiessling, W., Koeberl, C., Kring, D.A., MacLeod, K.G., Matsui, T., Melosh, J., Montanari, A., Morgan, J.V., Neal., C.R., Nichols, D.J., Norris, R.D., Pierazzo, E., Ravizza, G., Rebolledo-Vieyra, M., Reimold, W.U., Robin, E., Salge, T., Speijer, R.P., Sweet, A.R., Urrutia-Fucugauchi, J., Vajda, V., Whalen, M.T., and Willumsen, P.S. 2010. The Chicxulub asteroid impact and mass extinction at the Cretaceous-Paleogene Boundary. *Science*, 327: 1214-1218.

Seal, R.R. II. 2006. Sulfur isotope geochemistry of sulfide minerals. *Reviews in Mineralogy and Geochemistry*, 61: 633-677.

Self, S., Blake, S., Sharma, K., Widdowson, M., and Sephton, S. 2008. Sulfur and chlorine in Late Cretaceous Deccan magmas and eruptive gas release. *Science*, 319: 1654-1657.

Self, S., Thordarson, T., and Widdowson, M. 2005. Gas fluxes from flood basalt eruptions. *Elements*, 1: 283-287.

Self, S., Widdowson, M., Thordarson, T., and Jay, A.E. 2006. Volatile fluxes during flood basalt eruptions and potential effects on the global environment: A Deccan perspective. *Earth and Planetary Science Letters*, 248: 518–532.

Sen, A.M. 2001. Acidophilic sulphate reducing bacteria: Candidates for bioremediation of acid mine drainage pollution. Ph.D. Thesis, University of Wales, Bangor, United Kingdom.

Sen, A.M., and Johnson, D.B. 1999. Acidophilic sulfate-reducing bacteria: Candidates for bioremediation of acid mine drainage, pp. 709-718 *In:* Amils, R., and Ballester, A. (Eds.). Biohydrometallurgy and the environment toward the mining of the 21st century. Process Metallurgy 9B. Elsevier, Amsterdam. 1712 p.

Senko, J.M., Zhang, G., McDonough, J.T., Bruns, M.A., and Burgos, W.D. 2009. Metal Reduction at low pH by a *Desulfosporosinus* species: Implications for the biological treatment of acidic mine drainage. *Geomicrobiology Journal*, 26:71-82.

Sepkoski, J.J. Jr. 1996. Patterns of Phanerozoic extinctions: A perspective from global databases. pp. 35–52 *In:* Walliser, O.H. (Ed.) Global Events and Event Stratigraphy. Springer, Berlin. 333 p.

Sheehan, P.M., Hansen, T.A. 1986. Detritus feeding as a buffer to extinction at the end of the Cretaceous. *Geology*, 14: 868–70.

Shen, Y., Buick, R., and Canfield, D.E. 2001. Isotopic evidence for microbial sulphate reduction in the early Archaean era. *Nature*, 410: 77-81.

Shen, Y., and Buick, R. 2004. The antiquity of microbial sulfate reduction. *Earth-Science Reviews*, 64: 243-272.

Sheth, H.C., Pande, K., and Bhutani, R. 2001. ^{40}Ar-^{39}Ar ages of Bombay trachytes: Evidence for a Palaeocene phase of Deccan volcanism. *Geophysical Research Letters*, 28: 3513-3516.

Signor, P. W. III, and Lipps, J.H. 1982. Sampling bias, gradual extinction patterns and catastrophes in the fossil record. *Geological Society of America Special Paper*, 190: 291-296.

Sigurdsson, H., Bonté, Ph., Turpin, L., Chaussidon, M., Metrich, N., Steinberg, M., Prade, Ph., and D'Hondt, S. 1991a. Geochemical constraints on source region of Cretaceous/Tertiary impact glasses. *Nature*, 353: 839- 842.

Sigurdsson, H., D'Hondt, S., Arthur, M.A., Bralower, T.J., Zachos, J.C., Fossen, M., and Channell, J.E.T. 1991b. Glass from the Cretaceous-Tertiary boundary in Haiti. *Nature,* 349: 482-487.

Sigurdsson, H., D'Hondt, S., and Carey, S. 1992. The impact of the Cretaceous/Tertiary bolide on evaporite terrane and generation of major sulfuric acid aerosol. *Earth and Planetary Science Letters*, 109: 543-559.

Sim, M.S., Bosak, T., and Ono, S. 2011. Large sulfur isotope fractionation does not require disproportionation. *Science*, 333: 74-77.

Simpson, J.F. 1966. Evolutionary pulsations and geomagnetic polarity. *Geological Society of America Bulletin*, 77: 197-204.

Smit, J. 1999. The global stratigraphy of the Cretaceous-Tertiary boundary impact ejecta. *Annual Review of Earth and Planetary Sciences*, 27: 75-113.

Smit J, and Hertogen J. 1980. An extraterrestrial event at the Cretaceous-Tertiary boundary. *Nature*, 285: 198–200

Sørensen, D., Christensen, J., and Jørgensen, B.B. 1981. Volatile fatty acids and hydrogen as substrates for sulfate-reducing bacteria in anaerobic marine sediment. *Applied and Environmental Microbiology*, 42: 5-11.

Srivasta, S.K. 1970. Pollen biostratigraphy and paleoecology of the Edmonton Formation (Maestrichtian), Alberta, Canada. *Palaeogeography, Palaeoclimatology, Palaeoecology*, 7: 221-276.

Stackebrandt, E., Stahl, D.A., and Devereux, R. 1995. Taxonomic relationships. pp. 49-87 *In:* Barton, L.L. (Ed.). Sulfate-reducing bacteria. Plenum Press, New York. 352 p.

Stahlmann, J., Warthmann, R., and Cypionka, H. 1991. Na^+-dependent accumulation of sulphate and thiosulphate in marine sulphate-reducing bacteria. *Archives of Microbiology*, 155: 554-558.

Sweet, A.R., and Braman, D.R. 1992. The K-T boundary and contiguous strata in western Canada: Interactions between paleoenvironments and palynological assemblages. *Cretaceous Research*, 13: 31-79.

Sweet, A.R., and Braman, D.R. 2001. Cretaceous-Tertiary palynofloral perturbations and extinctions within the *Aquilapollenites* Phytogeographic Province. *Canadian Journal of Earth Sciences*, 38: 249-269.

Sweet, A.R., Braman, D.R., and Lerbekmo, J.F. 1999. Sequential palynological changes across the composite Cretaceous-Tertiary (K-T) boundary claystone and contiguous strata, western Canada and Montana, USA. *Canadian Journal of Earth Sciences*, 36: 743-768.

Swisher, C.C.III., Dingus, L., Butler, R.F. 1993. $^{40}Ar/^{39}Ar$ dating and magnetostratigraphic correlation of the terrestrial Cretaceous-Paleogene boundary and Puercan Mammal Age, Hell Creek – Tullock formations, eastern Montana. *Canadian Journal of Earth Sciences*, 30: 1981-1996.

Swisher, C.C. III, Grajales-Nishimura, J.M., Montanari, A., Margolis, S.V., Claeys, P., Alvarez, W., Renne, P., Cedillo-Pardo, E., Maurrasse, F.J-M.R., Curtis, G.H., Smit, J., and McWilliams, M.O. 1992. Coeval $^{40}Ar/^{39}Ar$ ages of 65.0 million years ago from Chicxulub crater melt rock and Cretaceous-Tertiary boundary tektites, *Science,* 257: 954-958.

Tanner, R. 1997. Cultivation of bacteria and fungi. p. 52-60. *In*: Hurst, C.J. Knudsen, G.R., McInerney, M.J., Stetzenbach, L.D., and Walter, M. V. (Eds.) Manual of Environmental Microbiology. American Society for Microbiology, Washington, DC. 894 p.

Tappan, H. 1968. Primary production, isotopes, extinctions and the atmosphere. *Palaeogeography, Palaeoclimatology, Palaeoecology*, 4: 187-210.

Textor, C., Graf, H.F., Herzog, M., and Oberhuber, J.M. 2003. Injection of gases into the stratosphere by explosive volcanic eruptions, *Journal of Geophysical Research*, 108: 17 p. doi:10.1029/2002JD002987.

Therrien, F., Eberth, D.A., Braman, D.R., and Zelenitsky, D.K. 2007. High-resolution organic carbon isotopic record across the Cretaceous-Tertiary boundary in south-central Alberta: Implications for the post-impact recovery rate of terrestrial ecosystems and use of $\delta^{13}C$ as a boundary marker. *Canadian Journal of Earth Sciences,* 44: 529-542.

Thiemens, M.H. 1999. Mass independent isotope effects in planetary atmospheres and the early solar system. *Science*, 283: 341-345.

Thode, H.G. Sulphur isotopes in nature and the environment: An overview. 1991. pp. 1-26 *In:* Krouse, H.R. and V.A. Grinenko (Eds.) Stable isotopes in the assessment of natural and anthropogenic sulphur in the environment. SCOPE 43. John Wiley & Sons, Chichester. 440 p.

Thode, H.G., Kleerekoper, H., and McElcheran, D.E. 1951. Isotopic fractionation in the bacterial reduction of sulphate. *Research (London)*, 4: 581-582.

Thode, H.G., Monster, J., and Dunford, B. 1961. Sulphur isotope geochemistry. *Geochimica et Cosmochimica Acta*, 25: 150-174.

Thordarson, T., and Self, S. 1998. The Roza Member, Columbia River Basalt Group: A gigantic pahoehoe lava flow field formed by endogenous processes? *Journal of Geophysical Research*, 103: 27411–27445.

Trudinger, P.A. 1992. Bacterial sulfate reduction: current status and possible origin, pp. 367-377 *In* Schidlowski, M., Golubic, S., Kimberley, M.M., McKirdy, D.M., and Trudinger, P.A. (Eds.). Early organic evolution: Implications for mineral and energy

resources. Springer-Verlag, Berlin. 556 p.

Tschudy, R.H. 1984. Palynological evidence for change in continental floras at the Cretaceous Tertiary boundary. pp. 315-337. *In:* Berggren, W. A., and Van Couvering, J.A. (Eds.). Catastrophes in Earth history: The new uniformitarianism. Princeton University Press. 487 p. doi:10.1029/EO066i031p00571-01

Tschudy, R.H., and Tschudy, B.D. 1986. Extinction and survival of plant life following the Cretaceous/Tertiary boundary event, Western Interior, North America. *Geology,* 14: 667-670.

Vandamme, D., and Courtillot, V. 1992. Paleomagnetic constraints on the structure of the Deccan Traps. *Physics of the Earth and Planetary Interiors*, 74: 241-261.

Vandamme, D., Courtillot, V., and Besse, J. 1991. Paleomagnetism and age determinations of the Deccan Traps (India): Results of a Nagpur-Bombay traverse and review of earlier work. *Review of Geophysics*, 29: 159-190.

Van Everdingen, R.O., Shakur, M.A., and Krouse, H.R. 1982. Isotope geochemistry of dissolved, precipitated, airborne, and fallout sulfur species associated with springs near Paige Mountain, Norman Range, N.W.T. *Canadian Journal of Earth Science*, 19: 1395-1407.

Van Everdingen, R.O., Shakur, M.A., and Krouse, H.R. 1985. Role of corrosion by H_2SO_4 fallout in cave development in a travertine deposit-evidence from sulfur and oxygen isotopes. *Chemical Geology*, 49: 205-211.

Wacey, D., Kilburn, M.R., Saunders, M., Cliff, J., and Brasier, M.D. 2011. Microfossils of sulphur-metabolizing cells in 3.4-billion-year-old rocks of Western Australia. *Nature Geoscience*, 4, 698–702. doi:10.1038/ngeo1238

Wagner, M., Roger, A.J., Flax, J.L., Brusseau, G.A., and Stahl D.A. 1998. Phylogeny

of dissimilatory sulfite reductases supports an early origin of sulfate respiration. *Journal of Bacteriology*, 180: 2975–2982.

Walker, J.C.G. and Brimblecombe, P. 1985. Iron and sulphur in the pre-biologic ocean. *Precambrian Research*, 28: 205-222.

Warthmann, R., and Cypionka, H. 1990. Sulphate transport in *Desulfobulbus propionicus* and *Desulfococcus multivorans*. *Archives of Microbiology*, 154: 144-140.

Waugh, D., and Hall, T. 2002. Age of stratospheric air: Theory, observations, and models. *Reviews of Geophysics*, 40. doi:10.1029/2000RG000101.

Wensink, H., and Klootwijk, C.T. 1971. Paleomagnetism of the Deccan Traps in the Western Ghats near Pona (India). *Tectonophysics*, 11: 175-190.

Westerhold, T., Röhl, U., Raffi, I., Fornaciari, E., Monechi, S., Reale, V., Bowles, J., and Evans, H.F. 2008. Astronomical calibration of the Paleocene time. *Palaeogeography, Palaeoclimatology, Palaeoecology*, 257: 377-403.

Westrich, J.T., and Berner, R.A. 1984. The role of sedimentary organic matter in bacterial sulfate reduction: the G model tested. *Limnology and Oceanography*, 29: 236-249.

Whelpdale, D.M. 1992. An overview of the atmospheric sulfur cycle. pp. 5-26 *In:* Howarth, R.W., Stewart, J.W.B., and Ivanov, M.V. (Eds.) Sulphur cycling on the continents: wetlands, terrestrial ecosystems and associated water bodies. SCOPE 48. John Wiley and Sons, Chichester. 350 p.

Widdel, F. 1988. Microbiology and ecology of sulfate- and sulfur-reducing bacteria. pp. 469–585 *In:* Zehnder, A.J.B. (Ed.) Biology of anaerobic microorganisms. John Wiley and Sons, New York. 872 p.

Widdel, F., and Hansen, T.A. 1992. The dissimilatory sulfate- and sulfur-reducing bacteria, p. 583-624. *In:* Balows, A., Trüper, H.G., Dworkin, M., Harder, W., and Schleifer, K.H. (Eds.). The prokaryotes, 2nd edition, Volume 1. Symbiotic Associations, Biotechnology, Applied Microbiology. Springer, New York. 1012 p.

Wilf, P., Johnson, K.R., and Huber, B.T. 2003. Correlated terrestrial and marine evidence for global climate changes before mas extinction at the Cretaceous-Paleogene boundary. *Proceedings of the National Academy of Science*, 100: 599-604.

Witham, C.S., Oppenheimer, C., and Horwell, C.J., 2005. Volcanic ash leachates: a review and recommendations for sampling methods. *Journal of Volcanology and Geothermal Research*, 141: 299–326.

Woese, 1987. Bacterial evolution. *Microbiology Review*, 51: 221-271.

Wolbach, W.S., Lewis, R.S., and Anders, E. 1985. Cretaceous extinctions; Evidence for wildfires and search for meteoritic material. *Science*, 230: 167-170.

Wortmann, U.G., Bernasconi, S.M., and Böttcher, M.E. 2001. Hypersulfidic deep biosphere indicates extreme sulfur isotope fractionation during single-step microbial sulfate reduction. *Geology*, 29: 647–650.

Wu, J. 1981. Evidence of sea spray produced by bursting bubbles. *Science*, 212: 324-326.

Yanagisawa, F., and Sakai, H. 1983. Thermal-decomposition of barium-sulfate vanadium pentaoxide silica glass mixtures for preparation of sulfur-dioxide in sulfur isotope ratio measurements. *Analytical Chemistry*, 55: 985-987.

Young, E.D., Galy, A., and Nagahara, H. 2002. Kinetic and equilibrium mass-dependent isotope fractionation laws in nature and their geochemical and cosmochemical significance. *Geochimica et Cosmochimica Acta*, 66: 1095–1104.

Zachos, J.C., Aubry, M.-P., Berggren, W.A., Ehrendorfer, T., Heider, F., and Lohmann, K.C. 1992. Chemobiostratigraphy of the Cretaceous/Paleocene boundary at Site 750, southern Kerguelen Plateau. *Proceedings of the Ocean Drilling Program, Scientific Results*, 120: 961–977.

Zeikus, J.G., Dawson, M.A., Thompson, T.E., Ingvorsen, K., and Hatchikian, E.C. 1983. Microbial ecology of volcanic sulphidogenesis: Isolation and characterization of *Thermodesulfobacterium commune gen. nov. and sp. nov*. *Journal of General Microbiology*, 129: 1159–1169.

Zmolek, P., Xu, X.P., Jackson, T., Thiemens, M.H., and Trogler, W.C. 1999. Large mass independent sulphur isotope fractionations during the photopolymerization of (CS_2)-^{12}C and (CS_2)-^{13}C. *Journal of Physical Chemistry A*, 103: 2477-2480.

Appendix I : Growth media for acidophilic sulfate-reducing bacteria

I.1 Strain M1: *Desulfosporosinus sp.* (optimal pH 4.0)

This isolate and the recipes for the preparation of the growth medium for its culture were provided by David Barrie Johnson, Bangor University, Bangor, United Kingdom. Some modifications were made to this medium for the purpose of the experiments described in this document. When applicable, these are indicated. All solutions should be stored at 4°C.

Table I.1: Chemically-defined growth medium for the *Desulfosporosinus sp.* (M1) strain

Component	Concentration in solution
Heterotrophic basal salts solution*	20 mL/L
Trace elements solution*	1 mL/L
Yeast extract	0.02% (w/v)
Glycerol	5 mM
$ZnSO_4$	5 mM
K_2SO_4	0.5 M

** see below*

In a base of double-deionized and degassed water, add all components and adjust pH to 4.0 with H_2SO_4 before autoclaving for sterilization. When the solution is cool, add F_2SO4 from a 1 M, pH 2.0 filter-sterilized stock solution, to a final concentration of 0.5 mM. Incubate medium overnight in an anaerobic chamber before inoculating with sulfate-reducing bacteria.

Table I.2: Composition of heterotrophic basalt salts solution for growth of the *Desulfosporosinus sp.* (M1) strain.

Compound	Concentration (g/L)
$ZnSO_4 \bullet 7H_20$	10
$CuSO_4 \bullet 5H_2O$	1
$MnSO_4 \bullet 4H_2O$	1
$CoSO_4 \bullet 7H_2O$	1
$Cr_2(SO_4)_3 \bullet 15H_2O$	0.5
H_3BO_3	0.6
$Na_2MoO4 \bullet 2H_2O$	0.5
$NiSO_4 \bullet 6H_2O$	1
$Na_2SeO_4 \bullet 10H_2O$	1
$Na_2WO_4 \bullet 2H_2O$	0.1
$NaVO_3$	0.1

To prepare the trace elements solution, adjust the pH of 800 mL of double deionized and water to pH 2.0 with H_2SO_4. Add the compounds listed above in the order given, allowing each compound to dissolve before the next compound is added. Check and adjust pH if necessary. When the last compound has been added, complete the total volume to 1 L, adjust the pH to 2.0 if necessary, and autoclave to sterilize. It should benoted that the sodium vanadate may require several days to dissolve completely.

Table I.3: Composition of trace elements solution for growth of the *Desulfosporosinus sp.* (M1) strain.

Compound	Concentration (g/L)
$Na_2SO_4 \bullet 10H_2O$	7.5
$(NH_4)_2SO_4$	22.5
KCl	2.5
$MgSO_4 \bullet 7H_2O$	25
KH_2PO_4	2.5
$Ca(NO_3)_2 \bullet 4H_2O$	0.7

Add components to 1 L of double deionized water and autoclave for sterilization.

The recipe for the growth medium described above is used for the maintenance of cultures: the presence of reactive metals (e.g. Fe, Mg, Zn) in the solution helps reduce the toxicity of the sulfides produced during the reduction of sulfate by facilitating their precipitation out of solution. For the purpose of the experiments described in this document, the presence of these elements was minimized to avoid the precipitation of sulfides, which would affect isotopic mass balance considerations. For the isolate M1, we replaced ZnSO4 and FeSO4 with K_2SO4 (8 mM) and Na_2SO4 (10 mM). The pH was adjusted using HCl. The composition of the trace metal and heterotrophic basal salts solutions was not changed.

The inoculum for the experiment was prepared by transferring the maintenance culture to Fe/Mg-free medium at least three times to minimize the precipitation of sulfides.

I.2 Strain GBSRB4.2: *Desulfosporosinus sp.* (optimal pH 4.2)

This isolate and the recipes for the preparation of the growth medium for its culture were provided by John Senko, University of Akron, Akron, Ohio, U.S.A. The vitamin and trace metal solutions are derived from Tanner (1997). Some modifications were made to this medium for the purpose of the experiments described in Chapter 3. When applicable, these are specified.

Table I.4: Chemically-defined growth medium for the *Desulfosporosinus sp.* (GBSRB4.2) strain.

Compound	Concentration
$(NH_4)_2SO_4$	10 mM
$MgSO_4$	2 mM
Glucose	5 mM
Tryptic soy broth (TSB)	0.5 g/L
Trace metals solution*	10 mL/L
Vitamin solution*	10 mL/L
$FeSO_4$ (in 0.4 mM solution)	16 mM

** see below*

This medium was prepared by adding, in the anaerobic chamber (N_2 95%, H_2 5%) each component of the growth medium to the prescribed concentration to degassed double deionized water. Once the pH was adjusted, the medium was dispensed into the appropriate container (serum tubes or vials for maintenance culture, large pyrex bottles for experimental cultures) and these were sealed and taken out of the anaerobic chamber for autoclaving. The inoculum for the experiment was prepared by transferring the maintenance culture to Fe/Mg-free medium at least three times to minimize the precipitation of sulfides from solution.

Table I.5: Composition of the trace metal solution for the strain *Desulfosporosinus sp.* (GBSRB4.2)

Component	Concentration (g/L)
Nitrilotriacetic acid (from trisodium salt)	2.0
$MnSO_4 \bullet H_2O$	1.0
$Fe(NH_4)_2(SO_4)_2 \bullet 6H_2O$	0.8
$CoCL_2 \bullet 6H_2O$	0.2
$ZNSO_4 \bullet 7H_2O$	0.2
$CuCl_2 \bullet 2H_2O$	0.02
$NiCl_2 \bullet 6H_2O$	0.02
$Na_2MoO_4 \bullet 2H_2O$	0.02
Na_2SeO_4	0.02
Na_2WO_4	0.02

The trace metal solution was prepared by adding each component in the prescribed concentration to one liter of double-deionized water. The solution was not autoclaved.

Table I.6: Composition of the vitamin solution for the strain *Desulfosporosinus sp.* (GBSRB4.2)

Component	Concentration (g/L)
Pyridoxine•HCl	10
Thiamine•HCl	5
Riboflavin	5
Calcium pantothenate	5
Thioctic acid	5
ρ-Aminobenzoic acid	5
Nicotinic acid	5
Vitamin B_{12}	5

Component	Concentration (g/L)
MESA (mercaptoethanesulfonic acid)	5
Biotin	2
Folic acid	2

The trace metal solution was prepared by adding each component in the prescribed concentration to one liter of double-deionized water.

In the growth medium for the isolate GBSRB4.2, $MgSO_4$ and $FeSO_4$ were replaced with $(NH_4)_2SO_4$ (8 mM) and Na_2SO_4 (10 mM) and pH was adjusted using HCl instead of H_2SO_4. The composition of the trace metal solution was not changed.

Appendix II: Sulfur reduction line

A significant portion of the PhD candidate's time was spent building a sulfur extraction line at the University of Ottawa, in the Earth Sciences Department (geobiology lab, Dr. Fortin). The design of this extraction line was based on a similar installation at McGill University, in the Earth and Planetary Sciences Department (Dr. Wing). Some improvements and modifications were made to this design by the candidate, namely to minimize the need to rely on complex glass parts that are expensive to make, fragile, and require the work of a professional glassblower, as well as to take advantage of the equipment already available at the University of Ottawa. This extraction line will be dismantled and moved to the G.G. Hatch Stable Isotope Lab facilities at the University of Ottawa. Included in this appendix are a description of this installation and of the parts used to build it.

Figure II.1: Sulfur extraction line at the Department of Earth Sciences, University of Ottawa. Up to six samples can be treated independently, each with its own adjustable gas pressure valve and mantle heater. The sample vials can be used interchangeably for the CRS reduction and the Thode reduction methods.

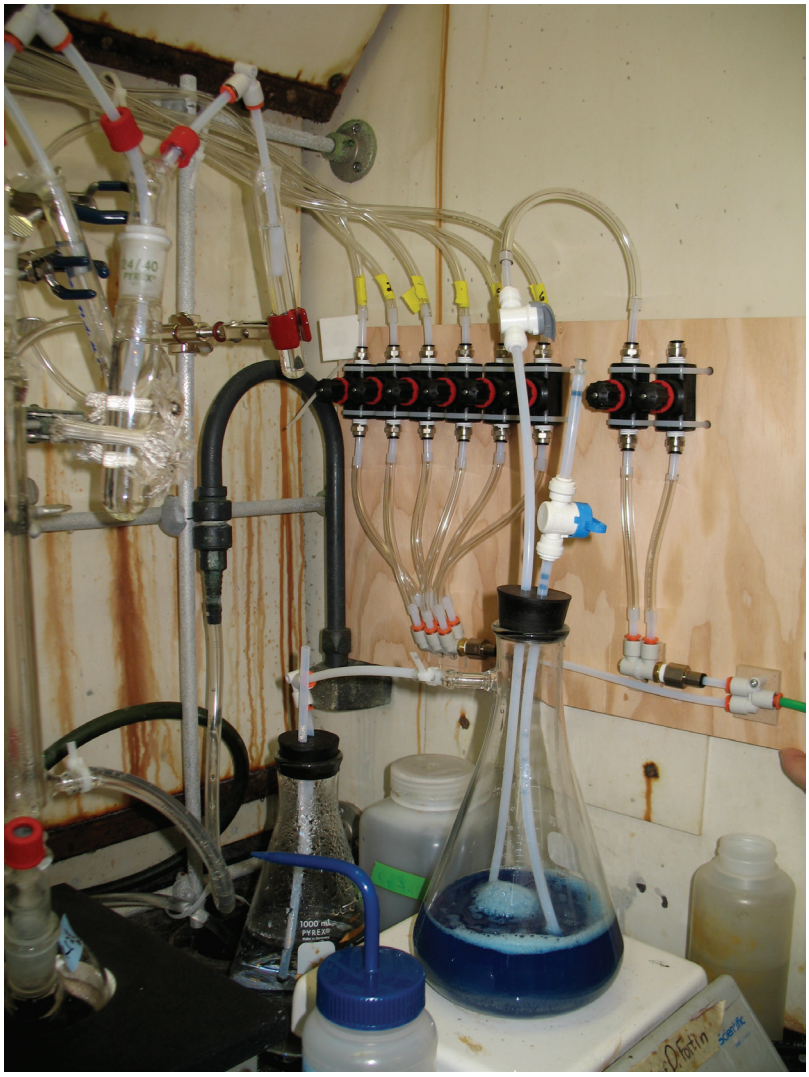

Figure II.2: Setup for the preparation of the CRS reagent and gas pressure regulators (behind).

Extraction line - sample sections

The samples are introduced into the flask via one of the three openings (Figure IIa). The central opening is fitted onto a Liebig-type condenser of any length (in this setup, 320-mm condensers were used). Allihn-type condensers are also appropriate, but types with very high surface area (e.g., coiled condensers, Graham-type) should be avoided as at temperatures required for CRS or Thode reduction, condensation forms inside the coils and prevents gases from flowing through the condenser.

A second flask opening is fitted with a 24/40 joint with GL-14 screw threading. As I was unable to find a manufacturer producing standard 24/40 joints fitted with GL-14 threading, I had a glassblower affix the new threading to existing thermometer adapters with a 24/40 joint. A glass rod connected to the gas inflow is passed through this GL-14 cap, which is fitted with a sillicone ring liner. For the extraction of Thode-reducible sulfates, the third and last opening is simply closed using a glass stopper, while for the extraction of chromium-reducible sulfides, it is fitted with a 24/40 male joint with GL-14 threading fitted with a septum. The sample can be introduced through the septa once the flask has been flushed with N_2 gas to remove oxygen. The septa used in this particular installation are Labco Ltd. septa for Exetainer caps and can be pierced several times before requiring replacement.

The top opening of the condensers are fitted with a 24/40 joint with GL-14 threading fitted with a GL-14 cap and silicone ring. Teflon tubing is inserted into this opening and connected to a single opening 24/40 vial via a push-to-connect 90° tube fitting coupling attached to a 24/40 joint with double GL-14 threading inserted into a cylindrical flask. The second opening of this joint features a GL-14 cap with silicone ring, into which a section of teflon tubing is inserted. This teflon tubing is then inserted into the sample vial.

Cold water is circulated via polypropylene tubing through all six condensers connected in series. All other tubing used in the extraction line is composed of teflon to minimize reaction of organic compounds and the “sticking” of H_2S to the lines. The 6-place heating mantle used features 6 individual temperature controllers.

CRS reagent setup

An Erlenmeyer flask is positioned onto a stir plate and fitted with a rubber or silicone stopper that has been pierced with two holes smaller than the diameter of the teflon tubing (this has to be air tight to avoid reoxidation of the chemicals). Teflon tubing is

inserted into each hole and each section is fitted with a valve. One valve controls access to the chemical with a syring and luer lock adapter, the other is connected to the gas panel controller for N_2 intake. The side outlet on the Erlenmeyer flask is connected to a section of polypropylene tubing that enters a 90° coupler directed into another

The CRS reagent (Figure II.2) can be removed from the flask through a 1/4 inch teflon tube fitted with a female luer lock adapter.

Gas panel controller

The gas panel controller consists in a series of needle-valves and manifolds fixed to a wooden plate inside the fume hood. A main line connected to a N_2 tank enters the panel from the right side (front of the fume hood, Figure II.2) and is split into two lines: one line is used for the two needle valves on the right side of the panel (one for the CRS reagent preparation and a spare valve) and the other split further into six for the six sample lines in the extraction line. Each valve can be controlled separately and with great precision.

Table II.1: List of parts used in the sulfur extraction line

Component	Supplier	Part number
Extraction line and reagent preparation		
3-neck round bottom flask, 24/40 joints, 250 mL	Chemglass Inc.	CG-1524
Liebig condenser, 24/40 joint, 320 mm	Chemglass Inc.	CG-1218-01
GL-14 cap with aperture	Chemglass Inc.	CGB-195-01
24/40 joint	Chemglass Inc.	
GL-14 Screw Thread Tube, on 12mm OD x 1.5mm W tubing, 100mm OAL	Chemglass Inc.	CGB-194-01
Silicone Sealing Ring, fits GL-14 Cap, fits tubing O.D. 5.5mm to 6.5mm	Chemglass Inc.	CGB-197-01
Teflon liners - long - for 24/40 standard taper joint[a]	Chemglass Inc.	CG-116-15
Teflon liners - medium - for 24/25 standard taper joint[a]	Chemglass Inc.	CG-116-06
Adapter, Thermometer, Inlet, 24/40 Inner Joint, 80mm Height, #7, Chemglass Inc.	Chemglass Inc.	CG-1042-01
Extreme-Temperature Tubing Made with Teflon® PTFE (1/4» OD- outside diameter)	McMaster-Carr	5033K31
Polypropylene female luer lock - 1/8	McMaster-Carr	51525K293
Septa for Labco Exetainer® 16.5mm Screw Caps	Labco Ltd.	VW101

Component	Supplier	Part number
Reagents		
Zinc	Fisher Scientific	14409
Hypophosphorous acid in 50% water	Sigma-Aldrich	214906
Hydroiodic acid	Sigma-Aldrich	248649
Chromium chloride hexahydrate	Fisher Scientific	AC-21336
Gas panel controller		
FDA Plastic Ball Valve 1/4» Tube OD - push to connect * push to connect	McMaster-Carr	4379K53
Easy-set polyester needle valve - dual direction (1/4»)	McMaster-Carr	4891K72
Plug - 1/4 inch	McMaster-Carr	5111K504
Polybutylene & Brass Push-to-Connect Fitting Wye for 1/4 Tube OD	McMaster-Carr	5111K547
Polybutylene & Brass Push-to-Connect Fitting Tee for 1/4 Tube OD, Gray	McMaster-Carr	5111K527
Polybutylene & Brass Push-to-Connect Fitting 90° Elbow for 1/4 Tube OD, Gray	McMaster-Carr	5111K488
Polybutylene & Brass Push-to-Connect Fitting Coupling for 1/4 Tube OD, Gray	McMaster-Carr	5111K468
Polybutylene Manifold Swivel Tube Fitting 6 Outlets, for 1/4 Tube OD, 1/4 NPT Thread	McMaster-Carr	5203K75
Polybutylene Manifold Swivel Tube Fitting 2 Outlets, for 1/4 Tube OD, 1/4 NPT Thread	McMaster-Carr	5203K18
Polybutylene & Brass Push-to-Connect Fitting Wye for 1/4 Tube OD, Gray	McMaster-Carr	5111K548
Nylon and Nickel-Plated Brass Tube Fitting Adapter for 1/4 Tube OD X 1/4» NPT Male Pipe	McMaster-Carr	5779K109
Nylon and Nickel-Plated Brass Tube Fitting Adapter for 1/4 Tube OD X 1/4 NPT Female Pipe	McMaster-Carr	5779K131
Extreme-Temperature Tubing Made with Teflon® PTFE (1/4 OD- outside diameter)	McMaster-Carr	5033K31

[a]Either size can be used with the 24/40 joints.